GROWTH OPTIMIZATION OF *Synechococcus elongatus PCC 7942* IN LAB FLASK AND 2D PHOTOBIOREACTOR

by

DAVID KUAN

B.A.Sc., The University of British Columbia, 2010

A THESIS SUBMITTED IN PARTIAL FULFILLMENT OF
THE REQUIREMENTS FOR THE DEGREE OF

MASTER OF APPLIED SCIENCE

in

The Faculty of Graduate and Postdoctoral Studies
(Chemical and Biological Engineering)

THE UNIVERSITY OF BRITISH COLUMBIA
(Vancouver)

August 2013

Abstract

One of the most promising mechanisms for the production of high value biologically active products is through the cultivation of microalgae. In addition to serving as a carbon capture system, this photosynthetic microorganism has demonstrated potential for recombinant protein expression as an approach towards sustainable development in biotechnology. Extensive studies on cyanobacterium *Synechococcus elongatus* PCC 7942 have assessed the dual function of carbon capture with product generation such as biodiesel and recombinant protein. In order to maximize CO_2 fixation and production rates of valuable product, a high cell growth rate needs to be achieved. Consequently, challenges in photobioreactor operation and cultivation need to be addressed, such as CO_2 mass transfer limitations, light availability, and minimizing energy consumption. Thus, the effects of the major growth factors need to be studied.

In this research, the objectives were to optimize the specific growth rate and biomass concentration of *S. elongatus* by investigating the effects of medium composition, light intensity, temperature, and CO_2 concentration. Preliminary studies at the shake flask scale revealed that an optimization of components in BG-11 medium resulted in no significant improvements for the specific growth rate and biomass concentration. However, a maximum specific growth rate of 0.0519 h^{-1} and a maximum biomass concentration of 0.496 g/L were achieved at 33°C and 120 $\mu E/m^2/s$.

A 1 L airlift photobioreactor was used to investigate the effects of light intensity, CO_2 concentration, and gas flow rate on the specific growth rate and biomass concentration. Additional experiments carried out in this photobioreactor revealed that air enriched with 5% CO_2 at 1 L/min, 33°C, and 120 $\mu E/m^2/s$ achieved a maximum biomass concentration of 1.006 g/L at a reduced specific growth rate of 0.0234 h^{-1}. Further increases in CO_2 % and light intensity, as well as light/dark cycles, reduced the growth rate and biomass concentration. Mass transfer experiments also revealed that 5% CO_2 provided the best growth conditions, as growth was significantly limited by CO_2 when supplied with air, whereas 10% CO_2 reduced the pH and consequently reduced the specific growth rate.

Preface

This research is part of a collaboration with Dr. S. Yewalkar of the University of British Columbia and Dr. F. Nano and his research team of the University of Victoria. The microalgae strains were isolated by Dr. Nano. The experiments and data analysis in Chapter 4 were performed by Dr. Yewalkar and me. The experiments and data analysis in Chapters 5 and 6 are my original work.

Table of Contents

List of Tables

List of Figures

List of Symbols and Abbreviations

Symbol	Units	Description
Bo		Bodenstein number
C_S	g/L	Saturation concentration
D_{CO2}	mg/L	Dissolved CO_2
D_{O2}	mg/L	Dissolved O_2
k_La	h^{-1}	Volumetric mass transfer coefficient
μ	h^{-1}	Specific growth rate
ρ	g/m^3	Density
Re		Reynolds number
Sh		Sherwood number
Sc		Schmidt number
v	m/s	Flow velocity
V	L	Volume
X	g/L	Biomass concentration

Abbreviation	Description
CTR	Carbon dioxide transfer rate
CUR	Carbon uptake rate
GHG	Greenhouse gas emissions
ILI	Incident light intensity
PBR	Photobioreactor
vvm	Gas volume flow per unit of liquid volume per minute

Acknowledgements

First, a thank you for the funding received from the National Science and Engineering Research Council (NSERC), without which I wouldn't have had this opportunity.

Next, I would like to give my most sincere thank you to my supervisors Dr. Sheldon Duff, Dr. Dusko Posarac, and Dr. Xiaotao Bi for their continued guidance, encouragement, and mentorship. You've helped me to really grow as an engineer and an individual and for that I am truly grateful. I would also like to thank Dr. Swati Yewalkar for providing her expertise and assistance in conducting this research, as well as Dr. Francis Nano and his research team for providing the microalgae strains. Also thanks to my lab mates for helping to create such an enjoyable environment to work in.

Finally, I would like to thank my friends, Mom and Dad, and sister for their unwavering support they provided throughout my journey.

To my family

1 Introduction

1.1 The need for economical CO_2 capture

Increasing concerns of the effects of climate change has elicited a response for better solutions to mitigate greenhouse gas (GHG) emissions. Humans are accelerating the accumulation of GHGs through combustion, waste gas emissions, and poor land use practices. Efforts to reduce the impacts of climate change are making significant progress towards the goal of reducing Canada's greenhouse gas emissions by 17% from 2005 levels by 2020. As of August 2012, 2020 emissions are projected to be one half of the way to the target (Environment Canada, 2012a). In the past decade, the Canadian government has taken a robust approach in reducing these emissions to tackle climate change (Environment Canada, 2012b).

The most prevalent of GHGs is CO_2, which accounted for 79% of total Canadian GHG emissions (Environment Canada, 2012a). GHG mitigation generally involves reductions in anthropogenic emissions, increasing the capacity of carbon sinks (ex. plants and algae), and the use of renewable energy (e.g. wind power). Commercial viability of carbon capture technologies has been a challenge as these methods have not been shown to be economical. This can be attributed to high operating and disposal costs. The 2009 federal budget has allocated $1 billion over 5 years towards the development of new technologies and is expected to generate at least $2.5 billion in clean energy investment (Flaherty, 2009). Much of this funding has been dedicated toward large-scale carbon capture and storage facilities primarily concerning the electricity and oil/gas sectors. As shown in Figure 1, both these sectors combined to produce 253 million tons of carbon dioxide equivalents, or 36.6% of Canada's total GHG emissions (Environment Canada, 2012c). The need to reduce industrial GHG emissions is imperative.

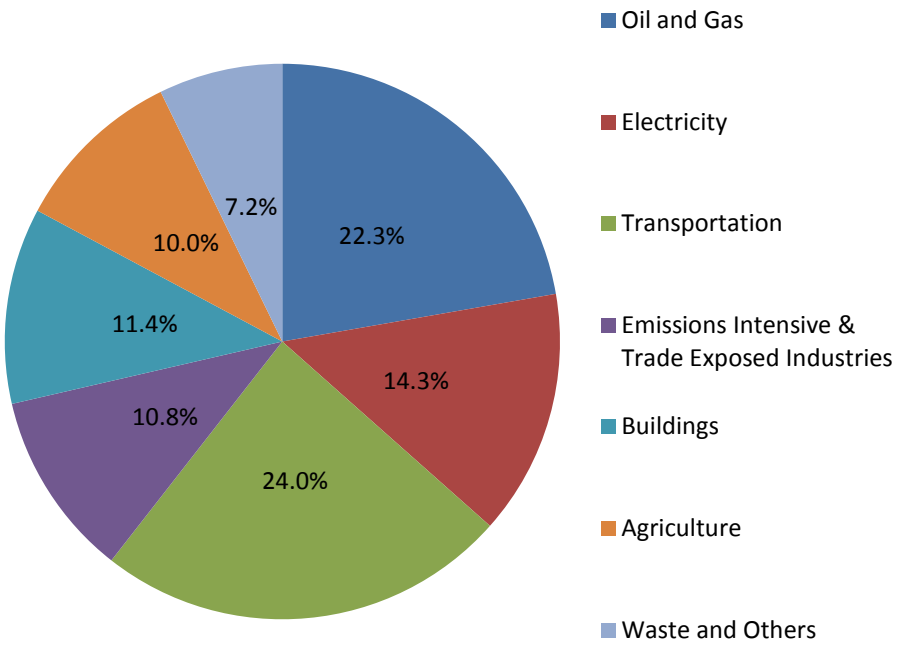

Figure 1: GHG emissions by economic sector (Mt CO_2e) (Environment Canada, 2012a)

1.2 Microalgae as a direct CO_2 mitigation technology

Recent developments on green technologies have had success in mitigating climate change. Three conceptually different modes of atmospheric CO_2 reduction include reducing fossil fuel consumption, removing CO_2 from the atmosphere, and capturing CO_2 from emissions before it is released into the atmosphere (Benemann, 1997). An example of the latter mode is the cultivation of microalgae in open ponds to deal with point source emissions. This has been attractive for its potential to fix CO_2 directly from the atmosphere or flue gases using photosynthesis, and convert it to biomass. This biomass can then be converted into bioproducts or biofuels. What sets microalgae apart from other microorganisms is that they are capable of taking in CO_2 and light energy. They are abundant in almost every habitat because of their tolerance to extreme environmental stresses. However, to date, direct mitigation methods with microalgae are generally associated with higher capital costs and the use of greater amount of resources. It is estimated to cost between \$50-\$250/ton of carbon to remove CO_2 from a conventional power plant using algal technology, when economically feasible sequestration costs should be about \$10/ton of carbon (PowerplantCCS, 2010). Estimates only consider the carbon fixed in biomass. The cost would be higher if carbon losses and costs from electricity, transportation, etc. were

included. Open ponds require land, water, and appropriate climatic conditions, making microalgae a less favourable option (J. Lee & Lee, 2003). Toxic gases present in flue gas such as SO_x and NO_x pose a problem so a pretreatment step is required to minimize their inhibitory effects before introducing CO_2 to the reactors (J. N. Lee et al., 2000). In other words, cultivating algae strictly for commercialization of biomass/biofuel to offset carbon capture costs is not economical. Rather, Benemann (1997) argued that microalgae are better used for specific biological technologies to produce high value products while simultaneously capturing CO_2, which requires the use of photobioreactors. If utilization of CO_2 into high-value compounds is possible, then CO_2 removal costs can be minimized. This has been the driving force in the research on the conversion of CO_2 into useful algae-based products. It has been shown that the application of microalgae for carbon capture can be economical by genetically modifying them to produce therapeutic proteins and other biological products (Specht et al., 2010).

One development that has come to fruition is the application of microalgae to capture CO_2 from a cement plant in Bowmanville, Ontario (Pond Biofuels, 2011). Pond Biofuels has become the first company to successfully use CO_2 emissions to produce biomass by using microalgae as a carbon sink, as shown in Figure 2.

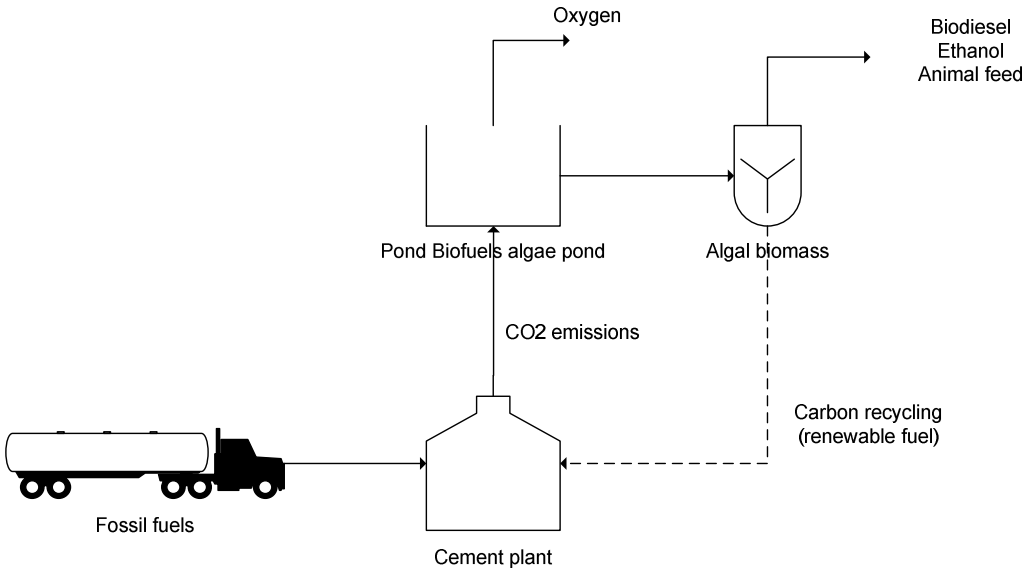

Figure 2: Pond Biofuels CO_2 capture process (Pond Biofuels, 2011)

The biomass can then be dried from industrial waste heat and used as fuel, or they can be used as animal feed. Emissions can be reduced by as much as 40% (Hodge, 2009). Of course,

combustion of algal biomass will release the captured CO_2; however, useful energy is generated as a result of the process. Although this only demonstrated the application of microalgae for production of low-value products, it opens the door for potential commercialization of high-value microalgal products from carbon capture applications.

Besides the additional ability to sequester carbon dioxide from the atmosphere, microalgae can produce a wide range of primary and secondary metabolites, such as proteins, lipids, vitamins, and other biologically active compounds (J. Kim & Lee, 2005). The prospect of using recombinant microalgae to develop high value products has only been a recent development; nonetheless pharmaceutical companies and biochemical producers alike have made strides in its research. The potential of using algae as a source of novel compounds has been reviewed by several researchers (Franklin & Mayfield, 2005; Walker et al., 2005). Of particular concern is determining the best conditions for microalgae growth to make the process economical. Optimizing algal growth rate can improve the production rate of the target metabolite. Cell growth rate depends on light intensity, nutrient type and concentration, temperature, and dissolved CO_2 concentration within the reactor (Sasi, 2009). With this in perspective, the focus of my research is to cultivate an engineered *Synechococcus elongatus* PCC 7942 strain as a vehicle for recombinant protein production in a bubble column and assess economic feasibility for industrial scale production. This provides the groundwork for further expansion of therapeutic and industrial products in the microalgae field.

1.2.1 Microalgal productivity

Biomass productivity is defined as the rate of production of algae biomass per unit volume, and it is highly dependent on the culture technique. Selection of a suitable cultivation method is crucial because it has a profound influence on productivity and purity and it depends on the purpose of the production facility. Biomass productivity is the production of algal biomass concentration per unit time for a given volume. Purity can indicate the contamination level or the percentage of recovered product. As a commonly used configuration for cultivation, open pond cultures are often large scale systems with nutrients provided by runoff water or effluent from wastewater treatment plants. Figure 3 illustrates a schematic of an open pond system (Seambiotic Ltd., 2010). Water is agitated by paddle wheels or similar rotating structures. The culture often consists of a mix of algal strains. This technology typically yields productivities of 14-50 $g \cdot L^{-}$

$^{1}\cdot day^{-1}$, making this a popular design for commercial production of biofuels. However, environmental conditions are difficult to control as these ponds are located outdoors, and this makes them susceptible to contamination and therefore lower purity.

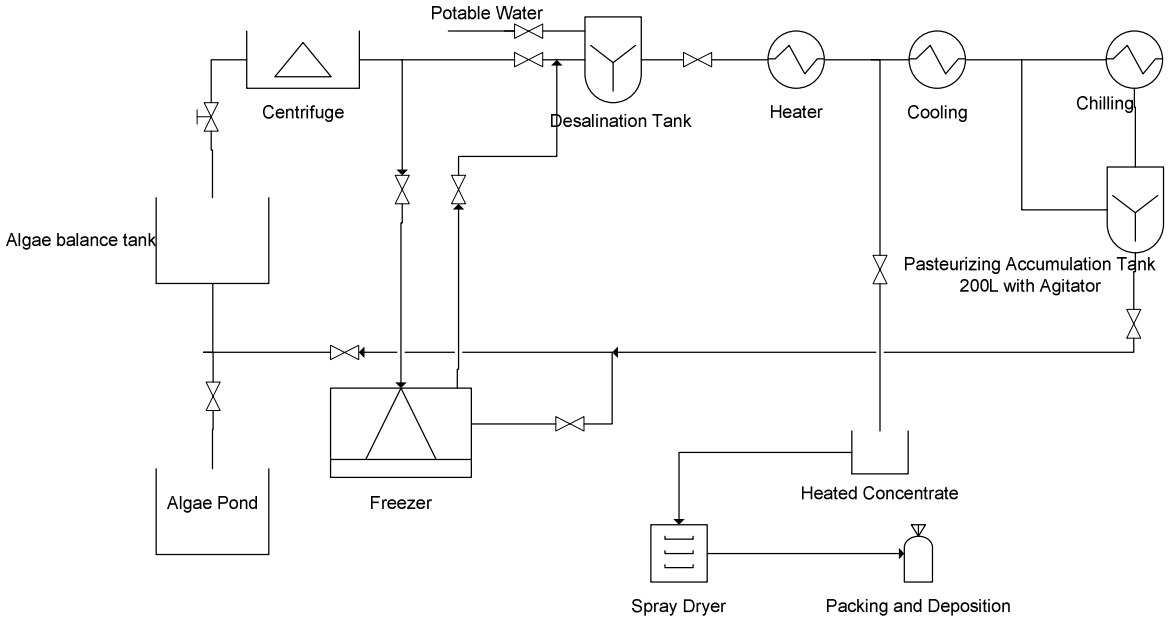

Figure 3: Open pond cultivation (Seambiotic Ltd., 2010)

Small scale production, such as in closed photobioreactors (PBR), allows for better control of growth conditions and sterility. Currently, closed PBRs are the most popular system for conducting research in optimizing algae growth and to make high-value products such as enzymes and food supplements. Closed PBRs provide a sterile environment that enables the growth of a single or several specific species to be optimized for producing a desired product. Water, nutrients, and CO_2 are supplied in a controlled manner. Internal PBR conditions such as pH, light intensity and temperature are controlled and monitored. They can be illuminated by artificial light or natural sunlight. Much work has been carried out to optimize these systems (Chisti & Moo-Young, 1993; Kajiwara et al., 1997; J. Kim & Lee, 2005). Although the potential for microalgae to achieve high productivities was based on projections of limited data from short term and laboratory experiments, they still possess features that can make them a valuable commodity in the biotechnology industry. In the laboratory, photosynthetic efficiency, which is the fraction of light energy that is converted into chemical energy, is usually at 20-24% (Benemann, 1997). Commercial microalgae cultivations are mostly done in open ponds where cells are exposed to sunlight. However, cell productivity does not increase in proportion to the

photosynthetic photon flux density. Table 1 compares the operating requirements for the two methods of algae cultivation.

Table 1: General characteristics of open pond and photobioreactor systems (National Research Council, 2012)

	Open pond system	**Photobioreactor**
Energy source	Natural sunlight	Focused sunlight/artificial light
CO_2 source	Atmosphere or introduced CO_2	CO_2 from carbon capture system
Nutrients	From waste water or introduced	Accurate dosing of nutrients
Capital cost	Low cost for simple engineering	High cost for sophisticated system
Economics	Generic analysis for energy-only schemes is not promising	High value co-products could give viability to niche markets
Electricity consumption	Modest power demand	High power demand
Algal product quality	Variable quality algae product with risk of contamination	High quality monoculture and secreted co-products possible
Potential products	Only suitable as a fuel precursor	Potential for high value products
Water use and loss	High water demand and high potential loss of evaporation	High water demand for solution management. Low evaporation loss
Land area	Large	Small

1.2.2 Current industrial applications using microalgae

For the past few decades, mass culturing microalgae has been a widely-used process for wastewater and water pollution treatments, biofuels production, pharmaceutical bioproducts and carbon sequestration (Benemann & Oswald, 1996). From a commercial perspective, microalgae have been used to produce both biofuels and high-value compounds (Table 2). In waste treatment ponds, microalgae provide oxygen to bacteria, which, in turn, break down biodegradable waste sludge (Alabi et al., 2009). Consequently, useful nutrients like CO_2 and phosphates are released and this promotes algae growth, turning waste into algal biomass. It also addresses the problem of eutrophication in watersheds. Kuehnle AgroSystems in Hawaii has implemented such a process at an oil refinery by removing CO_2 from wastewater (Higuchi, 2012). Kuehnle's system produced *Chlorella* by piping CO_2 and wastewater from Chevron's Hawaii refinery into tubular photobioreactors to accelerate algae growth. The algae were then converted into biofuel, which was used to reduce the refinery's greenhouse gas emissions. In November 2011, the project was the first successful algae production process using industrial CO_2 from an oil refinery.

As discussed previously, microalgae can also be used to fix CO_2 from flue gas by directing waste emissions into photobioreactors and the biomass generated can be harvested for biofuel production. In Israel, flue gas from a coal-fired power station was directed to a series of open algae ponds to produce dry algae biomass for biofuels (Ben-Amotz, 2008). The 1000 m^2 pilot project cultivated *Nannochloropsis sp*, and it had a maximum algae biomass yield of 25 kg/day.

The most successful application of microalgae to produce high-value compounds in a commercial scale has been the production of astaxanthin by Cyanotech using *Haematococcus* microalgae. This health supplement has been cultivated in shallow ponds installed with a paddlewheel to provide circulation i.e. raceway ponds (Guerin et al., 2003). The 40 hectare raceway ponds are located in Hawaii, where the low rainfall and year-round sunlight are most suitable for microalgae.

The commercial exploitation of non-transgenic microalgae as a nutritional supplement is well-developed. Other high-value products such as food additives, pigments, enzymes and anti-oxidants derived from algae exist but are extremely limited in the market. Polyhydroxyalkanoate (PHA), a biodegradable polyester produced by diatoms, is being commercialized for the plastics industry (Loo & Sudesh, 2007). The versatility of microalgae is advantageous across many applications. More examples of current algae-related applications are listed in Table 2.

Table 2: A selection of microalgal species and their products and application areas (Pulz & Gross, 2004)

Species/group	Product	Application areas	Basins/reactors
Spirulina platensis/Cyanobacteria	Phycocyanin, biomass	Health food, cosmetics	Open ponds, natural lakes
Chlorella vulgaris/Chlorophyta	Biomass	Health food, food supplement, feed surrogates	Open ponds, basins, glass-tube PBR
Dunaliella salina/Chlorophyta	Carotenoids, β-carotene	Health food, food supplement, feed	Open ponds, lagoons
Haematococcus pluvialis/Chlorophyta	Carotenoids, astaxanthin	Health food, pharmaceuticals, feed additives	Open ponds, PBR
Odontella aurita/Bacillariophyta	Fatty acids	Pharmaceuticals, cosmetics, baby food	Open ponds
Porphyridium cruentum/Rhodophyta	Polysaccharides	Pharmaceuticals, cosmetics, nutrition	Tubular PBR
Isochrysis galbana/Chlorophyta	Fatty acids	Animal nutrition	Open ponds
Phaedactylum tricornutum/Bacillariohyta	Lipids, fatty acids	Nutrition, fuel production	Open ponds, basins

1.2.3 Economics of microalgae cultivation

In the current market, the use of algae to mitigate CO_2 with biofuel production as the sole income stream is not economically feasible due to competitive crude oil prices of $93/barrel (as of January 2013). As a comparison, algal biofuels have been estimated to cost $240/barrel (includes CO_2 mitigation credits) (Lundquist et al, 2010). The biggest economic hurdle in commercialization of a closed microalgae cultivation system is the high capital cost (Alabi et al., 2009). Benemann (1997) reported costs of over $100/tonne for PBRs in Spain, Germany and Israel, as opposed to costs of around $10/tonne for open ponds. In PBRs, gas and liquid handling systems will be present, with spargers, valves and pumps. Biomass yields determine the frequency of harvesting and extraction.

Many microalgal strains can be grown in defined media for the purpose of maintaining high growth rates and the purity of cultures (Andersen, 2005). Some strains such as *Dunaliella* flourish in undefined media like wastewater, which is a cheap source of inorganic nutrients. However, restrictions may apply in a PBR because pre-treatment may be necessary to sterilize wastewater and meet other downstream process conditions. Medium costs are strain-dependent. Carbon can be supplied by industrial-grade CO_2 in PBRs or flue gas for any production scale. But other gases (sulphur oxides, nitrogen oxides, oxygen, etc.) must be considered as they have significant negative effects on the growth rate (Doucha et al., 2005). SO_2 can lower the pH to 4 if the concentration reaches 400 ppm, but this is commonly mitigated by adding NaOH (Oilgae, 2009). Nitrogen oxides can also affect the pH of the medium but to a lesser degree. Soot dust and heavy metals were found to have very little impact on algae growth.

Separation of biomass from the product stream in PBRs costs less than in open ponds due to higher biomass densities. Harvesting costs come from the electricity used for centrifugation and can make up 20-30% of the total cost of algal biomass (Molina et al., 2003).

Energy is also required for agitation of medium, delivery of gas, illumination, and heating. In some cases, cooling might be necessary for warmer climates. Over time, cells may adhere to the surface of the PBR, so this requires periodic cleaning and shutdown. Replacement of culture is also mandatory to maintain high optimal yields (Andersen, 2005). Other costs include production

of inoculum, and algae subculturing. It appears that, at the current economic state, production of high-value products is most profitable amongst all microalgae applications.

1.3 Microalgae as a platform for production of high value bioproducts

Select strains of microalgae can naturally produce high-value compounds; they can produce complex molecules which are otherwise difficult to produce by chemical synthesis (Borowitzka, 1995). These include antibodies (Schillberg et al., 2003), polysaccharides (Walker et al., 2005), and carotenoids (Pulz & Gross, 2004). They are an important source of chemical products that are applied in the feed, food, nutrition, and pharmaceutical industries.

What makes microalgae even more attractive in addition to their ability to capture CO_2 is that they can be genetically modified to produce recombinant products that have important value in the chemical and pharmaceutical applications. This opens up the possibility of producing a greater variety of valuable molecules that was not technologically feasible before. In the past three decades there has been significant focus on selection of algae strains for pharmacologically-active compounds. These microorganisms are now being looked upon as genetically-modified hosts for production of biopharmaceuticals, polymers, vaccines, enzymes, and antibodies.

Perhaps most importantly, algae are now recognized for their potential to reduce material costs compared to conventional biochemical production plants, and for the potential for scale-up. The desirable solution to carbon capture is to combine the benefits of carbon fixation in algae with the production of high-value compounds.

1.3.1 Advantages of microalgal protein production

Microalgae strains are generally simpler to cultivate commercially compared to macroalgae. High-value products are defined as any product when multiplied by its fraction in biomass has a value of over US$ 10/kg (Carlsson et al., 2007). In the algae commercialization industry, the products classified under this definition have been limited because most have been in the early stages of development. Producing therapeutic proteins in microalgae has many economic and qualitative benefits, such as reduced health risks from pathogen contamination and relatively high yields. Furthermore, existing infrastructure in production facilities can be used to cultivate, harvest, store, and process transgenic organisms and require relatively little capital investment. It

has been estimated that the cost of producing recombinant proteins in algae could be 10- to 50-fold lower than producing the same protein by *E. coli* fermentation, depending on the host transgenic plant or microalga (Kusnadi et al., 1997). Microalgae-derived products were estimated to have a global market value of US$ 5-6.5 billion in 2004 (Carlsson et al., 2007). US$ 1.25-2.5 billion were generated by the health food sector, US$ 1.5 billion from the production of docosahexanoic acid (DHA) and US$ 700 million from aquaculture. The United States is responsible for 50% of the global algae production. Algae production potential is greatest in regions where there is an abundance of land, water and sunlight; however, regions with these resources must also have the infrastructure to develop these production systems, limiting the number of locations suitable for cultivation. Although in its infancy, the use of transgenic microalgal systems as bioreactors for production of therapeutic and industrial organic compounds is promising. It is advantageous to use unicellular algae compared to higher plants as they have faster growth rates and can be grown at high densities in controlled reactors. A comparison of the various bioreactor systems currently available are listed in Table 3.

Table 3: Comparison of features of recombinant protein production from various bioreactor systems (Walker et al., 2005)

Features	**Bacteria**	**Yeast**	**Mammalian cell culture**	**Transgenic plants**	**Transgenic microalgae**
Production time	Short	Medium	Long	Long	Short
Production cost	Medium	Medium	High	Low	Very low
Reactor scale	Large	Large	Medium	Small	Small
Scale up cost	High	High	High	Low	Very low
Cost	Cheap	Cheap	Expensive	Cheap	Cheap
Production scale	Limited	Limited	Limited	Worldwide	Worldwide
Propagation	Easy	Easy	Hard	Easy	Very easy
Distribution	Feasible	Feasible	Difficult	Easy	Easy
Delivery vehicle	No	No	No	Possible	Possible
Gene size	Unknown	Unknown	Limited	Not limited	Not limited
Glycosylation	Absent	Incorrect	Correct	Correct	Correct
Protein yield	Medium	High	Medium-high	High	Unknown
Risk	Yes	Unknown	Yes	Unknown	Unknown
Safety to human	Low	Unknown	Medium	Medium	High

Theoretically, recombinant microalgae can potentially produce proteins at a fraction of the cost of conventional cell culture systems and higher plants. Production of algal biomass is estimated to cost $3/kg at commercial scale (Chisti, 2007). Approximately 25% of biomass is soluble protein, so if recombinant protein makes up 2% of soluble protein, facilities can presently produce recombinant protein at about $600/kg prior to purification. This is close to cost estimates for the least expensive protein expression systems in the current market (Rasala et al., 2010). Plant-based proteins are less likely to be contaminated with pathogens than those derived from animal cells because plants are not susceptible to human pathogens (Specht et al., 2010). Microalgae cells can also fold complex human proteins that bacteria and yeast may not fold well.

1.3.2 Potential applications of genetically-modified microalgae

There have been a few recent developments in the establishment of genetically-modified microalgae for production of high-value products. The most notable breakthrough for expression of human genes is the unicellular algae *Chlamydomonas reinhardtii.* It has been widely used in biology laboratories because its genome has been sequenced and has been cultured for many years. It is able to grow photosynthetically and heterotrophically, and can be cultured at a scale of up to 500,000 litres. From a genetic engineering perspective, the DNA of its chloroplasts, nucleus and other organelles can be easily altered. In studies by Tran (2012), *C. reinhardtii* was successfully modified to produce mammalian serum amyloid protein in 2007 and human antibody in 2010. In the most recent advancement, a malarial vaccine was developed (Dauvillée & Delhaye, 2010). These achievements open up the opportunity to make complex drugs economically and in larger quantities. More examples of potential products are listed in Table 4.

Table 4: Potential applications of genetically modified microalgae (Enzing & Nooijen, 2012)

Species/group	Product	Application areas	Reactor
Cyanobacteria	Antimicrobials, antivirals, antifungals	Pharmaceuticals	PBR
Spirulina, Ulva conblogbata	Neuroprotective agents	Pharmaceuticals	PBR
Chlamydomonas reinhardtii	Human therapeutic proteins	Pharmaceuticals	PBR
Nostoc Cyanobionts	Anti-cancer drugs	Pharmaceuticals	PBR

1.3.3 Challenges of using genetically modified algae

Programs for genetic modification of algae strains have lagged compared to research efforts for plants and microbes. Few companies have had algal-based products reach or approach the stage of regulatory approval. Because of the uncertainty of the regulatory process involving novel technology, there is an inherent high risk that slows down the product development stage. Every compound goes through vigorous screening, testing, and approval stages before it reaches the market. Statistically, in the pharmaceutical industry, about 3 compounds out of 1000 make it past the first round of clinical trials and only one would be commercialised (Watkins, 2002). For example, Mera Pharmaceuticals submitted an application to begin large-scale production of modified alga *C. reinhardtii*, which produced human immunoglobulin-A protein and other pharmaceuticals (Dunwell & Ford, 2005). However, because of a lack of experience with engineered algae, a turn of events led to a judicial decision requiring an environmental assessment before pilot trials could be conducted. These trials have never taken place. There have also been increasing concerns of the modified algae being released into the environment, which can threaten native organisms. Secondly, the highly scrutinized stages of drug development can take 12 to 15 years, which is attributed to the long discovery stage and preclinical testing, trials involving thousands of patients, and the FDA review. Thirdly, the cost of developing a new drug using conventional methods is estimated to be US $800 million to $1.7 billion. Both the cost of development and FDA approval time have been rising over the past years, indicating the challenge of having genetically-modified algae within the purview of biotechnology firms.

1.4 Synechococcus elongatus PCC 7942

Cyanobacterium *S. elongatus* PCC 7942 was chosen as the species for this research because it has been extensively studied by the international research community, most notably its acclimation to nutrient stresses and adaptation to variations in temperature and light intensity (Joint Genome Institute, 2013). This photoautotrophic organism is found in freshwater habitats. Like land-based plants, it is photosynthetic, meaning that it can convert light energy into useful chemical energy using a complex biological process. It grows best in BG-11 nutrient composition (I. S. Suh et al., 1998). In addition to physiological features, the genetic code of S. *elongatus* has been established and makes it an effective host for molecular genetics techniques

(Kajiwara et al., 1997). Numerous studies have been conducted on exogenous protein expression of this strain, as listed in Table 5 (Yamada et al., 1997).

Table 5: Previous studies of exogenous protein expression in *S. elongatus* PCC 7942

Exogenous protein	Source
Carbonic anhydrase	Human
β-galactosidase	*Escherichia coli*
Manganese superoxide dismutase	*Escherichia coli*
*lac*IQ repressor protein	*Escherichia coli*
α-amylase	*Bacillus amyloliquefaciens* A50
Entomocidal toxin	*Bacillus shaericus* 1593M
cI^{ts} repressor protein	Bacteriophage lambda
Fatty acid desaturase (*des*A)	*Synechocystis* PCC6803
Plastocyanin	*Anabaena* PCC7937
Phytoene desaturase	*Erwinia uredovora*
Ethylene-forming enzyme	*Pseudomonas syringae*

1.5 Closed photobioreactor design

Closed PBRs are ideal for the production of primary and secondary metabolites because they provide greater control of cell growth and metabolite production (I. S. Suh & Lee, 2001). Because closed PBRs are significantly smaller in size, it is necessary to maximize both productivity and photosynthetic efficiency. Various reactor configurations have been developed to address these factors. The three most common configurations of closed PBRs are tubular reactors, airlift reactors and bubble columns. A common feature among all closed photobioreactors is the high surface area to volume ratio for the purpose of increasing light exposure and biomass yields. Airlift reactors (Figure 4) are appealing because they require only a simple construction and can achieve circulation without moving parts (Chisti & Moo-Young, 1993). Gas-induced circulation of liquid is a key aspect of reactor design because it controls important parameters such as gas-liquid mass transfer, heat transfer and mixing. This setup also offers better O_2/CO_2 gas exchange compared to other configurations (I. S. Suh & Lee, 2001). Aeration rates must be chosen to balance a variety of factors. It has been shown that mixing of algal cultures has multiple effects on cell growth, namely shear forces on cell membranes and light penetration (Mirón et al., 2000). As liquid circulation increases, cells are exposed to greater

mechanical forces from bubbles and reactor surfaces, causing cell lysis and foaming. Mixing also controls mass transfer of nutrients, and removal of potential harmful metabolites.

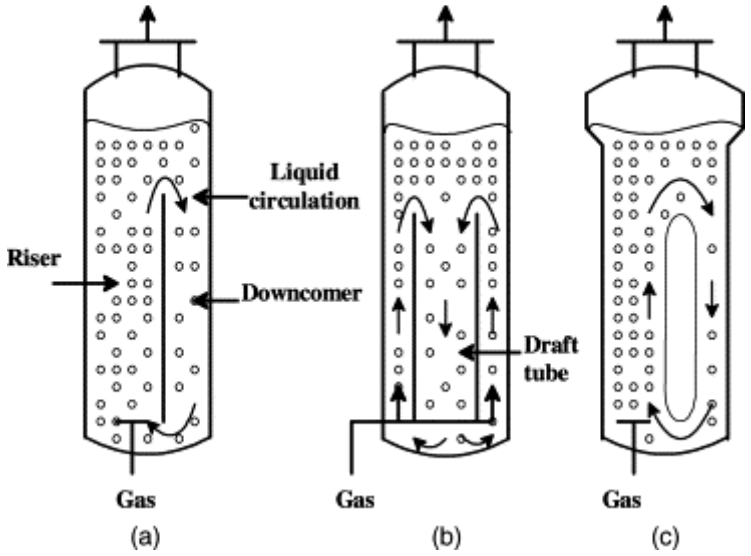

Figure 4: Airlift reactors (a) split-cylinder internal loop; (b) draft tube internal loop; (c) external loop (Kilonzo & Margaritis, 2004)

At the same time, aeration rates cannot drop below a certain lower limit to ensure a well-mixed culture. Efficient mass transfer of CO_2 is essential. Although aeration rate has an important influence on cell productivity, further consideration must be made on culture depth because bubbles can also affect light penetration (Mirón et al., 1999). The presence of bubbles reduces internal irradiance because they can refract and reflect some light away from the reactor. Kobayashi has shown using *Chlorella* sp. cultures that growth rate and biomass concentration decreased with increasing diameter of vertical tubes over the range 0.016-0.050 m (Kobayashi & Fujita, 1997). At a certain depth, the light intensity fell to growth-limiting levels and a dark zone was encountered. This depth was dependent on reactor geometry, light source and intensity, biomass concentration, and other factors.

A flat-plate photobioreactor, comprising of transparent flat panels and a relatively high surface area to volume ratio, has been developed to allow for more light energy available for cells (Sierra et al., 2008). This reduces the effects of shading within the reactor. However, exposure of cells to excess light will result in photoinhibition (Krupa et al., 1991). Studies of PBRs are thorough and advanced; however, there is a lack of research in the optimization of growth of certain microalgal species in PBRs, including the freshwater cyanobacterium *S. elongatus* PCC 7942. Due to these

advantages, experimental work in this study was conducted with a flat-plate airlift photobioreactor.

1.5.1 Design of airlift reactors

Airlift reactors have no focal points of energy dissipation and shear distribution is homogeneous throughout (Merchuk & Gluz, 2002). A typical flat-plate airlift photobioreactor is shown in Figure 5. The riser is located above the sparger, where gas bubbles are introduced into the liquid phase. Circulation of the liquid is mainly driven by the density gradient between the riser and downcomer (Chisti & Moo-Young, 1993). The riser is sparged with gas, lowering the bulk density in this section. The downcomer is almost completely free of bubbles so the bulk density there is relatively higher. This induces a liquid circulation rate that is dependent on the geometry of the reactor, gas flow rate, and liquid and gas physical properties. It is a major characteristic of airlift reactors because this controls the circulation time, mixing, and mass transfer. The gas-liquid separation chamber is designed such that most bubbles from the riser are released from the liquid, leaving the downcomer with a negligible amount of bubbles. The gas entrainment chamber allows for bubbles to escape because expansion of the cross-sectional area reduces the liquid velocity at the entrance of the downcomer, giving more time for the bubbles to rise. To ensure that cultures are always well-mixed, a sufficient aeration rate should be utilized. Conversely, high aeration rates are not recommended because this would introduce unnecessary shear forces and larger bubbles that can decrease internal light intensities.

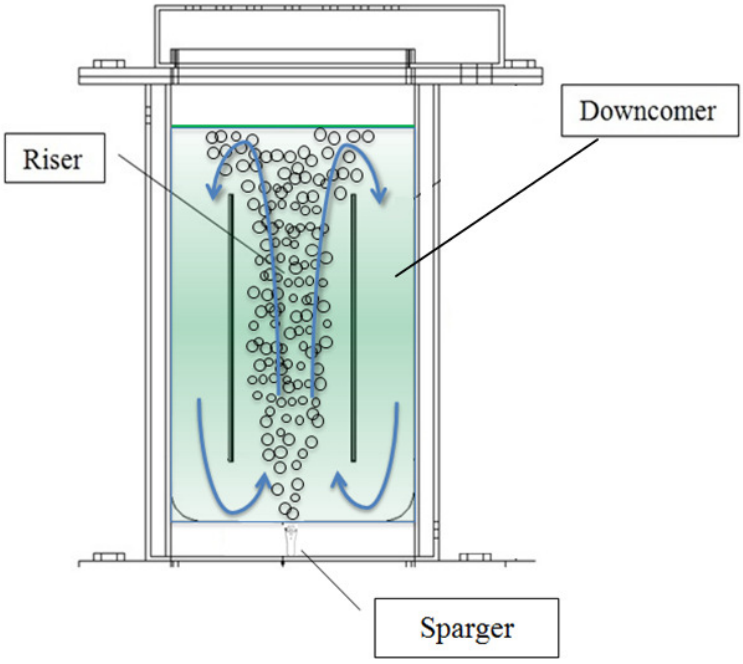

Figure 5: Flat-plate airlift photobioreactor

The key hydrodynamic parameters in a reactor are gas hold-up, liquid circulation velocity and the mixing time. For airlift reactors, gas hold-up is calculated using the following equation:

$$\varepsilon_R = \frac{V_{DR} - V_R}{V_{DR}} \quad (1)$$

where V_{DR} is the dispersed riser volume and V_R is the ungassed riser volume plus the gas entrainment volume. A useful characterization of flow pattern in a reactor is the mixing time, which can be quantitatively measured. Mixing time is the time required to reach the desired degree of homogeneity (for example 95%) after tracer injection. Axial mixing in loop reactors is commonly characterized by the Bodenstein number *Bo,* which is the ratio between the mixing effects of the axial dispersion coefficient and bulk movement of medium (Onken & Träger, 1990):

$$Bo = \frac{w_L \cdot L}{D_{ax}} \quad (2)$$

Where w_L is liquid velocity, L is length of flow path, D_{ax} is effective axial dispersion coefficient. A reactor is considered well mixed when $Bo<0.1$ and acting as plug flow at $Bo>20$ (Mirón et al., 2000).

1.6 Optimizing growth of microalgae

1.6.1 Overview of media for microalgae

Media are important because they provide the nutrients for microorganisms' metabolism and growth. They are generally composed of three components: macronutrients, trace elements, and vitamins. Macronutrients like nitrogen and phosphorous provide the nutrients essential for growth of all algae (Oilgae, 2009). However, trace elements can vary with different algae strains. Each trace element has an important function; for example, iron is required for electron transfer, and magnesium is needed for chlorophyll production. Lack of sufficient trace metals will limit the magnitude of growth. Each nutrient is usually prepared as a stock solution. Stock solutions are useful because they provide convenience and consistency; repeated individual weighing of chemicals would otherwise be time-consuming and prone to error. Microalgae are commonly grown in chemically defined media to ensure a pure and consistent cell culture environment. Undefined media contain complex ingredients and a mixture of numerous components in unknown concentrations. Undefined media are suitable for applications that require growing greater variety of microalgae or for economical reasons.

1.6.2 Medium and pH buffer selection

Some medium recipes like BG-11 (Table 6) are formulated for multiple freshwater algae species; others are derived from detailed studies of a particular organism. For the purpose of optimizing the specific growth rate for a chosen species, it is necessary to establish specific nutrient requirements. BG-11 medium has shown to be successful in supporting growth of *S. elongatus*, thus this was chosen as the base case medium for the optimization experiments.

Table 6: BG-11 composition

Component	mM
$NaNO_3$	17.6
K_2HPO_4	0.22
$MgSO_4 \cdot 7H_2O$	0.03
$CaCl_2 \cdot 2H_2O$	0.2
$C_6H_8O_7 \cdot H_2O$	0.03
$C_6H_{11}FeNO_7$	0.02
$Na_2EDTA \cdot 2H_2O$	0.002
Na_2CO_3	0.18
Trace metals	

Each component in the medium plays an important role in sustaining cell growth. $NaNO_3$ serves as the main source of nitrogen, which is converted by the bacteria to produce organic compounds like amino acids (Srivastava et al., 2013). The phosphorus in K_2HPO_4 is involved in a variety of physiochemical reactions and is important for the metabolism of cells. $MgSO_4$ provides sulphur, which is also an essential nutrient that is found in amino acids, peptides, vitamins, and secondary metabolites (Jain et al., 2006). It is also the magnesium source that induces chlorophyll production. $CaCl_2$ plays an important role in regulating osmotic pressures in cells (Srivastava et al., 2013). $C_6H_8O_7$ is a central part of the citric acid cycle, which is a series of chemical reactions used to generate energy (Siegesmund, 2011). $C_6H_{11}FeNO_7$ provides the iron required for photosynthetic apparatus (Shcolnick et al., 2009). Na_2EDTA is a chelating agent that removes harmful heavy metal ions (De Philippis et al., 2011). Na_2CO_3 provides an additional source of inorganic carbon (Schwarz et al., 2011) and adds a buffering capacity to the medium. Trace metals act as cofactors for enzymatic reactions in the cell (Todar, 2012). The pH of the medium is also buffered to prevent any abrupt changes in pH that may potentially hinder cell growth.

1.6.3 Effects of temperature on growth

In general, algae growth rates increase with rising temperatures until an optimum temperature is reached, after which growth declines. For every microalgal species, temperature greatly influences cellular chemical composition, uptake of nutrients, and carbon dioxide fixation. In most research involving *S. elongatus* PCC 7942, the subcultures of the strain were cultivated at a constant temperature of 30°C (Kajiwara et al., 1997). The effect of temperature on the rates of biological processes is well understood; however, each species responds differently to these changes (Konopka & Brock, 1978). For example, *Microcystis* isolates possess a thermal growth optimum between 28.8 and 30.5°C (Krüger & Eloff, 1978), while *Chlorella sorokiniana* has a thermal growth optimum at 35°C (Wageningen UR, 2011). In addition, there has been a lack of research focusing on the effects of temperature on the growth of *S. elongatus* PCC 7942. PBRs provide the ability to control temperature. Unlike outdoor reactors, fluctuations in ambient temperature will not affect the internal temperature of the PBR.

1.6.4 Gas-liquid mass transfer

Monitoring dissolved CO_2 concentrations and CO_2 transfer rates is a standard procedure in microalgae cultivation to ensure adequate delivery of CO_2 for algae. In this experiment, the on-

line dissolved CO_2 data were used to determine k_La, the volumetric mass-transfer coefficient for the CO_2-medium system.

CO_2 is supplied to the culture medium by sparging CO_2-enriched air through the medium. Thus, CO_2 enters the reactor in air bubbles of fairly narrow size distribution. Empirical data and theory suggest that the major resistance to CO_2 and O_2 transfer is the liquid film surrounding the gas bubbles (Doran, 2012). Rates of mass transfer are often described by the classic two-film theory, where the main resistance to mass transfer lies in the liquid film.

For the estimation of theoretical k_La values at conditions in which CO_2 concentrations are too small to be measured (ie. CO_2 in air), the Rand and Marshall equation (Eq. 3) is useful (Bird et al., 2007). Assuming forced convection around the gas bubbles during operation of the photobioreactor, the Sherwood (*Sh*) equation for a spherical bubble is:

$$Sh = 2 + 0.60Re^{1/2}Sc^{1/3} \quad (3)$$

where *Re* is the Reynolds number and *Sc* is the Schmidt number . *Re* is a dimensionless group that indicates the ratio of inertial and viscous forces in a fluid system (Eq. 4).

$$Re = \frac{\rho v d}{\mu} \quad (4)$$

where ρ is the density of the bulk liquid, v is the bubble velocity relative to the liquid, d is the diameter of the bubble and μ is the viscosity of the liquid.

Sc is another dimensionless group that indicates the ratio of viscosity and mass diffusivity (Eq. 5).

$$Sc = \frac{\mu}{\rho D_{CO2}} \quad (5)$$

where D_{CO2} is the diffusivity of CO_2 in the liquid phase. Equation 5 is valid for constant physical properties and small net mass transfer rates. k_La can then be estimated using Equation 6:

$$k_L = \frac{D}{L} Sh \quad (6)$$

where D is the diffusivity of CO_2 in water and L is the characteristic length. Similar equations can be used to determine k_La for oxygen (using D_{O2} instead of D_{CO2}).

Gas holdup is also important because it controls the residence time of gas in the liquid. In addition to bubble size, it controls the gas-liquid interfacial area available for mass transfer (Chisti & Moo-Young, 1988).

1.6.5 Effects of light intensity on growth

1.6.5.1 Photosynthesis

Photosynthesis is the biological process of using light energy to produce chemical energy and stored in the molecular bonds of organic molecules (e.g. sugars) (Lai et al., 2005). This process occurs in plants and photoautotrophic algae like cyanobacteria. In cyanobacteria (ie. blue-green algae), photosynthetic reactions take place in light-harvesting organelles called phycocyanin (Mazel et al., 1988). CO_2 is reduced to form carbohydrates, with water as an electron donor and O_2 as a waste product. The overall chemical reaction is:

$$nCO_2 + nH_2O \text{ (+ light energy)} \rightarrow (CH_2O)_n + nO_2 \qquad 7$$

The process of photosynthesis is dependent on the light intensity, which can also be expressed as the irradiance or the quantity of incident light on a surface. The unit for irradiance is μmol photons/m^2/s or μE/m^2/s (i.e. microeinsteins/m^2/s). Photosynthesis is a combination of two reactions: a light phase and a dark phase (Prezelin, 1981). Light phase reactions only occur when cells are exposed to light while dark phase reactions occur in the absence of light. The purpose of the light-dependent reactions is to convert available light energy into a form that can be used readily in metabolic processes. Energy of the sunlight is converted to a biochemical reductant $NADPH_2$ (nicotinamide-adenine dinucleotide phosphate) and a high energy compound ATP (adenosine triphosphate) (Masojidek et al., 2004). The dark phase reactions involve the utilization of the $NADPH_2$ and ATP molecules produced by the light dependent reactions. The mechanisms of carbon fixation, called the Calvin cycle, occur here. The basic process of photosynthesis is illustrated in Figure 6.

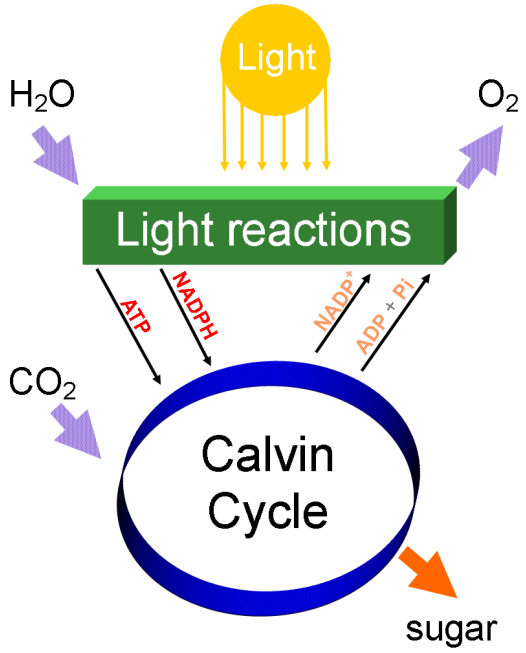

Figure 6: Photosynthesis (Mayer, 2008)

1.6.5.2 Light Distribution

Because light is the main source of energy for phototrophic algae, the distribution and intensity of light is one of the important factors for growth. Light attenuation is the main limitation in algae growth in cultivation systems due to decreases in light intensity and mutual shading (C. Lee, 1999). According to Lambert's Law of Absorption, light intensity decreases along the path length in the photobioreactor as illustrated in Figure 7:

$$I_{out} = I_{in} e^{-a_c C_{alg} l} \qquad 8$$

where I_{out} = light intensity exiting (μE/m^2/s)

I_{in} = light intensity at interface where light enters (μE/m^2/s)

a_c = spectral-averaged absorption coefficient (m^2/g)

C_{alg} = algae concentration (g/m^3)

l = path length (m)

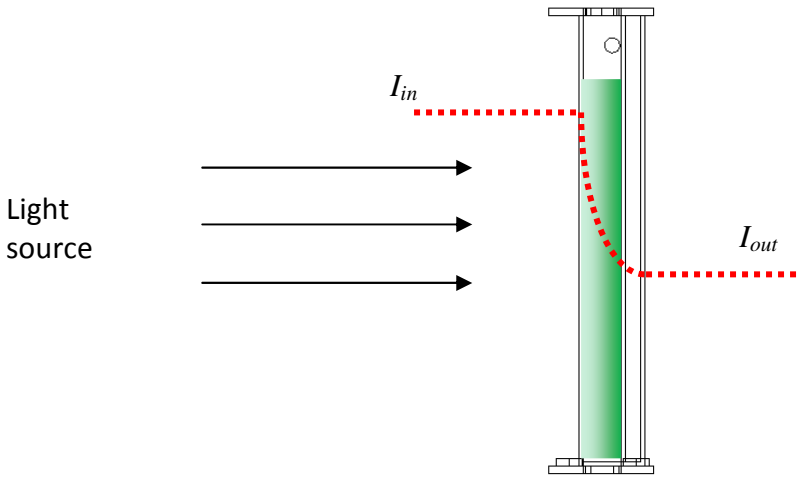

Figure 7: Light intensity changes with distance in absorbing medium

This law allows for determination of the light gradient inside the photobioreactor. Initially, the light strikes the reactor with constant intensity but past the surface, it is converted to photonic energy in algae cells. As a result, less light exits the reactor than entered. Integration of the above equation over the path length gives the average light intensity I_{av}.

$$I_{av} = \frac{I_{in}}{a_c C_{a\lg} l}\left[1 - \exp(-a_c C_{a\lg} l)\right] \qquad 9$$

At very low light intensities, the rate of photosynthesis is equal to the rate of respiration (compensation point), resulting in no cell growth. As the intensity increases, photosynthesis increases until it reaches a light saturation point, where growth rate is at a maximum (Krupa et al., 1991). Higher light intensities will lead to a reversible damage of the photosynthetic apparatus of algae and decrease the photosynthetic rate (Lönneborg et al., 1988). This phenomenon, called photoinhibition, can be also triggered by a combination of light and other environmental factors such as low temperatures or drought. This effect can be reversed if the algae cells are exposed to favourable growth conditions. It is essential to determine the light intensity in which *S. elongatus* reached the light saturation point and to operate as close as possible to it.

Algae cells absorb almost all the light projected on them but not all can be used for photosynthesis (N. Kim et al., 2002). At high cell densities, almost all light is absorbed by a thin top layer of cells, leaving the rest with less available light (self-shading) and decreases the

photosynthetic efficiency. Figure 8 shows that light intensity decreases as penetration depth or cell concentration increases (C. Lee, 1999). The growth rate of microalgae depends on the light energy available to the cells. In the early stage of growth, microalgal cells adjust to conditions and start to grow exponentially. The organisms reach a maximum growth rate, but at the same time, mutual shading effects become more apparent. On average, less light is available for each cell, so the specific growth rate starts to decline. The biomass concentration continues to increase but the growth rate begins to decrease. Graphically, the biomass concentration increases linearly with time. This linear growth phase in batch cultures is a common observation for microalgae during photoautotrophic growth.

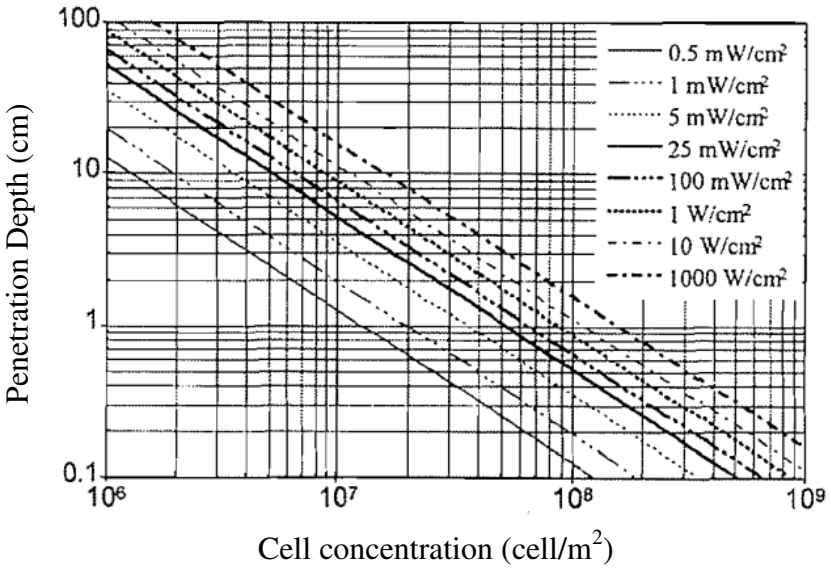

Figure 8: Light penetration depth of *Chlorella kessleri* as a function of light intensity (W/cm^2) and cell concentration (cell number/mL)

Minimizing the effect of mutual shading requires reducing the light path length of algae culture for a more homogeneous light distribution. This is facilitated by proper mixing to ensure that individual cells are not stationed entirely in the dark or light zones of the photobioreactor. The intensity of light is sometimes expressed as the average light irradiance per algal cell.

Since *S. elongatus* has a preferable absorption spectrum of 631-684 nm (Espinosa et al., 2007), light used for all experiments has been selected to provide energy within this spectrum. The best light source for this spectrum and application is a compact fluorescent light bulb (CFL) that provides 6500K color temperature. The color temperature of a light source is the temperature of

an ideal black body that radiates light identical to that of the light source (Wyszecki & Stiles, 1982). CFLs are cost effective, energy efficient and stable over the extended operating time (Geider & Osborne, 1992).

1.6.5.3 Light/dark cycles

The presence of light and dark cycles also has been suggested to have a beneficial effect on the growth of *S. elongatus*. Photosynthesis is comprised of light dependent and light independent reactions so it is preferable to utilize a light/dark pattern for optimal growth. Literature involving photobioreactors has suggested that mixing rates create an artificial light/dark effect (Phillips & Myers, 1954). Turbulence causes individual cells to move between the high intensity of the front surface and the low intensity of the back surface. Some studies have focused on the effect of different light/dark cycles (Jacob-Lopes et al., 2009). Jacob-Lopes' results indicated that duration of light periods was a significant factor in the performance of photobioreactors. Biomass production and CO_2 fixation was observed to decrease as the duration of the light period decreased, with the exception of 12:12 (light hours:dark hours) cycles. This can be explained by the circadian rhythm of microalgae, in which cells have adapted to grow best under 12:12, like natural sunlight patterns (Suzuki & Johnson, 2001). Specifically for *S. elongatus*, it is not known if culturing in photobioreactors with diurnal cycles will save energy and improves cell growth in comparison to continuous lighting. This is to be investigated.

1.6.6 Effects of O_2 and CO_2 on growth

Microalgae are naturally adapted to atmospheric oxygen so exposure to air during growth is not a concern (Pope, 1975). At atmospheric conditions, the solubility of oxygen in water (7 ppm at 35 ºC and 1 atm air) is extremely low. However, high levels of O_2 and CO_2 can inhibit growth. There were some known cases in which high concentrations of O_2 led to growth inhibition. For *Chlorella pyrenoidosa*, oxygen inhibition was only evident at 50% vvm O_2 or higher, resulting in a dissolved O_2 concentration of at least 15.7 ppm (Shelp & Canvin, 1980). Other microalgae respond differently at high O_2 concentrations; however, there have been no published data on the effects of oxygen inhibition for *S. elongatus* (Pope, 1975).

For *S. elongatus*, inhibition from CO_2 was observed at concentrations greater than 5% (Kajiwara et al., 1997). There was also evidence of growth inhibition at inlet CO_2 concentrations above

10% (Kajiwara et al., 1997). Due to the equilibrium reactions of CO_2 in water, carbonic acid is also produced (Poling et al., 2001).

$$CO_{2(l)} + H_2O_{(l)} \Leftrightarrow H_2CO_{3(l)} \quad 10$$

At equilibrium, only a small fraction (0.2-1%) of dissolved CO_2 is converted to H_2CO_3. Nevertheless, high inlet CO_2 concentrations will produce a greater concentration of H_2CO_3, causing pH to drop and adversely affect cell growth. For microalgae growth, CO_2 and HCO_3^- are the most important carbon sources. *S. elongatus* PCC 7942 has been shown to be capable of growing at over 0.9 g/L in culture aerated with CO_2-enriched air. Kajiwara determined growth characteristics of *S. elongatus* for CO_2 fixation by cultivating under various inlet CO_2 concentrations in a photobioreactor and comparing final biomass yields and growth rates to determine which conditions gave the best yields. His external loop airlift column achieved the highest specific growth rate of 0.048 h^{-1} at 5% CO_2. At higher CO_2 concentrations, the maximum biomass concentration and specific growth rate have been observed to be lower than 0.048 h^{-1}, signifying that elevated CO_2 concentrations above 5% CO_2 did not correlate to higher biomass productivities. In this case, excess CO_2 acidified the medium at levels that inhibited growth. Yet productivities grown with CO_2-enriched air were at least 30% higher than for culture grown with air. It is paramount to understand the effects of inlet CO_2 concentration and pH changes on growth to minimize the inhibitory effects while achieving high biomass productivity. Nonetheless, the findings suggested that *S. elongatus* is capable of growing at elevated CO_2 concentrations, paving the way for the application of industrial waste emissions as a carbon source.

1.6.7 Effects of agitation on growth

As discussed previously, at high algae concentrations, almost all the available light is absorbed by the top cell layer. Thus, mixing must be sufficient to maintain cell suspension and light homogeneity. Improper mixing could also lead to sedimentation, uneven thermal distribution, and inefficient gas exchange. Mixing also decreases the boundary layer surrounding each cell, promoting the uptake of nutrients and release of metabolic products. Sources have shown that both growth rate and maximum biomass concentration increased when the aeration rate increased, with CO_2 concentration constant at all times (Zhang et al., 2002; Q. Hu et al., 1996). Furthermore, it was concluded that if a gas containing a low CO_2 concentration was used, a high

critical k_La value would be required to meet the CO_2 requirement for algae growth. This indicated that there was room for optimizing the vertical airlift photobioreactor by varying the aeration rate.

1.7 Previous Research on Optimization of Growth of Microalgae

Studies on growth optimization of numerous microalgal species have been performed over the past few decades, but in most cases, high growth rates have been elusive. One study demonstrated that μ_{max} of *S. elongatus* decreased from 0.033 h^{-1} to 0.0290 h^{-1} as the light intensity increased by a factor of 16 in an external loop photobioreactor (Sasi, 2009). In terms of the growth response from varying the inlet CO_2 concentration, cultivation with air produced the lowest μ_{max} of 0.015 h^{-1}, while 5% CO_2 concentration resulted in the highest μ_{max} of 0.043 h^{-1}, but further increases in CO_2 concentration did not generate an increase in μ_{max}.

Information on the growth optimization of *S. elongatus* PCC 7942 has been limited but still provided useful data on the effects of growth by varying different conditions. For instance, Kajiwara performed batch cultivations of this strain in an external loop airlift reactor (Kajiwara et al., 1997). It was found that varying the gas flow rate from 0.2 L/min to 1 L/min did not affect growth when the inlet CO_2 concentration, light intensity and temperature were fixed at 5%, 73 $\mu E/m^2/s$ and 30°C, respectively. This indicated that mass transfer of dissolved CO_2 was not a limiting factor of cell growth at CO_2 concentrations of 5% or higher. In addition, for cultivations with the inlet CO_2 concentration ranging from 5% to 30%, the highest μ_{max} (0.044 h^{-1}) and X_{max} (0.88 g/L) was observed at 5%. This observation was similar to that of *Chlorella vulgaris* (Sasi, 2009). In the experiments where light intensity was varied between 41 $\mu E/m^2/s$ and 135 $\mu E/m^2/s$, μ_{max} and X_{max} increased as the light intensity increased. However, the responses decreased at light intensities above 108 $\mu E/m^2/s$, which implied the presence of photoinhibition. Most importantly, cultivations grown in CO_2-enriched air yielded greater specific growth rates and final cell mass concentrations, showing promise for applications centred on CO_2 fixation with algae.

1.8 Modelling microalgae growth

1.8.1 Cell growth models

In general, batch cultures of microorganisms experience 5 growth phases: lag phase, exponential phase, declining phase, stationary phase, and death phase (Figure 9). The duration of each phase

depends on the initial cell concentration, concentrations of the nutrients, pH, temperature, and other factors. During the lag phase, cells acclimatize to the medium. Cells synthesize new enzymes required for cell multiplication and there may be a small increase in cell mass but that is usually apparent near the end of the phase. Following the lag phase is the exponential growth phase. Cells adapt and multiply rapidly and a "balanced growth" is achieved: all components of the cell increase at the same rate. The growth rate is independent of concentrations of medium components as they are in excess; cell numbers increase exponentially with time. Past the end of this phase, the growth rate begins to decline but the biomass concentration continues to increase. At the stationary phase, medium nutrients are exhausted and the cells stop multiplying but existing cells continue to grow in size. Formation of inhibitory products like organic acids may also occur. Cells are still metabolically active, and can produce secondary metabolites. Eventually, cells enter the final phase, the death phase, where cells lyse and the number of living cells decreases.

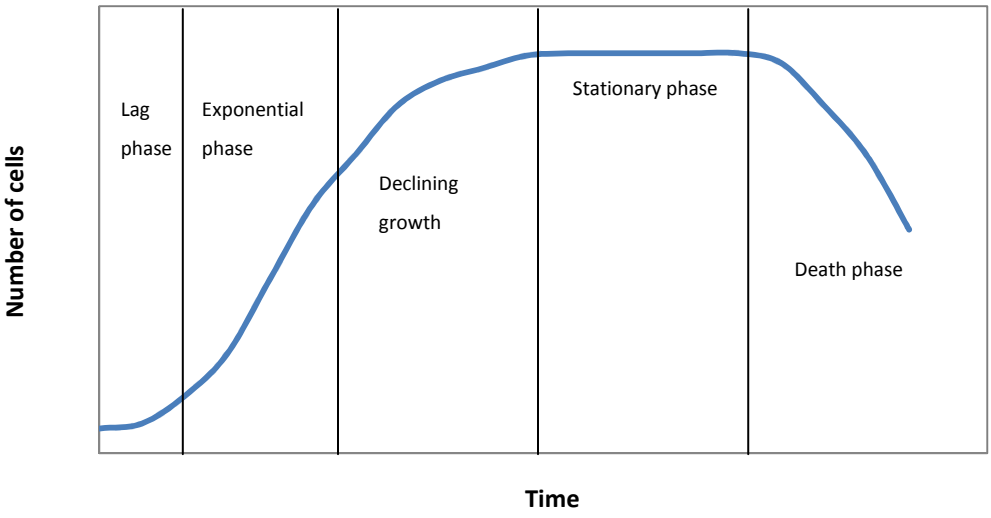

Figure 9: Typical growth curve for batch cultivation

Mathematical models have been developed, based on time dependent changes of the specific growth rate μ, for prediction of cell growth in batch cultures (Lin et al., 2000). The most commonly used expression is the classic Monod equation (Monod, 1949):

$$\mu = \frac{\mu_{\max} S}{K_S + S} \qquad 11$$

where μ_{max} is the maximum specific growth rate, S is the substrate concentration, and K_s is the saturation constant of the rate-limiting substrate when the specific rate of growth is half of the maximum. The specific growth rate is defined as the rate of increase in cell mass per unit time as measured in batch culture. Traditional growth models for batch and fed-batch cultures mostly involved unstructured kinetic models and variations of the Monod equation (Goudar et al., 2005). Unstructured kinetic models are impractical because they require a large number of parameters from a system of differential equations. For example, in the model introduced by Dhir specifically for mammalian cell growth in a fed-batch culture (Dhir et al., 2000), the rate of change of live cell concentration X was

$$\frac{dX}{dt} = \mu X \tag{12}$$

μ was a function of the concentration of four limiting substrates G, Q, L and A.

$$\mu = f(G, Q, L, A) \tag{13}$$

Equations 14-17 represented the rate of change of each substrate, with each equation involving several parameters.

$$\frac{dG}{dt} = f(G, X) \tag{14}$$

$$\frac{dQ}{dt} = f(Q, X) \tag{15}$$

$$\frac{dL}{dt} = f(L, Q, X) \tag{16}$$

$$\frac{dA}{dt} = f(A, Q, X) \tag{17}$$

Although Dhir's model adequately described experimental data, like other unstructured kinetic models, it was computationally not practical for modelling growth because it involved the non-linear estimation of a large number of parameters. Analytical solutions of these equations are not applicable because they assume that specific growth rates are constant. This is not the case in batch mode. For heterotrophic microorganisms, the growth rate decreases over time because the concentration of the limiting nutrient decreases during growth (Ernst, 2004). In bacteria like *E.*

coli, the limiting substrate is typically glucose under aerobic conditions. Thus one can simply plot the Monod growth model with glucose concentration as the substrate. However it is difficult to model *S. elongatus* growth with Monod because, as autotrophs, it produces its own intracellular substrate from extracellular components and this is difficult to quantify.

Another approach is polynomial fitting, which is useful over the whole duration of growth and the specific growth rates are simple to compute. However, cellular and product concentrations show exponential behaviour and are difficult to describe with polynomials. Polynomials are also especially sensitive to outliers, yielding unrealistic trends.

1.8.2 Logistic growth model

Logistic equations have adequately described bacterial growth curves. A logistic growth model, as introduced by Yang (Yang et al., 2011), was chosen to model microalgae growth:

$$\frac{dX}{dt} = \mu_{\max}\left(1 - \frac{X}{1 + X_{\max}}\right)X \qquad 18$$

Where μ_{max} is the maximum specific growth rate of the microalgae, X is the biomass concentration, and X_{max} is the maximum biomass concentration. The disadvantage of the model is that it does not apply for the declining phase; the model assumes that X approaches X_{max} as t increases. But since experiments were not typically run long enough to observe a declining phase, the model adequately described the first four growth phases which were the primary focus of this research.

2 Research Objectives

The objective of this project was to maximize the specific growth rate and biomass concentration of *S. elongatus* PCC 7942 cells in a 2D airlift photobioreactor and demonstrate the potential for production of high-value products using microalgae. A set of experiments was performed to complete this study. To evaluate whether microalgae is an ideal vehicle for production of value-added products, the following objectives were performed.

First, the effect of laboratory-scale shake flask conditions on the growth of *S. elongatus* was studied. The independent variables that were included in the study were medium composition, light intensity, and temperature. To gain an understanding of how the three variables affected the specific growth rate and biomass concentration, a logistic growth model was used. This was followed by the determination of optimized parameters which resulted in the highest specific growth rate and biomass concentration for the ranges investigated.

Next, to analyze the effects of CO_2 concentration and mixing on cell growth, studies were conducted in a 2D airlift photobioreactor, operating in a batch configuration and in axenic conditions. Similar to the methodology from the shake flask experiments, a logistic growth model was implemented with experimental data to investigate the effects of different variables on the specific growth rate and biomass concentration. Optimized conditions from the shake flask scale were applied to the airlift reactor studies. The independent variables of interest were inlet CO_2 concentration, aeration rate, and light intensity. Light/dark cycles were also investigated to see whether provision of regulated illumination intervals improved cell growth.

3 Materials and Methods

3.1 *Synechococcus elongatus* PCC 7942

Wild type *Synechococcus elongatus* PCC 7942 was selected as the representative microalgal strain for experimentation. It was isolated and provided by Dr. Francis Nano from the University of Victoria (UVic).

3.1.1 Subculturing of *S. elongatus* in BG-11 liquid medium

The method of conserving microalgal cultures was by continued maintenance under controlled conditions, which involved routine liquid media and agar media preparation using aseptic techniques. The purpose of using liquid media was to prepare inoculum for experiments. The purpose of using agar media was to preserve monoculture for future use, and these are typically kept for two months before they are replaced. Liquid media involved serial subculturing, in which inoculum from a late log phase culture was transferred to fresh, sterilized BG-11 medium. This organism was subcultured at 30°C under a continuous light intensity of 80 μE/m^2/s using Philips 6500k 60W compact fluorescent lamps. All experiments were conducted with the seed culture, taken during the exponential growth phase (approximately 96 hours from the inoculation time). To prepare a 100 mL flask of subculture, 10 mL of 96 hour-old culture is transferred to 90 mL of BG-11. This was cultured in 250 mL Erlenmeyer flasks and agitated at 120 rpm in a New Brunswick Innova® 42 shaking incubator (Figure 10).

Figure 10: Incubation of subcultures

3.1.2 Preparation of BG-11 liquid medium

To prepare BG-11 medium, stocks of each component were made first according to the recipe from the University of Texas (UTEX). Components in BG-11 medium are listed in Table 7 below (UTEX, 2009). Following this, $NaNO_3$, $MgSO_4 \cdot 7H_2O$, $CaCl_2 \cdot 2H_2O$, $C_6H_8O_7 \cdot H_2O$ (citric acid), $C_6H_{11}FeNO_7$ (ammonium ferric citrate), and $Na_2EDTA \cdot 2H_2O$ were mixed in deionized water and then autoclaved in a Midmark® M11 autoclave. The other components were not added into the solution until after the autoclave process to prevent precipitation of components. HEPES pH buffer was not used in the experiments to simplify the factorial design and to reduce the number of potential carbon sources.

Table 7: BG-11 medium stock solutions (UTEX, 2009)

Component	Quantity per litre of media	Final Concentration
$NaNO_3$	10 mL	17.6 mM
K_2HPO_4	10 mL	0.22 mM
$MgSO_4 \cdot 7H_2O$	10 mL	0.03 mM
$CaCl_2 \cdot 2H_2O$	10 mL	0.2 mM
$C_6H_8O_7 \cdot H_2O$	10 mL	0.03 mM
$C_6H_{11}FeNO_7$	10 mL	0.02 mM
$Na_2EDTA \cdot 2H_2O$	10 mL	0.002 mM
Na_2CO_3	10 mL	0.18 mM
BG-11 Trace Metals Solution	1 mL	(see recipe below)
Trace metals solution		
H_3BO_3	-	46 µM
$MnCl_2 \cdot 4H_2O$	-	9 µM
$ZnSO_4 \cdot 7H_2O$	-	0.77 µM
$Na_2MoO_4 \cdot 2H_2O$	-	1.6 µM
$CuSO_4 \cdot 5H_2O$	-	0.3 µM
$Co(NO_3)_2 \cdot 6H_2O$	-	0.17 µM

3.1.3 Preparation of BG-11 agar plates

To make BG-11 agar plates, agar medium was first made. The concentrations from Table 7 were added to distilled water for a total of 500 mL. In a separate container, 15g of agar were added to 500 of distilled water. After autoclaving both solutions, they were allowed to cool to 45-50°C. 3g $Na_2S_2O_3 \cdot 5H_2O$, which served as a source of sulphur, was added to the agar solution. Next, both agar and liquid solutions were mixed together and quickly poured into 30 Petri plates, which

were left to cool. To transfer microalgal colonies from agar, a wire loop was sterilized over a Bunsen burner flame and allowed to cool before use. Once cooled, the loop was used to transfer a colony of cells from one Petri plate to another and subsequently streaked across the plate into four quadrants, as shown in Figure 11. The time it took for cells to mature into colonies was about 2 weeks. To ensure that the subcultures used as inoculum contained only *S. elongatus* monoculture, 10 mL of BG-11 was inoculated with a single colony from the Petri plate. The colony was then allowed to mature into a culture growing in the exponential phase (96 hours after inoculation), and then used as seed culture for 100 mL medium.

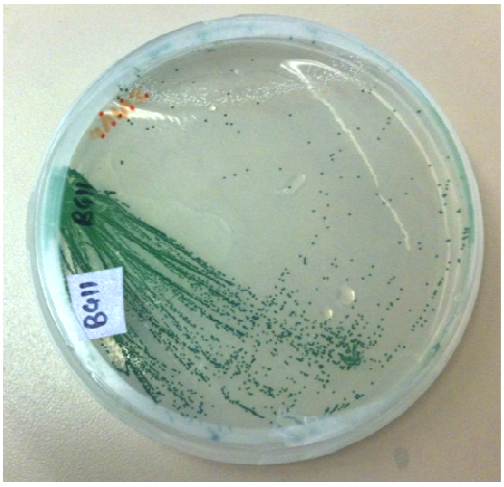

Figure 11: Petri dish of *S. elongatus*

3.1.4 Sterilization

To ensure that all working materials were not contaminated with foreign microorganisms, aseptic conditions had to be established. Sterilization was important in maintaining isolated strains of *S. elongatus* and keeping experiments free of potential unwanted variables. In the shake flask scale, two methods of sterilization were used: filter sterilization and autoclave sterilization. Autoclave sterilization was used to sterilize BG-11 medium, Erlenmeyer flasks and foam plugs, and all equipment that would contact with the medium. The medium and equipment were placed in the autoclave at a temperature of 121°C and 28 psia for 30 minutes. Filter sterilization was used to sterilize several BG-11 components that may precipitate under autoclave conditions. To filter sterilize, the mixture was passed through a 0.45 micron Millex-GP Filter. To sterilize the photobioreactor, the chamber was soaked in 0.6% sodium hypochlorite for 60 minutes at room temperature, followed by thorough rinsing in sterile deionised water in a sterile environment.

The sodium hypochlorite solution was made by diluting 15 mL household bleach (containing 5% hypochlorite) in 1.25 L water.

3.2 Measurement of biomass concentration

A reliable way of tracking cell growth is by measuring biomass concentration using a spectrophotometer. To determine the cell concentration, the optical density (OD) was measured at 600 nm using a Shimazu spectrophotometer. Before any estimation of biomass concentrations can be made, a calibration curve between the OD and dry cell weight was constructed (Figure 12). To determine the biomass concentration for a specific OD, a 2 mL sample was taken from a growth flask of 100 mL volume during a late exponential phase. Five 1:2 serial dilutions were made from this sample and the ODs were recorded. The volume of the remaining culture (98 mL) was recorded, then placed in an oven and dried overnight at 90°C (Yun et al., 1997). Following overnight drying, the sample was moved to a desiccator where it could cool without absorbing moisture. After 1 hour of cooling, a dry weight measurement was recorded. Dividing this by the recorded volume gave the biomass concentration of the original sample. The biomass concentrations of other dilutions were calculated. Sampling was performed in duplicate.

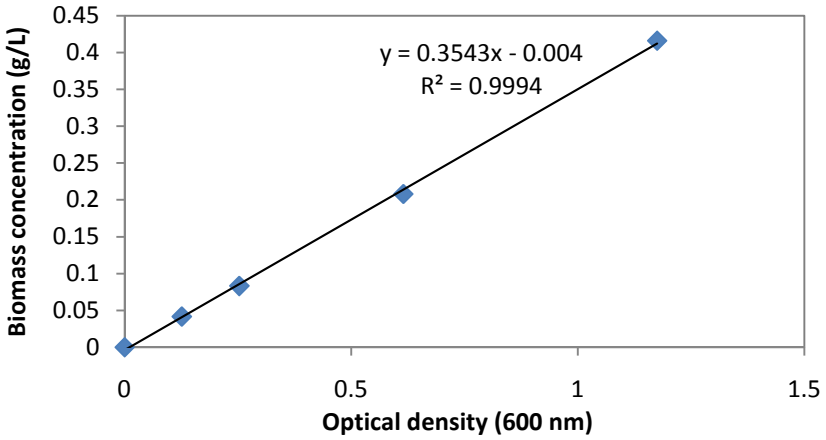

Figure 12: Determined relationship between dry cell concentration and optical density

The biomass concentration was calculated using the following equation:

$$X = 0.3542A - 0.004 \qquad 19$$

where X is biomass concentration (g/L) and A is optical density. The biomass concentration of all subsequent samples was measured by the optical density based on this relationship.

3.3 Logistic growth model and carbon uptake rate

After integration of Eq. 18, the experimental data were fitted by non-linear least squares using multiple sets of data to the following model equation:

$$X = \frac{X_o X_{\max} e^{\mu_{\max} t}}{X_{\max} - X_o + X_o e^{\mu_{\max} t}} \qquad 20$$

where X_o is the initial biomass concentration. In Figure 13, the continuous line represented a logistic fit of growth from experimental data. μ_{max} was determined by the solver function in Microsoft Excel. All other parameters can be directly retrieved from experimental data.

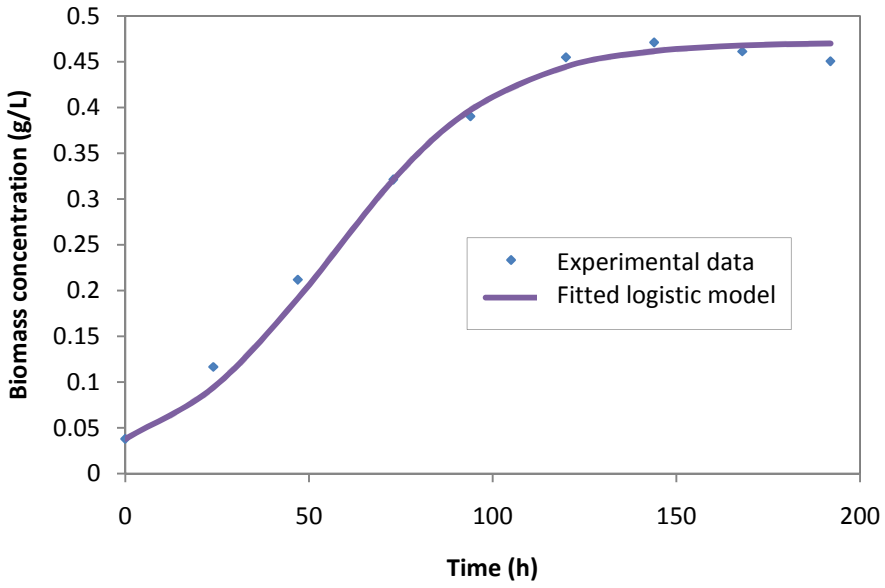

Figure 13: Example of a logistic growth curve

Carbon uptake rates (CUR) are calculated indirectly from the biomass concentration, assuming that CO_2 is converted into organic carbon via photosynthesis. Since *S. elongatus* PCC 7942 metabolized only CO_2 as a carbon source, the amount of CO_2 consumed was estimated directly from cell mass. Results from an elemental analysis of *S. elongatus* done by Kajiwara showed that

the cells comprised of 46.5% carbon. This led to an equation for calculating the CUR (Kajiwara et al., 1997).

$$CUR(g/L/h) = \frac{dX}{dt} \cdot 0.465 \cdot \frac{44}{12} \quad (21)$$

where *dX/dt* is the biomass growth rate, 44 is the molecular weight of CO_2, and 12 is the molecular weight of carbon. Elemental analysis showed that the 0.465 g of carbon per gram of dry cell mass (Kajiwara et al., 1997). It was observed to be constant among all growth phases.

3.3 Optimization of medium composition

Growth media are an important determinant of cell growth and composition because they provide the nutrients for metabolism and growth. Some of the medium recipes like BG-11 are formulated for many freshwater algae species; others are derived from detailed studies of a particular organism. For the purpose of optimizing growth for a chosen species, it is necessary to establish specific nutrient requirements.

3.3.1 Defining conditions for screening medium composition

A screening design was used to find components of BG-11 medium that had significant effects on μ_{max} and X_{max}. A full factorial experimental design was carried out for 5 components: ammonium ferrous citrate, $NaNO_3$, $CaCl_2$, K_2HPO_4, and Na_2CO_3. The concentrations used in the experimental design are outlined in Table 8. The other components that made up BG-11 were also present in the medium, and they had the same concentrations as listed in Table 7. Each run was carried out in 250 mL shake flasks, incubated at 30°C and at 120 rpm in a shaker. Four fluorescent lamps were mounted at the top of the shakers to provide an average incident light intensity of 80 $\mu E/m^2/s$.

Table 8: Experimental design for screening of medium components

Parameter	Concentrations (mM)
$C_6H_{11}FeNO_7$	0, 0.02
$NaNO_3$	0, 17.6
$CaCl_2$	0, 0.2
K_2HPO_4	0, 0.22
Na_2CO_3	0, 0.18

3.3.2 Defining conditions for optimization of medium composition

Following the screening experiments, a central composite experimental design was used to study the effects of the concentration of each BG-11 component on μ_{max} and X_{max}. Table 9 outlines the concentrations of each component used in the design. Analysis of growth in flasks was conducted in a randomized order. Temperature, light intensity, and agitation rate were identical to those used in the screening experiments.

Table 9: Central composite design for optimization of BG-11 medium components

Component	Concentration (mM)				
$NaNO_3$	4.4	8.8	17.6	35.2	70.4
K_2HPO_4	0.055	0.11	0.22	0.44	0.88
$CaCl_2$	0.05	0.1	0.2	0.4	0.8
$C_6H_{11}FeNO_7$	0.005	0.01	0.02	0.04	0.08
Na_2CO_3	0.045	0.09	0.18	0.36	0.72

3.4 Experimental setup of photobioreactor

Large scale work was carried out in a 2D photobioreactor. The photobioreactor setup is illustrated in Figure 14. The photobioreactor was connected to a CO_2 cylinder (supplied by Praxair) and a building-compressed air nozzle. Gas from the CO_2 cylinder was regulated by two flowmeters; one to handle flow rates less than 150 mL/min and the other for higher flow rates. A manual switch valve allowed for gas to be directed to either flowmeter. Between the flowmeter setup and the reactor was a pressure relief valve set at 5 psig to prevent pressure build-up. A 0.45 μm filter was also placed on the gas line to remove foreign microorganisms and therefore minimize the risk of contamination. An outlet gas port at the top flange of the reactor allowed for exhaust gases to be directed back to the fume hood. The photobioreactor was equipped with a dissolved CO_2 electrode (VL-PC), an oxygen electrode (VWR), and one sampling port. Another port was also built in to the top flange if needed.

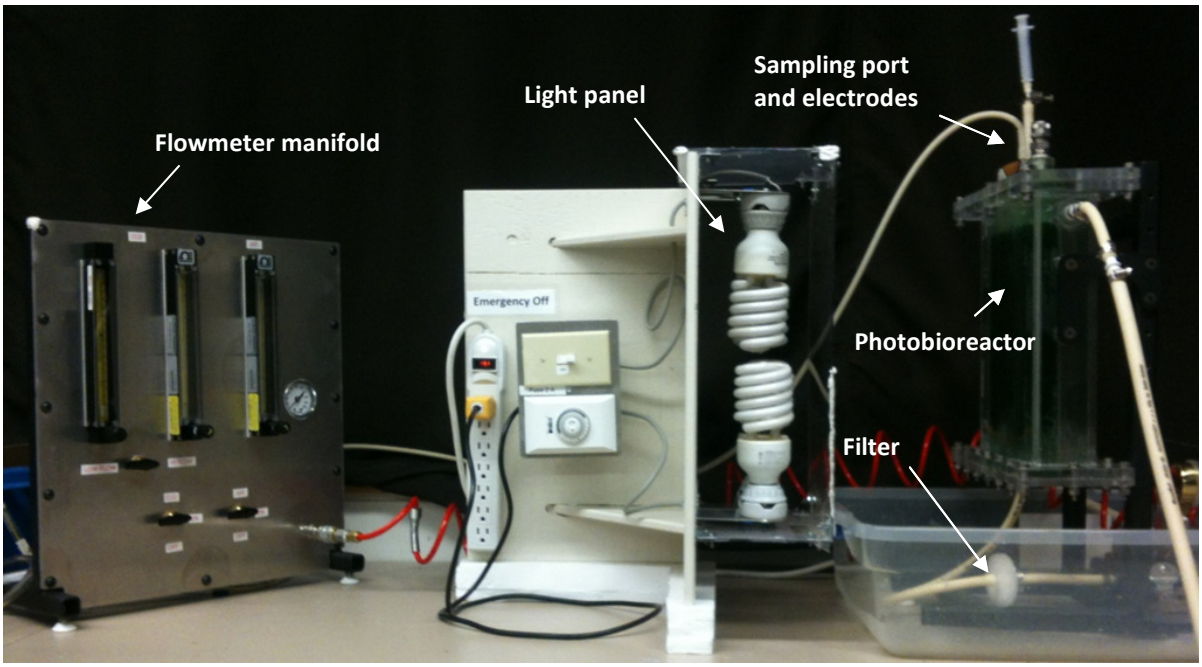

Figure 14: Photobioreactor setup

The dissolved CO_2 electrode was connected to a Thermo Orion A710+ pH meter. The electrode calibration curve is shown in Figure 15. Calibration of the electrode was performed by measuring the electrode responses of serial dilutions of a 1000 ppm CO_2 standard. Both pH and dissolved oxygen were measured using a VWR Symphony meter. Installation of a pH probe in the reactor was not possible due to space constraints, so pH was measured offline. All parameters except pH were recorded in-situ every 10 minutes by the Labtech Notebook software. The photobioreactor was illuminated continuously at the front surface by 4 CFL bulbs (Philips 60W, 6500k color temperature).

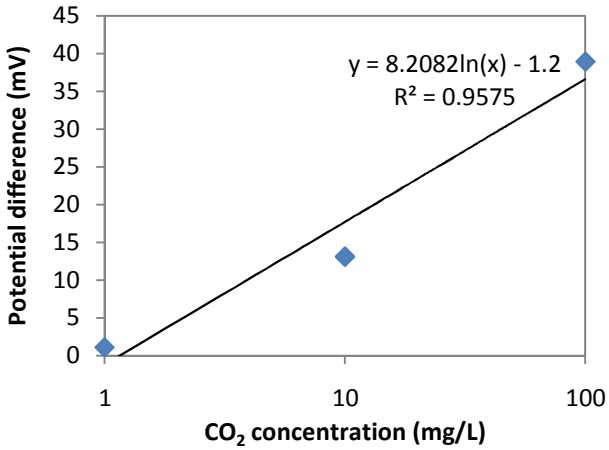

Figure 15: Dissolved CO_2 electrode calibration

3.4.1 Calculation of the concentrations for each carbon species

The CO_2 electrode was an ion-selective type, and it had a membrane that allowed the passage of only dissolved CO_2. When dissolved CO_2 passed through the membrane, it entered the probe in the form of H_2CO_3. However, the probe does not have the ability to measure the concentrations of other inorganic carbon species in the solution. An understanding of the dissociation reactions of CO_2 is required to determine such concentrations and therefore calculate the concentration of total dissolved inorganic carbon c, where c can be defined as:

$$c = [H_2CO_3] + [HCO_3^-] + [CO_3^{2-}] \quad (22)$$

Carbonic acid dissociates in two steps (Haynes et al., 2012):

$$H_2CO_3 + H_2O \Leftrightarrow H_3O^+ + HCO_3^- \qquad pK_{a1}\ (33\ °C) = 6.316 \quad (23)$$

$$HCO_3^- + H_2O \Leftrightarrow H_3O^+ + CO_3^{2-} \qquad pK_{a2}\ (33\ °C) = 10.27 \quad (24)$$

Where the pK_a values are derived from a water-CO_2 system. Figure 16 shows the concentrations of each CO_2 species at pH between 0 and 14 for c=1.

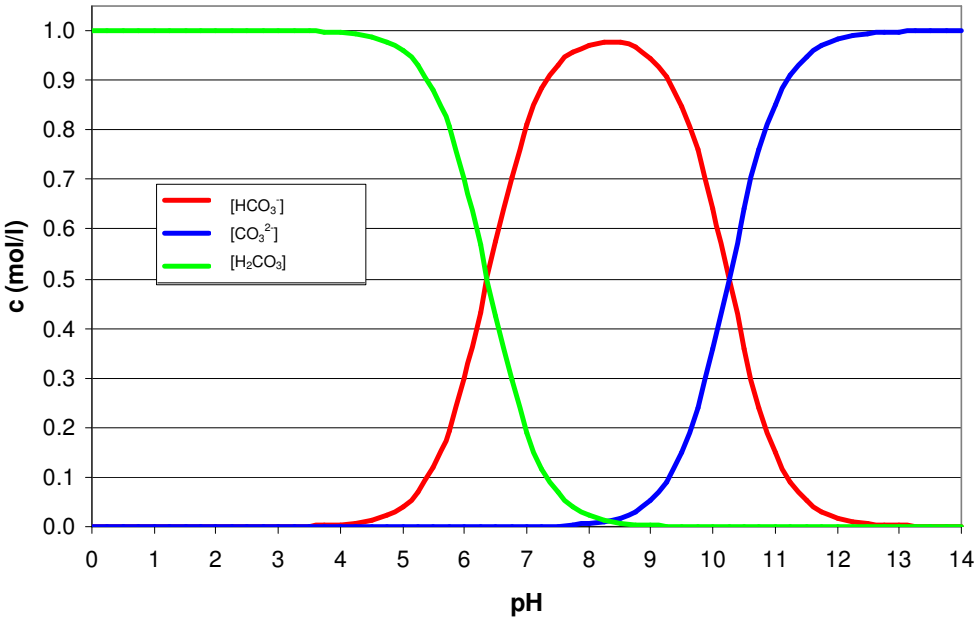

Figure 16: CO_2 species and pH (Haynes et al., 2012)

By definition:

$$x = 10^{-pH} \quad (25)$$

To calculate *c*, we can derive the following equation from the equilibrium constants:

$$c = \frac{[H_2CO_3](x^2 + K_{a1}x + K_{a1}K_{a2})}{x^2} \quad 26$$

pH values and $[H_2CO_3]$ were known from experimental data. As pK_a values have not been determined for CO_2-BG11 medium system, the pK_a values for the water-CO_2 system were used for calculations instead.

3.4.2 Specifications of photobioreactor

A diagram of the airlift photobioreactor is shown in Figure 17. A vertical flat-plate airlift photobioreactor was selected as a suitable configuration because it provided a short light path length, high surface area to volume ratio for minimal dark zones, and a simple design (Q. Hu et al, 1998). The reactor had an internal depth of 2.54 cm, width of 16 cm, and an internal height of 28 cm. One of the rationales for choosing a "two-dimensional" design was that a single vertical tubular photobioreactor bubble-column or airlift reactor cannot exceed about 0.2 m in diameter (Chisti & Moo-Young, 1993) or light availability would be hindered (Mirón et al., 2000). Secondly, a thin and flat design allowed for simple measurement of light intensity that would otherwise not be possible with a curved reactor surface. Two-dimensional systems have made it easier to attain quantitative flow information such as bubble size, liquid superficial velocity, and gas hold-up. An internal loop circulation was induced by a sparger and a pair of 6" baffles, forming riser and downcomer regions of equal volumes.

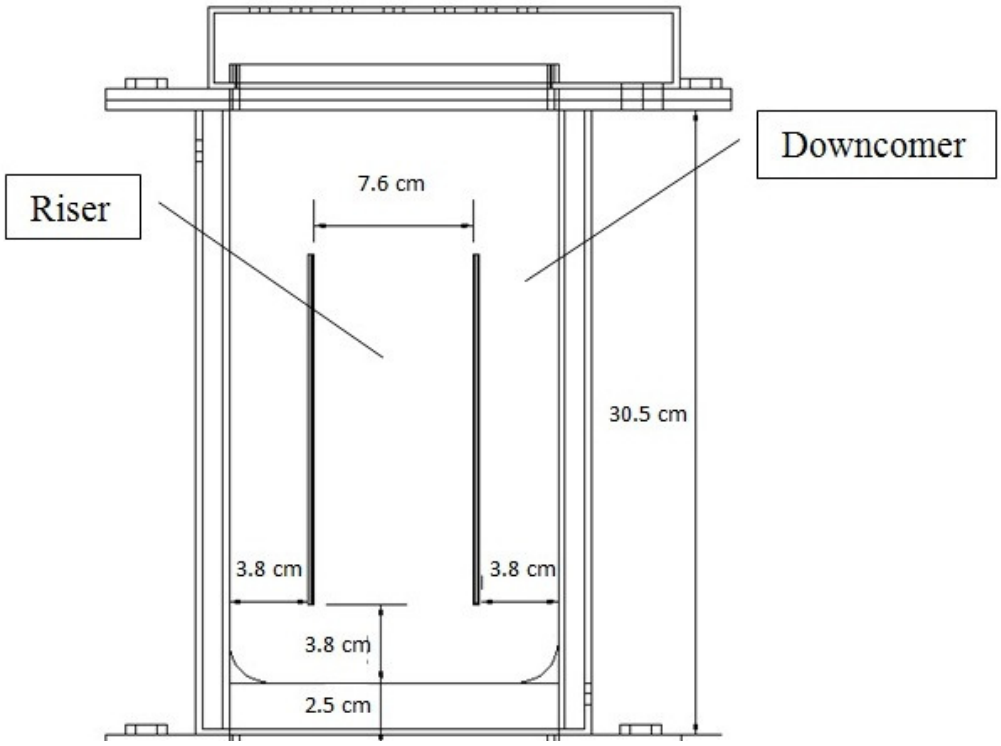

Figure 17: Reactor dimensions

An acrylic block was installed to provide a rounded bottom, with a partition in the centre for insertion of a glass sparger, pictured in Figure 18. This block removed blind zones and minimized the settling of cells. The sparger was supplied by Cansci Glass Ltd and used for all photobioreactor experiments in this study. The sparger had an average pore size of 4.0-5.5 microns. At a working volume of 1 L, there was a headspace of 5 cm and gas-liquid separator height of 2.5 cm. The temperature was regulated by a 2 cm water jacket surrounding the sides and back of the reactor, with circulating warm water from a water bath. The system was operated at atmospheric pressure for all experiments.

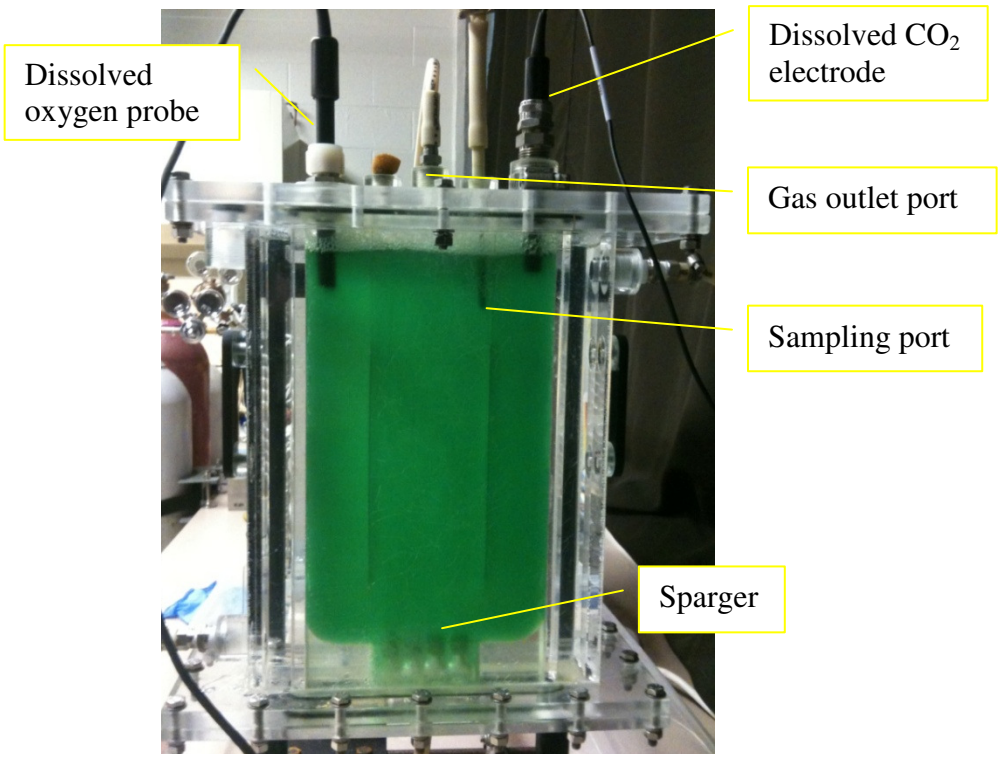

Figure 18: Front view of photobioreactor

3.5 Hydrodynamic parameters of the photobioreactor

Macroscopic flow structures of gas-liquid fluidization systems were studied through flow visualization using the 2D airlift photobioreactor under various operating conditions. The gas flow rates in the reactor were adjusted by valves and measured by flowmeters. The effects of gas flow rate on superficial liquid velocity, bubble size, gas hold-up, and mixing times were examined. Eight gas flow rates were used: 0.25, 0.5, 0.75, 1, 1.25, 1.5, 1.75, 2 L/min.
For non-Newtonian fluids such as biological suspensions, fluid behaviour is assumed to be similar to that of water due to the relatively low mass fraction of the solid phase (algae).

3.5.1 Procedure for determining mixing time

A tracer experiment was designed for determining the mixing time of the reactor at various gas flow rates, and Bodenstein number. The acid tracer experiment was based on a procedure devised by Miron (2004). The method measured the mixing time, defined as the time to reach a 5% deviation of the steady state concentration. Before each experiment, the system was purged with N_2 gas to strip out dissolved CO_2. The pH of the medium was lowered to 2 with HCl and bubbled with air for 20 minutes to remove carbonates. Then it was raised to 4.5 by adding 12M sodium hydroxide. The acid tracer (0.66 mL of 35% HCl) was then added instantaneously into

the 1L BG-11 medium at the centre of the surface of the sparger. Air was used as the sparging gas. The pH detection point was 2.5 cm below the gas-liquid interface, located above one of the downcomers, and the tracer injection point was 1.2 cm above the detection point. Changes in pH were detected with a Cole Parmer pH electrode. Readings were automatically recorded every 0.8 seconds, which was the minimum time permitted by the pH meter. The theoretical mixing time t_m for 95% homogeneity was calculated using the following equation (Petrović et al., 1995):

$$t_m = 53.5 U_G^{-0.31} \left(\frac{H}{D} \right)^{0.12} V_R^{0.19} V_D^{0.5} V_S^{-0.26} \tag{27}$$

where U_G is the superficial gas velocity, H is the height of riser, D is the characteristic diameter of the whole reactor, V_R is the riser volume, V_D is the downcomer volume, and V_S is the separator volume. The superficial liquid velocity was calculated by dividing the distance of the circulation path $2H$ by the peak interval time in pH readings. The pH readings were converted to hydrogen ion concentrations, and the dimensionless concentration C_T was calculated using the following equation:

$$C_T = \frac{[H^+]_{inst} - [H^+]_{initial}}{[H^+]_{final} - [H^+]_{initial}} \tag{28}$$

The experimental mixing time was found by determining the time taken for C_T to reach 0.95 in the readings starting from the time of tracer addition.

3.5.2 Procedure for determining the Bodenstein number

The Bodenstein number characterized axial mixing in the PBR, and this is described in the following equation (Blenke, 1979):

$$c_r = \sum (c_r)_{x_U} = \sum_{x_U = \tau_U - 2}^{x_U = \tau_U + 2} \left(\frac{Bo}{4\pi\tau_U} \right)^{1/2} \exp\left[-\frac{(x_U - \tau_U)^2}{4\tau_U} Bo \right] \tag{29}$$

Where c_r is the predicted dimensionless concentration, x_U is the dimensionless distance, and τ_U is the dimensionless time. Experimental c_r was calculated using the formula:

$$c_r = \frac{c(t) - c_\infty}{c_\infty} \tag{30}$$

Where $c(t)$ is the concentration at time t and c_∞ denotes the steady state concentration. x_U is the relative flow path, which is defined by:

$$x_U \equiv \frac{L}{L_U} \tag{31}$$

which is the ratio of the distance travelled L and the characteristic length $L_U=2H$ of one circulation. In this case, the characteristic length was 12 inches (twice the length of each baffle). τ_U is the ratio of time t to the mean circulation time t_U. The mean circulation time was found by measuring the time interval between peaks of the tracer profile. Once x_U and τ_U were computed, the experimental c_r was fitted to Eq. 29 with Bo as the fitting parameter. This was achieved using the solver function in Excel. Once Bo is determined in Eq. 29, D_{ax} can be subsequently calculated in Eq. 2 (Onken & Träger, 1990). This information can be used to compare mixing of the internal loop airlift reactor at air flow rates between 0.25 L/min and 1 L/min. This range for the flow rates was chosen because these have been commonly used in airlift photobioreactors for microalgae cultivation (Kajiwara et al., 1997).

3.5.3 Procedure for calculating gas hold-up

Gas hold-up ε_R was calculated by recording the change in dispersed liquid riser volume V_{DR} relative to the initial liquid riser volume V_R. Since the cross-sectional area of the riser was the same along the height of the riser h, the gas hold-up was calculated simply by measuring the change in height of the gas-liquid interface. This is expressed as:

$$\varepsilon_R = \frac{V_{DR} - V_R}{V_{DR}} = \frac{h_{DR} - h_R}{h_{DR}} \tag{32}$$

3.5.4 Procedure for determining volumetric mass transfer coefficient

The medium used for mass transfer experiments was BG-11. Effects of cells were not analyzed to simplify the experiments. The pH value of the fresh medium was not adjusted and was initially at about 8.4. The volumetric mass transfer coefficient of oxygen (k_La) was determined by the dynamic gassing-out method. First, the medium is scrubbed free of oxygen and CO_2/carbonates by nitrogen gas (supplied by Praxair). Aeration was then initiated at a constant air flow rate and the increase in dissolved O_2 (D_{O2}) and CO_2 (D_{CO2}) was logged by computer. To analyze the effects of temperature on k_La, a low temperature of 23°C and a high temperature of 33°C were observed. CO_2-enriched air was introduced at CO_2 concentrations of 5% and 10%, at

a constant total gas flow rate of 0.5 L/min. To analyze the effects of gas flow rate and CO_2 concentrations on k_La, experiments were conducted at total gas flow rates of 0.5, 1, 1.5, and 2 L/min. CO_2 concentrations were adjusted to 5% and 10%. The temperature was maintained at 33°C.

The following equation represents the carbon dioxide transfer rate *CTR* into the culture medium:

$$CTR = \frac{dC}{dt} = k_L a(C_S - C) \qquad 33$$

Where C [mol/m^3] is the dissolved CO_2 concentration in the bulk liquid at any time t [s], C_S is the saturation concentration of CO_2 in the liquid, and k_La is the volumetric mass transfer coefficient. Integration of Eq. 33 yields an equation where k_La can easily be calculated:

$$k_L a = \frac{1}{t}\ln\left[\frac{C_o - C_S}{C - C_S}\right] \qquad 34$$

where C_o is the initial dissolved CO_2 concentration at time t=0.

Calculation of k_La using Eq. 34 is justified when the following conditions are met: the liquid phase mixing time, the response time of the CO_2/O_2 electrodes, and the gas phase residence time must be lower than the time constant for CO_2/O_2 transfer [1/k_La] (Boogerd & Kuenen, 1990).

To observe physical changes of the gas-liquid system, bubble size was measured by image processing software ImageJ, as shown in Figure 19. A total of 100 measurements were taken for each gas flow rate (Appendix B).

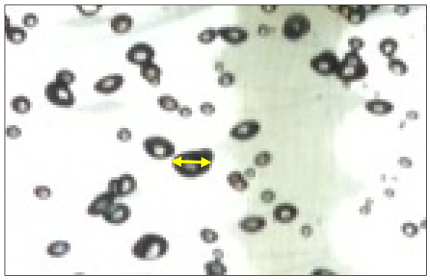

Figure 19: Measurement of bubble diameter with ImageJ

3.6 Procedure for optimization of μ_{max} and X_{max} in shake flasks

A central composite design was used to investigate the effects of light intensity and temperature on μ_{max} and X_{max}. The experiment consisted of 8 different conditions and 5 center points for a total of 13 runs. Three replicate experiments were carried out for reproducibility. The reaction conditions used in the experimental design are outlined in Table 10. Light intensity was varied by changing the height of the light panel, which was suspended over the flasks. Incident light intensities (ILI) were measured using an Apogee MQ-200 quantum sensor. Temperature was controlled by the incubator and the agitation rate was set at 120 rpm. Air was used as the source of CO_2. Gas exchange between the shake flask and the external environment occurred at the mouth of the flask, through foam plugs. The foam plugs maintained axenic conditions inside the flasks. In each experiment, 10 mL inoculum was added to 90 mL of BG-11 medium and grown in 250 mL flask. The flasks were kept in two Innova incubators (Models 4230 and 42). Initial biomass concentrations were 0.03-0.05 g/L. One mL samples were taken daily from each flask for OD measurements.

Table 10: Central composite design for optimization of μ_{max} and X_{max} using two factors

Light intensity ($\mu E/m^2/s$)	Temperature (°C)
150	30
79	30
200	35
150	30
150	23
100	25
150	30
221	30
200	25
150	37
100	35
150	30
150	30

3.7 Procedure for optimization of μ_{max} and X_{max} in photobioreactor

A full factorial experimental design was used to study the effects of light intensity, CO_2 concentration, and gas flow rate on μ_{max} and X_{max}. The reactor operating conditions used in the experimental design are outlined in Table 11. Temperature was kept constant at 33°C by a water

bath. Light intensity was varied by changing the distance between the light panel and the reactor, as shown in Figure 20.

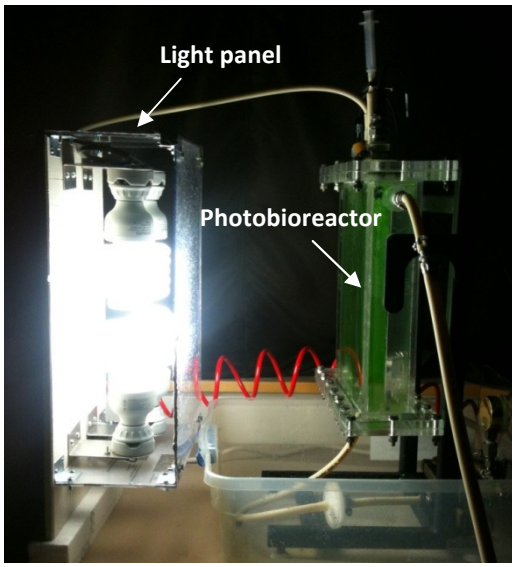

Figure 20: Photobioreactor and light panel setup

The laboratory in which this reactor was located was not exposed to external sources of light; the reactor was subjected to light only from the light panel. Analysis of each run was conducted in a randomized order. ILI was measured using an Apogee MQ-200 quantum sensor. At the beginning and at the end of each experiment, ILI was recorded to verify whether the ILI was constant during cultivation time. The ILI was the average of measurements at twelve different locations of the illuminated surface. Exiting light intensities were recorded at twelve different locations of the back surface of the reactor, and then averaged to give the mean exiting light intensity. ILI were within 5% of the mean, showing little variance over the surfaces of the reactor.

Table 11: Experimental design for optimization of μ_{max} and X_{max} using two factors in photobioreactor

CO_2 concentration (%)	Inlet flow rate (L/min)	Light intensity (µE/m^2/s)
Air	1	60
Air	1	120
5	1	60
5	1	120
10	1	60
10	1	120

4 Results for Shake Flask Scale Experiments

4.1.1 Screening of BG-11 medium components

A set of experiments designed to test the effects of a broad range of BG-11 component concentrations was conducted. The effects of $NaNO_3$, K_2HPO_4, $CaCl_2$, $C_6H_{11}FeNO_7$, and Na_2CO_3 on response variables μ_{max} and X_{max} were analyzed. Optimal BG-11 concentrations that maximized μ_{max} and X_{max} were then determined. The experiment consisted of two stages: a screening stage and a central composite design. The purpose of the screening experiment was to determine the range of concentrations that had significant impacts on the response variables. Using these concentrations, the next step was to integrate them into the optimization experiments and then determine the concentrations that gave the highest μ_{max} and X_{max}.

A full factorial design was developed for the screening study, as shown in Table 12, to assess the impact of each medium component on μ_{max} and X_{max}. Each independent variable was investigated at a high level and a low level which represented two different nutrient concentrations. The same initial concentrations for $MgSO_4$, $CaCl_2$, $C_6H_8O_7$, Na_2EDTA and trace metals from Table 6 of Materials and Methods were used in this design. The *t* test and regression analysis were done to determine whether the inclusion of a given component had a significant effect on μ_{max} and X_{max}.

Table 12: Full factorial design of BG-11 components

Independent variable	Symbol	Level	
		-1	1
$NaNO_3$ (mM)	X_1	0	17.6
K_2HPO_4 (mM)	X_2	0	0.22
$CaCl_2$ (mM)	X_3	0	0.2
$C_6H_{11}FeNO_7$ (mM)	X_4	0	0.02
Na_2CO_3 (mM)	X_5	0	0.18

For each shake flask, the algae were highly dispersed in the culture medium, and cells did not adhere to the surface throughout the cultivations. Thus, optical density measurement in each sample was a good representation of the biomass concentration.

As an example, Figure 21 shows the growth pattern obtained in a shake flask at high levels of each medium component listed in Table 12.

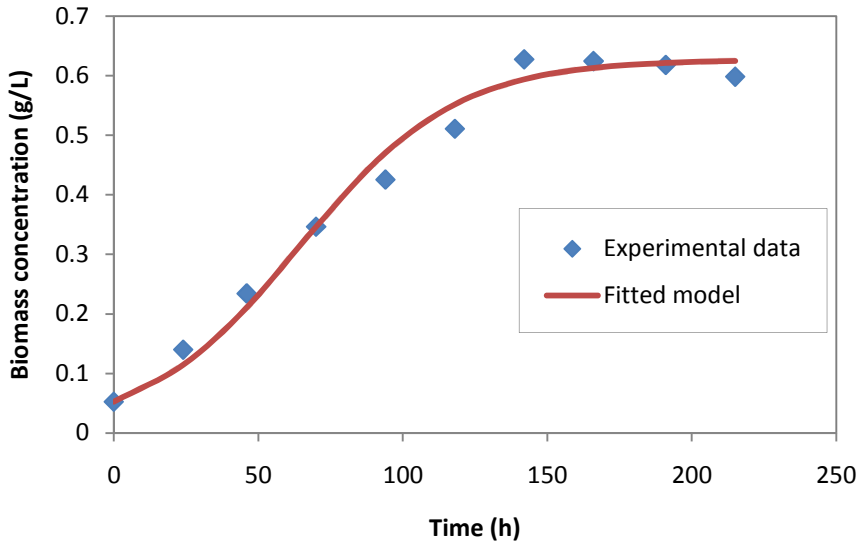

Figure 21: Growth curve and fitted logistic model for estimating μ_{max}

A lag phase was not apparent in the experimental data points in Figure 21. This absence may be explained by the lag phase being shorter in duration than the sampling rate (once per day), and thus was not detected. In most of the growth runs conducted, a lag phase was apparent in the experimental data points, and this meant that cells needed to acclimatize to new conditions. For the particular set of conditions in Figure 21, the exponential growth phase spanned approximately144 hours, and this was followed by a stationary phase. Most growth curves had exponential growth phases that ranged between 120 to 288 hours depending on the conditions. The biomass concentration was calculated from optical density measurements using Eq. 19. Next, μ_{max} was calculated using Eq. 20 using non-linear least squares for model fitting. X_{max} was taken from the highest optical density in each run. The results for each set of conditions are presented in Table 13.

Table 13: Results from the BG-11 medium factorial design

Component concentrations					Response		Initial pH
$NaNO_3$ (mM)	K_2HPO_4 (mM)	$CaCl_2$ (mM)	$C_6H_{11}FeNO_7$ (mM)	Na_2CO_3 (mM)	μ_{max} (1/h)	X_{max} (g/L)	
17.6	0.22	0.2	0.02	0.18	0.031	0.57	8.507
17.6	0	0.2	0.02	0.18	0.021	0.82	8.662
0	0	0.2	0	0	0.013	0.80	8.722
0	0.22	0	0.02	0.18	0.022	0.80	8.933
17.6	0.22	0.2	0.02	0	0.027	0.57	8.451
17.6	0	0.2	0	0	0.019	0.52	8.559
0	0	0	0	0	0	0.032	9.057
0	0.22	0	0	0	0.021	0.43	8.719
0	0.22	0.2	0	0	0.020	0.70	8.374
17.6	0	0	0	0.18	0	0.023	8.691
0	0	0	0.02	0	0.017	0.70	8.654
0	0.22	0.2	0	0.18	0.022	0.68	8.572
17.6	0	0	0	0	0	0.027	8.794
17.6	0	0.2	0.02	0	0.025	0.59	8.172
17.6	0	0	0.02	0	0.023	0.65	8.477
17.6	0.22	0	0.02	0.18	0.025	0.56	8.510
0	0	0.2	0.02	0.18	0.021	0.82	8.570
0	0	0.2	0	0.18	0.010	0.60	8.791
17.6	0.22	0.2	0	0	0.025	0.84	8.399
17.6	0	0.2	0	0.18	0.020	0.77	8.650
0	0.22	0.2	0.02	0	0.035	0.74	8.189
17.6	0.22	0	0	0.18	0.029	0.38	8.611
0	0.22	0.2	0.02	0.18	0.032	0.60	8.596
17.6	0.22	0.2	0	0.18	0.031	0.42	8.516
0	0	0	0	0.18	0.021	0.70	8.979
0	0.22	0	0	0.18	0.026	0.73	8.547
17.6	0	0	0.02	0.18	0.020	0.88	8.662
17.6	0.22	0	0	0	0.023	0.43	8.209
0	0	0.2	0.02	0	0.023	0.71	8.111
0	0.22	0	0.02	0	0.020	0.52	8.156
0	0	0	0.02	0.18	0.027	0.96	8.812
17.6	0.22	0	0.02	0	0.027	1.12	7.951

Table 14 lists the statistical values of each variable for the response to μ_{max}. The relative magnitude of each effect coefficient indicates its impact on the response and the sign of the value indicates whether it has a positive or negative impact on the response. Three components had a significant positive effect on μ_{max}: $C_6H_{11}FeNO_7$, $CaCl_2$, and K_2HPO_4. The same result was obtained by Deshmukh for optimization of BG-11 components using *Microcystis* (Deshmukh et al, 2013). Interactive effects between variables were not significant.

Table 14: Effects and coefficients of variables estimated using a screening design for response μ_{max}

Variable	Effect	Standard error	*t*-value	*p*-value	Confidence level (%)
$NaNO_3$	0.000	0.000	0.55	0.588	41.2
K_2HPO_4	0.044	0.009	4.67	0.000	100.0*
$CaCl_2$	0.024	0.010	2.27	0.032	96.8*
$C_6H_{11}FeNO_7$	0.365	0.104	3.52	0.002	99.8*
Na_2CO_3	0.014	0.012	1.24	0.228	77.2

*significant at 95% level (p<0.05)

Table 15 lists the statistical values of each variable for the response to X_{max}. $C_6H_{11}FeNO_7$ had a significant positive effect on X_{max}. Interactive effects were not significant. Based on the results of the screening design, the independent significances of factors $C_6H_{11}FeNO_7$, K_2HPO_4, and $CaCl_2$ on μ_{max} and X_{max} warranted further investigation. Although $NaNO_3$ and Na_2CO_3 were insignificant, including them in the subsequent optimization experiments can provide useful information on its effects on cell growth as nitrogen and carbon are the major elements that make up the cell.

Table 15: Effects and coefficients of variables estimated using a screening design for response X_{max}

Variable	Effect	Standard error	*t*-value	*p*-value	Confidence level (%)
$NaNO_3$	-0.005	0.005	-1.06	0.298	70.2
K_2HPO_4	0.133	0.369	0.36	0.721	27.9
$CaCl_2$	0.566	0.406	1.39	0.176	82.4
$C_6H_{11}FeNO_7$	11.005	4.063	2.71	0.012	98.8*
Na_2CO_3	0.325	0.451	0.72	0.478	52.2

*significant at 95% level (p<0.05)

An investigation of BG-11 medium components provided additional insight into the effects of pH on growth of *S. elongatus*. Initial pH was important in the analyses of X_{max} and μ_{max} because it influenced the initial growth rate and the duration of the lag phase, as these are tabulated in Table 13. Different pH values were observed because the component concentrations varied for each run. Initial pH readings ranged between 8 and 9 due to the alkalinity of the medium. During exponential growth phase, *S. elongatus* increased the alkalinity of the medium (pH 10-11), and this was likely caused by the removal of dissolved CO_2 (Summerfield & Sherman, 2008). The declining phase was associated with a pH decrease to 8-9. This was caused by cell death, during which photosynthetic activity ceased and, as a result, alkalinity levels dropped.

4.1.2 Optimization of BG-11 component concentrations

To determine the optimal component concentrations that maximize μ_{max} and X_{max} for the tested domain, a central composite experimental design was conducted. These results helped to explain the effects of component concentrations on μ_{max} and X_{max}. The response can be predicted for a particular set of conditions using the following equation:

$$y = \beta_0 + \sum_{i}^{k} \beta_i x_i + \sum\sum_{i<j} \beta_{ij} x_i x_j + \varepsilon \qquad 35$$

Where y is the predicted response, β_i is the coefficient of the equation, β_0 is the intercept of the plane, x_i and x_j are coded levels of variables, and ε is the error term. Table 16 shows the levels of the experimental variables used.

Table 16: Values of independent variables in different levels of the optimization design

Independent variable	Symbol	Level				
		-2	-1	0	1	2
$NaNO_3$ (mM)	X_1	4.4	8.8	17.6	35.2	70.4
K_2HPO_4 (mM)	X_2	0.055	0.11	0.22	0.44	0.88
$CaCl_2$ (mM)	X_3	0.05	0.1	0.2	0.4	0.8
$C_6H_{11}FeNO_7$ (mM)	X_4	0.005	0.01	0.02	0.04	0.08
Na_2CO_3 (mM)	X_5	0.045	0.09	0.18	0.36	0.72

Table 17 tabulates the responses for all 32 runs, including 10 axial points and 6 centre points. Table 18 and Table 19 summarize the significance of each medium component on X_{max} and μ_{max}, respectively. The effects of each variable were determined by JMP statistical software (V 7, SAS

Institute Inc., Cary, NC, U.S.A.). Coefficients with $p < 0.05$ identified the significant factors (a 95% confidence level).

Table 17: Experimental results from optimization of BG-11 component concentrations

Component concentrations					Response	
$NaNO_3$ (mM)	K_2HPO_4 (mM)	$CaCl_2$ (mM)	$C_6H_{11}FeNO_7$ (mM)	Na_2CO_3 (mM)	μ_{max} (1/h)	X_{max} (g/L)
8.8	0.11	0.1	0.01	0.09	0.0284	0.366
8.8	0.11	0.1	0.04	0.36	0.0262	0.459
8.8	0.11	0.4	0.01	0.36	0.0270	0.305
8.8	0.11	0.4	0.04	0.09	0.0227	0.334
8.8	0.44	0.1	0.01	0.36	0.0384	0.416
8.8	0.44	0.1	0.04	0.09	0.0385	0.349
8.8	0.44	0.4	0.01	0.09	0.0376	0.408
8.8	0.44	0.4	0.04	0.36	0.0280	0.525
35.2	0.11	0.1	0.01	0.36	0.0392	0.219
35.2	0.11	0.1	0.04	0.09	0.0253	0.473
35.2	0.11	0.4	0.01	0.09	0.0256	0.327
35.2	0.11	0.4	0.04	0.36	0.0226	0.249
35.2	0.44	0.1	0.01	0.09	0.0377	0.362
35.2	0.44	0.1	0.04	0.36	0.0465	0.334
35.2	0.44	0.4	0.01	0.36	0.0423	0.367
35.2	0.44	0.4	0.04	0.09	0.0330	0.445
4.4	0.22	0.2	0.02	0.18	0.0315	0.436
70.4	0.22	0.2	0.02	0.18	0.0268	0.249
17.6	0.055	0.2	0.02	0.18	0.0293	0.399
17.6	0.88	0.2	0.02	0.18	0.0488	0.375
17.6	0.22	0.05	0.02	0.18	0.0421	0.318
17.6	0.22	0.8	0.02	0.18	0.0226	0.349
17.6	0.22	0.2	0.005	0.18	0.0410	0.400
17.6	0.22	0.2	0.08	0.18	0.0322	0.461
17.6	0.22	0.2	0.02	0.045	0.0348	0.381
17.6	0.22	0.2	0.02	0.72	0.0401	0.306
17.6	0.22	0.2	0.02	0.18	0.0360	0.382
17.6	0.22	0.2	0.02	0.18	0.0345	0.382
17.6	0.22	0.2	0.02	0.18	0.0283	0.381
17.6	0.22	0.2	0.02	0.18	0.0287	0.403
17.6	0.22	0.2	0.02	0.18	0.0326	0.402
17.6	0.22	0.2	0.02	0.18	0.0319	0.374

Table 18: Optimization of BG-11 component concentrations for response X_{max} (R^2=0.91)

Variable	Effect	Standard error	*t*-value	*p*-value	Confidence level (%)
Base	0.386	0.0130	29.56	<0.0001	>99.99*
$NaNO_3$	-0.032	0.0067	-4.75	0.0006	99.94*
$C_6H_{11}FeNO_7$	0.022	0.0067	3.24	0.0079	99.21*
K_2HPO_4	0.018	0.0067	2.67	0.0217	97.83*
Na_2CO_3	0.022	0.0082	2.65	0.0228	97.72*
$CaCl_2$	0.0018	0.0067	0.26	0.7973	20.27

*significant at 95% level (p<0.05)

From the analysis of the response for X_{max}, $NaNO_3$ had a significant negative effect. This may have been evidence of excess $NaNO_3$ concentration in BG-11. The significant positive effect of $C_6H_{11}FeNO_7$ highlighted the importance of iron uptake in photosynthesis. K_2HPO_4 had a significant positive effect on X_{max}, and this showed that its role in the nitrate uptake process was important for the growth of *S. elongatus*. As expected, Na_2CO_3 was important in providing inorganic carbon and stabilizing pH to promote cell growth. However, $CaCl_2$ had an insignificant effect on X_{max}. These results indicated that the four components, $NaNO_3$, $C_6H_{11}FeNO_7$, K_2HPO_4, and Na_2CO_3 may act as a major or limiting factor in culture medium, and slight changes in their concentrations can affect X_{max}. The predicted response of X_{max} can be described by Eq. 36, using the effects coding from Table 16 (ie. -2, -1, 0, 1, 2.).

$$X_{\max} = 0.386 - 0.032X_1 + 0.018X_2 + 0.0018X_3 + 0.022X_4 + 0.022X_5 \qquad 36$$

From the analysis of the response for μ_{max} in Table 19, K_2HPO_4 had a significant positive effect. This may indicate that the K_2HPO_4 concentration in BG-11 was a limiting factor for the growth rate. Literature has shown that nitrogen to phosphate molar ratios (N:P) higher than 25 gave lower biomass growth among cyanobacteria (Bulgakov & Levich, 1999). In BG-11, the N:P ratio was 80, which explained why K_2HPO_4 was a limiting factor. Furthermore, it was believed that nitrate uptake was influenced by the availability of the phosphate ion, which is important for cellular metabolism and influences enzyme activity and the nitrate uptake process (Q. Hu, Westerhoff, & Vermaas, 2000). Hu has shown that in a phosphate-deprived culture, nitrate uptake did not occur in *S. elongatus*. The significant positive effect of K_2HPO_4 implied that phosphates were very important towards the nitrogen uptake process. This was consistent with

the results from the analysis of the response of X_{max} by $NaNO_3$. Conversely, $CaCl_2$ and $C_6H_{11}FeNO_7$ had significant negative effects on μ_{max}. Because it was previously shown that $C_6H_{11}FeNO_7$ had a positive effect on X_{max}, it demonstrated that iron had a more significant role in maintaining cellular reproduction, but it did not enhance the growth rate.

Table 19: Optimization of BG-11 component concentrations for response μ_{max} (R^2=0.89)

Variable	Effect	Standard error	*t*-value	*p*-value	Confidence level (%)
Base	0.0326	0.00153	21.35	<0.0001	>99.99*
K_2HPO_4	0.0052	0.00078	6.62	<0.0001	>99.99*
$CaCl_2$	-0.0033	0.00078	-4.28	0.0013	99.87*
$C_6H_{11}FeNO_7$	-0.0021	0.00078	-2.73	0.0197	98.03*
Na_2CO_3	0.0013	0.00071	1.7	0.1165	88.35
$NaNO_3$	0.00067	0.00078	0.86	0.4095	59.05

*significant at 95% level (p<0.05)

Na_2CO_3 and $NaNO_3$ had insignificant effects on μ_{max}. Na_2CO_3 had a more significant role in providing inorganic carbon, which was the major building block for cell reproduction, but had no correlation with the cellular growth rate. The predicted response of μ_{max} can be described in Eq. 37.

$$\mu_{\max} = 0.0326 + 0.00067X_1 + 0.0052X_2 - 0.0033X_3 - 0.0021X_4 + 0.0013X_5 \quad (37)$$

The significant factors of both X_{max} and μ_{max} had small *p*-values, and these were associated with large *t*-values because they imply that the coefficient is greater than its standard error. This confirmed that the fitted surface had maximum points. Using JMP statistical analysis, the concentrations for optimum growth were determined in Table 20. To confirm that the findings were indeed the concentrations that gave the highest X_{max} and μ_{max}, an experiment was conducted to compare cultivation of *S. elongatus* in unmodified BG-11 medium and optimized media. Experiments were performed in triplicates.

Table 20: Components of the original and modified media

Component	BG-11 concentrations	Concentrations for optimal X_{max} (mM)	Concentrations for optimal μ_{max} (mM)
$NaNO_3$	17.6	8.8	17.6
K_2HPO_4	0.22	0.44	0.44
$CaCl_2$	0.2	0.2	0.14
$C_6H_{11}FeNO_7$	0.02	0.04	0.01
Na_2CO_3	0.18	0.36	0.18

Figure 22 illustrates the cell concentrations and their fitted logistic curves in both optimized media and in the original BG-11 medium with respect to time. *S. elongatus* reached the maximum after 210 hours of cultivation. The growth was stable during the exponential growth phase and the culture pH ranged between 8.5 and 10.5.

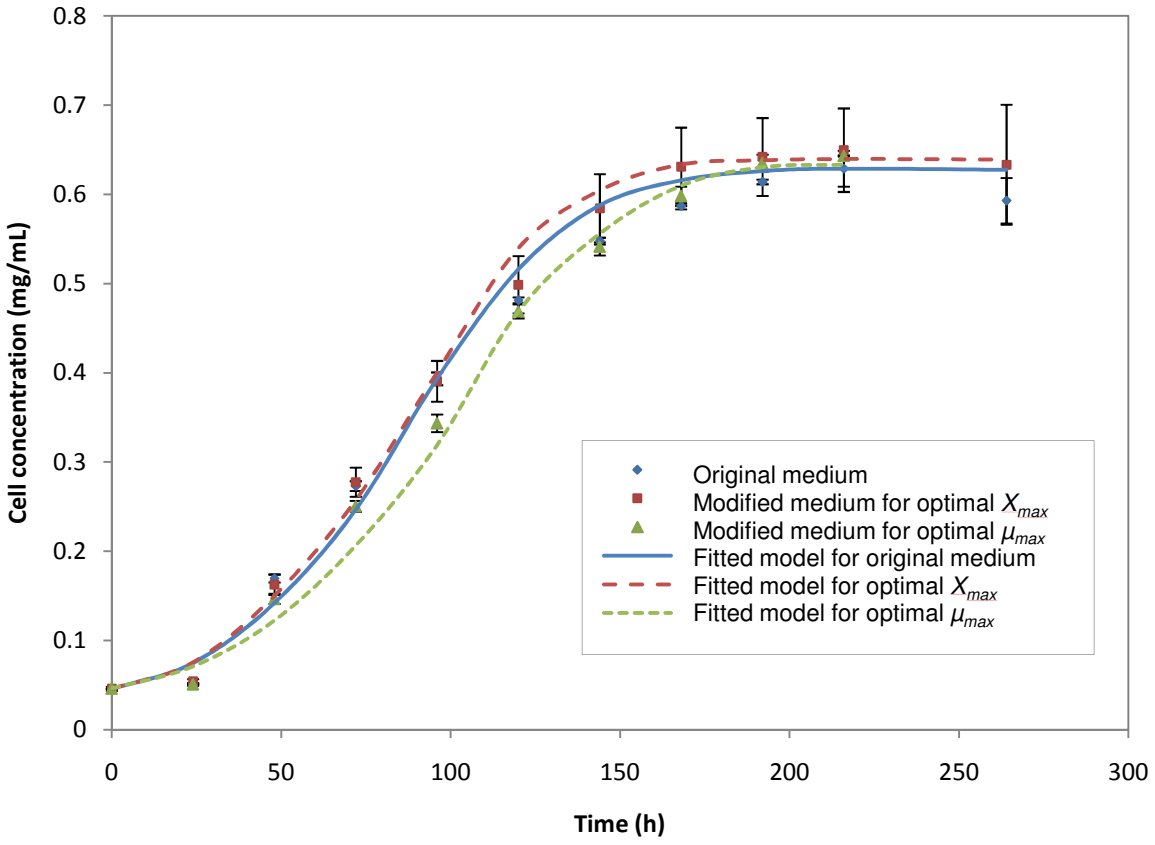

Figure 22: Growth in optimized media. Lines added to visualize data.

It was deduced that there was no significant difference in X_{max} and μ_{max} between the three runs as the standard deviations were relatively large.

Table 21: Summary of X_{max} and μ_{max}

Medium	X_{max} (g/L)	μ_{max} (h^{-1})
Unmodified BG-11 medium	0.629±0.020	0.0318±0.0009
Adjusted medium for optimal X_{max}	0.650±0.047	0.0314±0.0005
Adjusted medium for optimal μ_{max}	0.643±0.001	0.0294±0.0001

It was determined that CO_2 limitation in the medium was a likely cause of this effect, which was confirmed in subsequent carbon balance experiments (Figure 37). Under air, dissolved CO_2 is so severely limited that any changes in the nutrient composition had no effect on growth. If more CO_2 was available, it is likely that changes in nutrient composition would have a more profound effect on cell growth. Furthermore, X_{max} was larger for both adjusted media compared to the unmodified medium but the difference was not significantly great enough to draw this conclusion. Unexpectedly, the adjusted medium for optimal μ_{max} gave a slightly lower μ_{max} compared to the other two media. This was likely due to the logistic model fitting of the data, in which the fitting underestimated the experimental values. For these reasons, the concentrations of the unmodified BG-11 medium were used for optimization experiments in shake flasks and in the photobioreactor.

4.2 Effects of light intensity and temperature on growth of *S. elongatus* in shake flasks

For successful growth of microalgae in culture, the environment must be conditioned to meet the intrinsic requirements of *S. elongatus* for optimal growth. Following the initial results, which indicated that there were insignificant differences in X_{max} and μ_{max} for the original and optimized media, the original BG-11 component concentrations were used for subsequent experiments. A central composite design was developed for the optimization of light intensity and temperature on X_{max} and μ_{max}. This allowed for a reduced number of runs, while still producing statistically reliable results. Table 22 summarizes the optimization results obtained. The biomass concentration was calculated using the biomass calibration curve. The growth rate was calculated by fitting the biomass concentrations to the logistic growth model.

Similar to the growth curves from the medium optimization experiment, each curve in these experiments revealed a short lag phase (≤ 24 h), followed by an exponential phase (duration between 96 to 144 h) and the beginning of the stationary phase.

Table 22: Results from the optimization of light intensity and temperature

Temperature (°C)	Light intensity (μE/m^2/s)	μ_{max} (h^{-1})	X_{max} (g/L)
X_6	X_7		
30	150	0.0510	0.485
30	79.3	0.0533	0.444
35	200	0.0495	0.450
30	150	0.0492	0.485
23	150	0.035	0.335
25	100	0.0347	0.381
30	150	0.0493	0.485
30	220.7	0.0438	0.430
25	200	0.0337	0.358
37	150	0.0397	0.356
35	100	0.0499	0.505
30	150	0.0516	0.497
30	150	0.0507	0.497

Table 23 shows the significance of each factor on μ_{max}. Only temperature had a significant positive effect on μ_{max}. The 2nd order temperature effect showed that concavity was present on the response surface, i.e. there was an optimum temperature at 33°C. Interestingly, light intensity did not have a significant effect on μ_{max}. This may indicate that light is not a limiting factor in conditions between 79.3 and 220.7 μE/m^2/s in the shake flasks. No significant interactive effects between temperature and light were present in the model.

Table 23: Optimization of light intensity and temperature for response μ_{max}

Variable	Effect	Standard error	*t*-value	*p*-value	Confidence level (%)
	0.0504	0.00171	29.39	<0.0001	>99.99*
Temperature*temperature	-0.00669	0.00145	-4.60	0.0025	99.75*
Temperature	0.00463	0.00135	3.42	0.0112	98.88*
Light intensity	-0.00185	0.00135	-1.37	0.2137	78.63
Light intensity*light intensity	-0.00117	0.00145	-0.81	0.4454	55.46
Light intensity*temperature	0.000150	0.00192	0.08	0.9396	6.04

*significant at 95% level (p<0.05)

Figure 23 displays the response surface for μ_{max}. Within the tested range of conditions, μ_{max} were achieved at 33°C for the tested range of light intensities. Below 30°C, the cells experienced a

dramatic drop in μ_{max}. As previously mentioned, light intensity had no significant effect on μ_{max}. A slight decrease in μ_{max} was observed as the light intensity increased, which may indicate the presence of photoinhibition in the cells; however, this was not statistically significant. The highest μ_{max} in this response curve was 0.0519 h^{-1}, and this was attained at a temperature of 33°C and light intensity of 120 μE/m^2s. The model is represented by the following equation, where X_6 is the effects coding for temperature (ie. -1.414, -1, 0, 1, 1.414):

$$\mu_{\max} = 0.0504 + 0.00463X_6 - 0.00669X_6^2 \qquad 38$$

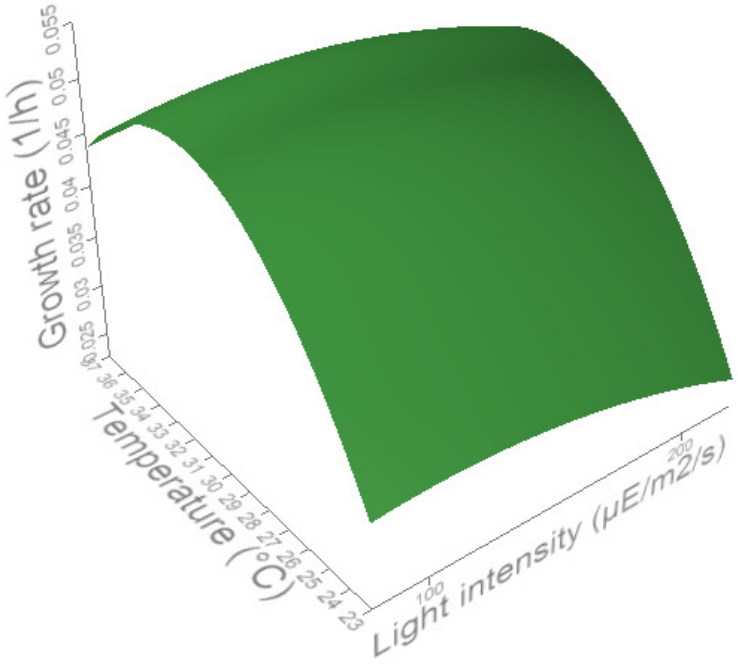

Figure 23: Response curve for μ_{max} as a function of temperature and light intensity (R^2=0.83)

Table 24 shows the significance of each factor on X_{max}. Similar to the response curve for μ_{max}, X_{max} depends on the temperature. It also displays the same trend of concavity as observed in the response for μ_{max}.

Table 24: Optimization of light intensity and temperature for response X_{max}

Variable	Effect	Standard error	*t*-value	*p*-value	Confidence level (%)
	0.490	0.0142	34.59	<0.0001	>99.99*
Temperature*temperature	-0.0641	0.0120	-5.34	0.0011	99.89*
Temperature	0.0307	0.0112	2.74	0.0288	97.12*
Light intensity*light intensity	-0.0184	0.0120	-1.53	0.1702	82.98
Light intensity	-0.0122	0.0112	-1.09	0.3110	68.90
Light intensity*temperature	-0.008	0.0158	-0.51	0.6289	37.11

*significant at 95% level (p<0.05)

The model is represented by the following equation:

$$X_{\max} = 0.490 + 0.0307X_6 - 0.0641X_6^2 \quad (39)$$

Figure 24 is the response surface model of X_{max}. Photoinhibition was observed to take effect at light intensities greater than 150 μE/m^2/s. The highest X_{max} was estimated to be 0.496 g/L, at a temperature of 33°C and a light intensity of 120 μE/m^2/s. Similar to the μ_{max} response curve, the response from temperature showed concavity. X_{max} decreased drastically at temperatures below 30°C. A similar trend was observed by Kajiwara et al. (1997). Although optimization of temperature was not conducted, Kajiwara et al. used light intensities between 40 μE/m^2/s and 135 μE/m^{2}s and a mixture of 5% CO_2 and air to cultivate *S. elongatus*. They found that 108 μE/m^2/s at 30°C gave the highest μ_{max} and X_{max}, 0.048 h^{-1} and 1.1 g/L, respectively. This apparent similarity in the optimal light intensities from two independent experiments hinted that responses of μ_{max} and X_{max} from changes in light intensity were not significantly affected by other factors.

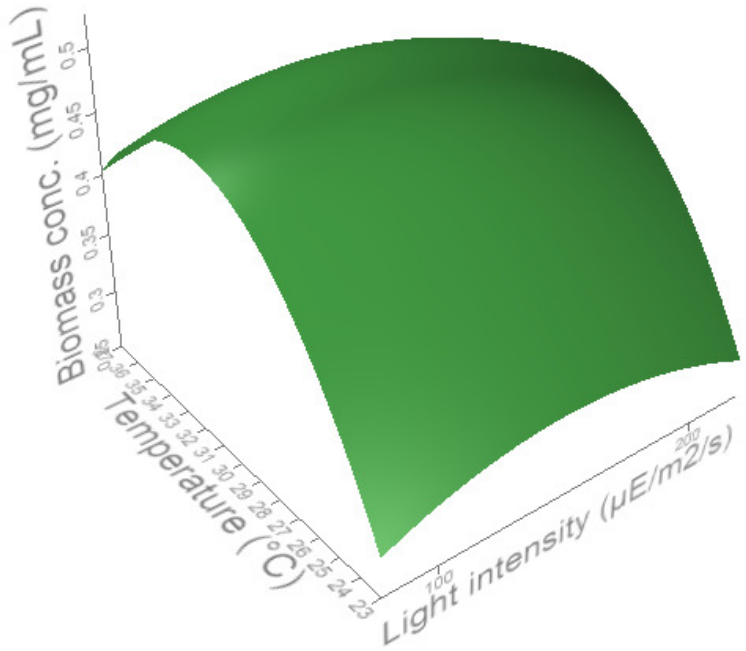

Figure 24: Response curve for X_{max} as a function of temperature and light intensity (R^2=0.85)

From these results, the highest μ_{max} and X_{max} predicted in the shake flask experiments were 0.0519 h^{-1} and 0.496 g/L, respectively. Both values were attained at a light intensity of 120 µE/m^2/s and a temperature of 33°C. These optimized parameters were subsequently used for the optimization experiments in the flat-plate photobioreactor.

5 Mass Transfer Studies in 2D Airlift Photobioreactor

5.1 Determination of Bodenstein number and gas hold-up in photobioreactor

To determine if axial liquid mixing was sufficient for flow rates between 0.25 L/min and 2 L/min in the flat-plate photobioreactor, *Bo* of the overall photobioreactor was calculated using Equations 29-31. Table 25 lists *Bo* and the mixing time for the given gas flow rates.

Table 25: *Bo* and t_m

Gas flow rate (L/min)	*Bo*	t_m (s)
0.25	48.7	4.0
0.5	37.1	3.2
0.75	17.8	2.8
1	11.9	2.6
1.25	11.5	2.4
1.5	11.5	2.3
1.75	11.3	2.2
2	11.3	2.1

As the gas flow rate increased from 0.25 L/min to 1 L/min, *Bo* decreased significantly. Beyond 1 L/min, *Bo* appeared to stabilize just above 11. This indicated that no further significant improvement in axial liquid mixing was achieved at gas flow rates above 1 L/min. It also was deduced that significant axial liquid mixing was present at flow rates above 0.5 L/min, but the photobioreactor did not have characteristics of a perfectly mixed reactor. Instead, the photobioreactor had *Bo* values typical of internal airlift reactors in the range between 10 and 60 (Gavrilescu & Tudose, 1999). The mixing time t_m necessary to achieve 95% homogeneity in the reactor was then calculated from *Bo* using equation 27. t_m was observed to decrease from 4 s to 2.1 s as gas flow rate increased from 0.25 L/min to 2 L/min. t_m was also observed to reach an asymptotic value of approximately 2, indicating that gas flow rates beyond 2 L/min would have insignificant improvement liquid in mixing. Results from the determination of *Bo* and t_m will provide insight into the volumetric mass transfer characteristics of dissolved CO_2 in the photobioreactor, and will determine if the tested operating parameters are sufficient for cell growth.

Measurement of the gas holdup was also essential for understanding its effects on mixing and mass transfer. The gas holdup was measured only at the riser section and the gas entrainment space above it. Figure 25 showed that the gas holdup increased linearly with the air flow rate. The total gas holdup reached 6.5% at 2 L/min, which was the maximum gas flow rate investigated. The linear relationship suggested that a greater gas holdup can be attained at higher air flow rates, and this could result in greater liquid circulation and greater gas-liquid interfacial area available for mass transfer of CO_2 and O_2 (Chisti & Moo-Young, 1988). However, experiments at higher flow rates could not be conducted due to operational limitations of the experimental setup.

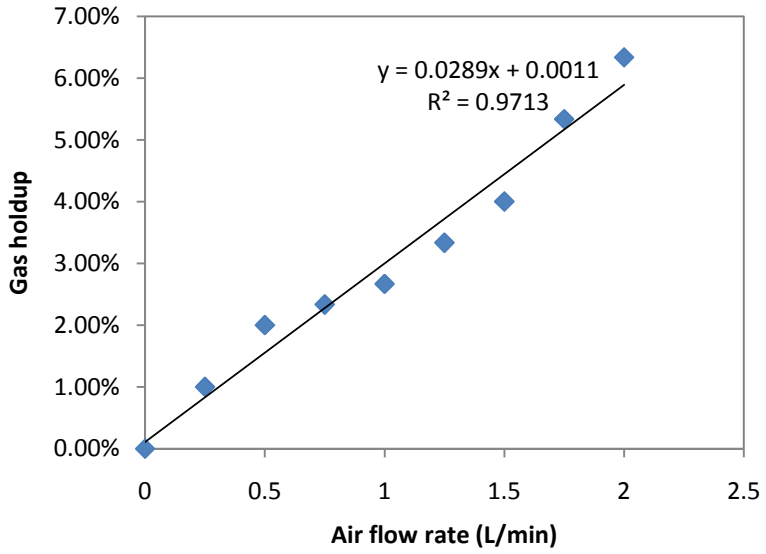

Figure 25: Relationship between gas holdup and gas flow rate

5.2 Aeration by CO_2-enriched air for mass transfer characterization in 2D photobioreactor

To optimize the aeration conditions for microalgal biomass production in an airlift photobioreactor, the effect of aeration rate on CO_2 mass transfer was investigated under given conditions. To understand whether cell growth was CO_2-limited under the experimental conditions, it was crucial to first analyze the mass transfer properties of the photobioreactor. The relationship between the volumetric mass transfer coefficient k_La and aeration rate was studied and parameters for enhanced k_La of CO_2 were determined. Air enriched with 5% or 10% (vvm) CO_2 was supplied for the experiments at rates of 0.5, 1, 1.5 and 2 L/min.

The following equation represents the CO_2 transfer rate into the culture medium:

$$\frac{dC}{dt} = k_L a(C_S - C) \qquad 40$$

where C (mol/m^3) is the dissolved CO_2 concentration (D_{CO2}) in the bulk liquid at any time t (s), and C_S is the saturation concentration of D_{CO2}. C_S was obtained by determining the maximum concentration recorded in the experiments.

In this experiment, the dynamic method is used to measure k_La. Integration of equation 1 yields an equation where k_La can easily be calculated:

$$k_L a = \frac{1}{t}\ln\left[\frac{C_o - C_s}{C - C_s}\right] \qquad 41$$

where C_o is the initial D_{CO2} concentration at time t=0. The same equations can be used to calculate k_La values for dissolved oxygen (D_{O2}). Measurements of D_{O2} were important in this study because they were required for calculations of k_La for D_{CO2} using the Rand and Marshall equations (Eq. 3).

As an example, Figure 23 shows the concentrations of D_{CO2} and D_{O2} at 33°C, constant gas flow rate of 0.5 L/min, and at 5% CO_2. These profiles were important for determining the saturation concentrations and volumetric mass transfer coefficients of D_{CO2} and D_{O2} for the specified conditions. The data was then regressed to fit the model described in Eq. 41 to yield k_La and C_S.

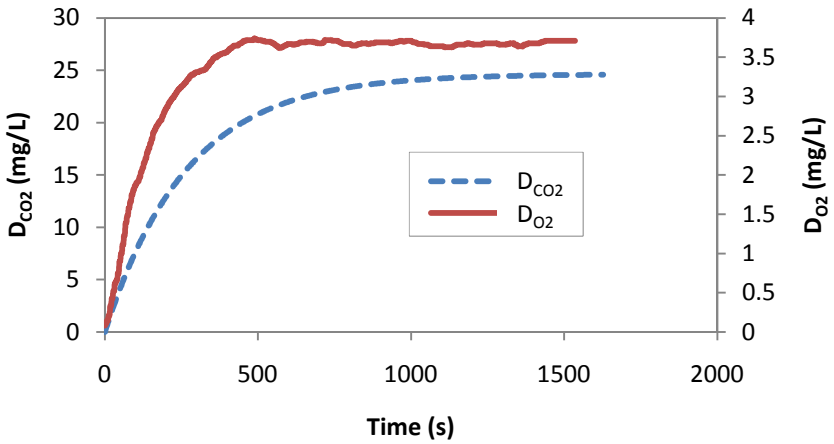

Figure 26: D_{CO2} and D_{O2} at 33°C, constant gas flow rate of 0.5 L/min, and at 5% CO_2

Figure 27, which shows k_La values for D_{CO2} at two temperatures and two inlet CO_2 concentrations, indicated that k_La values increased as the temperature increased from 23°C to 33°C. k_La values for D_{CO2} with air were not available as CO_2 concentrations were too low to be detected by the CO_2 electrode. A rise in temperature led to a decrease in surface tension of the liquid, generating smaller bubbles and higher k_La values (Bird, 2002). k_La values for D_{O2} showed no significant change as inlet CO_2 concentration increased.

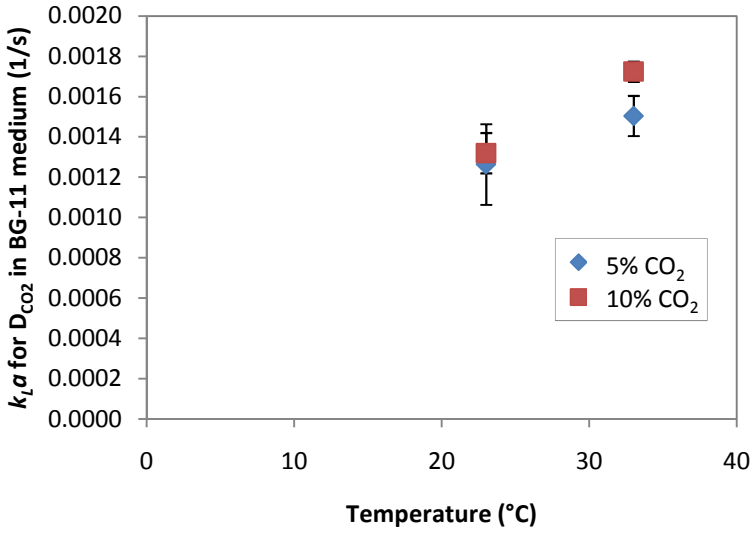

Figure 27: CO_2 k_La at 23°C and 33°C for a constant gas flow rate of 0.5 L/min

Figure 28 plots k_La values at various gas flow rates and CO_2 concentrations at a constant temperature of 33°C. As gas flow rate increased, k_La values rose. This was expected due to the additional mixing power the gas provided to the medium. The k_La values for 5% CO_2 were lower than the values at 10% CO_2 by approximately 10-24%. The dissociation of carbonic acid decreased the surface tension of the water, reducing the average bubble diameter and increasing total surface area (Beltran et al, 1998; Dos Santos & Levin, 2010). In other words, increasing the inlet CO_2 % increased k_La.

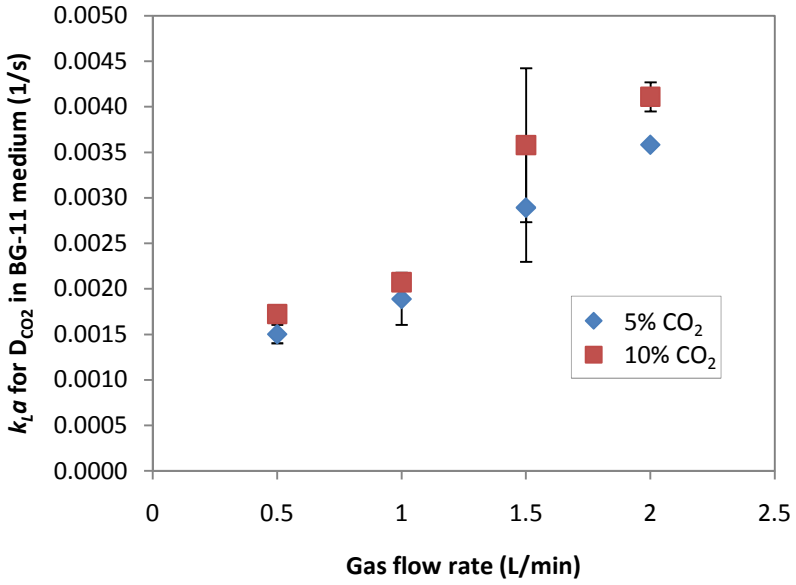

Figure 28: CO_2 k_La at various gas flow rates and a constant temperature of 33°C

For the same conditions, k_La values of D_{O2} in Figure 29 increased as inlet gas flow rate increased. These observations indicate that higher k_La values were possible at higher gas flow rates. The same relationship between the gas flow rate and k_La was also observed by Kazim (2011). However, the effect of shear stress on cells resulting from these higher gas flow rates was never previously investigated for this reactor configuration.

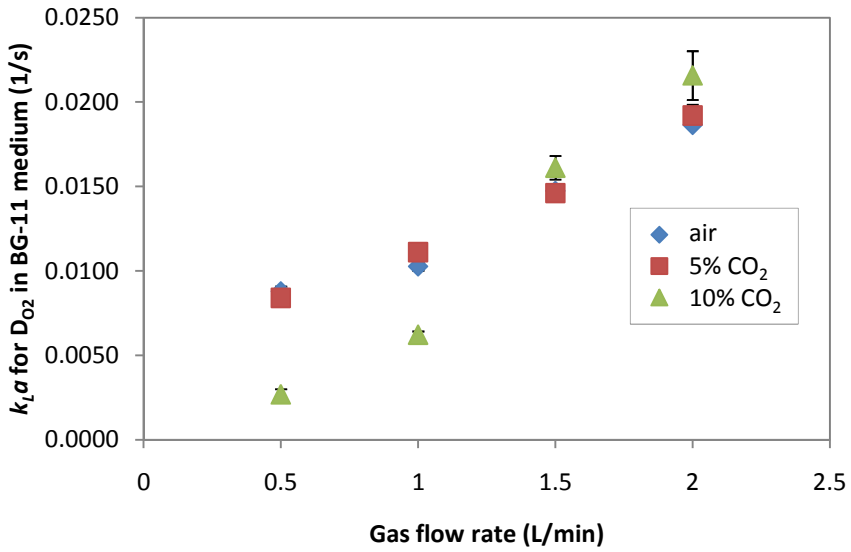

Figure 29: Oxygen k_La at various gas flow rates and a constant temperature of 33°C

Figure 29 showed that as the gas flow rate increased, k_La for oxygen also increased. There was a significant difference in k_La between 10% CO_2 and the other runs at flow rates below 1.5 L/min, but then k_La converged to similar values at 1.5 and 2 L/min. This was due to the higher gas flow rates that promoted greater liquid mixing by gas bubbles in the medium.

In Table 26, saturation concentrations for both D_{CO2} dropped as the temperature increased, which complied with literature results. This can be explained by the changes in water crystallinity. Elevated temperatures increase the kinetic energy of water molecules, disturbing its crystalline structure and allowing gas molecules to escape, thereby lowering gas solubility (Bird, 2002). At both temperatures of 23°C and 33°C, C_S values at 10% inlet CO_2 were almost double that of 5% inlet CO_2.

Table 26: Saturation concentration for CO_2 at 23°C and 33°C and a constant gas flow rate of 0.5 L/min

Temperature	CO_2 concentration	
	5% CO_2	10% CO_2
23°C	79.9 mg/L	151.9 mg/L
33°C	62.0 mg/L	116.3 mg/L

In Figure 30, C_S values for D_{CO2} at 5% and 10% CO_2 did not change significantly at the tested range of gas flow rates. Similarly, C_S values for D_{O2} were relatively constant.

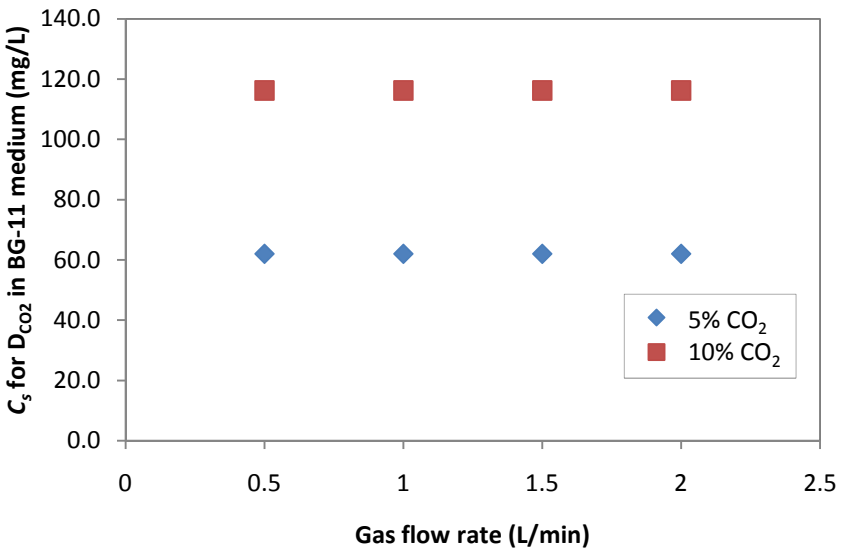

Figure 30: Saturation concentration of CO_2 at various gas flow rates and a constant temperature of 33°C

As shown in Figure 31, when varying the inlet CO_2 concentrations and gas flow rates, D_{O2} remained relatively constant. Calculations of superficial gas velocity showed that the reactor was in bubbly flow regime at the tested gas flow rates.

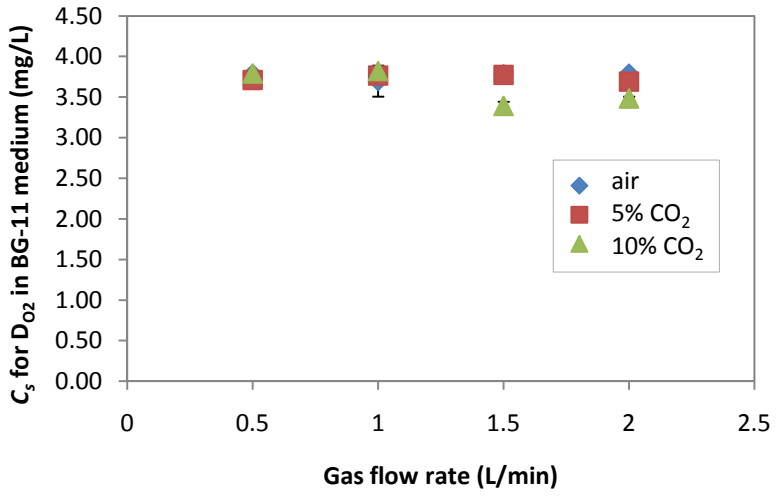

Figure 31: Saturation concentration of O_2 at various gas flow rates and a constant temperature of 33°C

Like the dependence of k_La on the gas flow rate, the gas hold up was found to be directly proportional to the gas flow rate at the tested parameters, as shown in Figure 32.

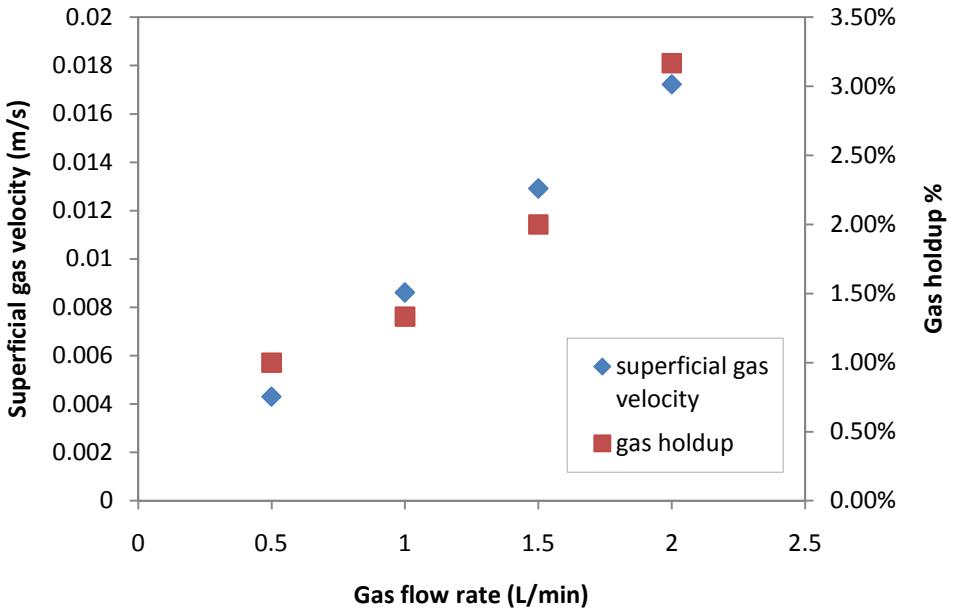

Figure 32: Superficial gas velocities and gas hold-ups at various flow rates

A summary of k_La values for CO_2 is tabulated in Table 27. Errors were obtained by calculating the standard deviation of the experimental data. Experiments were performed in duplicates.

Table 27: Comparison of k_La values at different inlet gas flow rates and CO_2 %. T=33°C

Flow rate (L/min)	k_La values for O_2-BG11 medium system (h^{-1})		
	0.04% CO_2	5% CO_2	10% CO_2
0.5 L/min	0.0088 ± 0.0004	0.0084 ± 0.0007	0.0027 ± 0.0003
1 L/min	0.0103 ± 0.0003	0.0111 ± 0.0000	0.0062 ± 0.0002
1.5 L/min	0.0147 ± 0.0004	0.0146 ± 0.0003	0.0161 ± 0.0007
2 L/min	0.0186 ± 0.0006	0.0192 ± 0.0006	0.0216 ± 0.0014
	k_La values for CO_2-BG11 medium system (h^{-1})		
	0.04% CO_2	5% CO_2	10% CO_2
0.5 L/min	-	0.0015 ± 0.0001	0.0017 ± 0.0001
1 L/min	-	0.0019 ± 0.0003	0.0021 ± 0.0001
1.5 L/min	-	0.0029 ± 0.0006	0.0036 ± 0.0008
2 L/min	-	0.0036 ± 0.0001	0.0041 ± 0.0002

A rise in temperature resulted in increases of CO_2 and O_2 k_La in the BG-11 medium and drops in the maximum dissolved CO_2 and O_2 concentrations. An increase in gas flow rate also led to an increase in both k_La values due to the higher rate of bubbles and agitation supplied to the medium. Increasing CO_2 concentration led to an increase in k_La value, possibly because of the

formation of carbonic acid and the associated reduction in the gas-water surface tension. Experimental results suggest that operation of the airlift photobioreactor at 33°C, 5% CO_2, and high gas flow rates will yield high volumetric mass transfer coefficients in the BG-11 system. However, light intensity and temperature optimization experiments conducted earlier in shake flasks suggested that studies at light intensities lower than 120 $\mu E/m^2/s$ should be carried out to determine its effects on cell growth. Although increasing the gas flow has been shown to improve k_La values, providing high flow rates is energy intensive. Given the *Bo* values in Table 25, selecting a flow rate of 1 L/min provides the necessary CO_2 transfer while sustaining good axial liquid mixing. This is equivalent to 1 vvm (gas volume flow per unit of liquid volume per minute), which is commonly used in airlift photobioreactors (Hong et al, 2013). Keeping the flow rate and temperature constant at 1 L/min and 33°C will allow for a reduced number of runs and greater focus on the effects of light intensity and inlet CO_2 concentration on the growth of *S. elongatus*.

6 Optimization of X_{max} and μ_{max} in photobioreactor

Following the initial results, which indicated that a temperature of 33°C yielded the highest X_{max} and μ_{max} and a gas flow rate of 1 L/min provided sufficient CO_2 mass transfer, an experiment designed and conducted to test a range of growth conditions. The effect that light intensity and CO_2 concentration had on X_{max} and μ_{max} in the photobioreactor was analyzed. Optimal reactor conditions that maximized total biomass yield were then determined.

A factorial experimental design was developed for this study. The range of each variable was chosen based on results from the previous light and temperature experiments and the mass transfer experiment. Light intensities greater than 120 μE/m^2/s induced photoinhibition. Gas flow rates of at least 1 L/min were shown to provide good CO_2 mass transfer. Conditions that maximize X_{max} and μ_{max} were therefore sought. Table 28 outlines the reactor conditions studied. The gas flow rate was kept constant at 1 L/min and the temperature was also maintained at 33°C. The results from this experiment on growth in the photobioreactor are presented in Table 29. Growth curves are plotted in Appendix C.

Table 28: Factorial design of reactor conditions

Independent variable	Symbol	Level		
		-1	0	1
Light intensity (μE/m^2/s)	X_7	60	n/a	120
CO_2 %	X_8	0.04	5	10

The light intensity had a relatively insignificant effect on both μ_{max} and X_{max} in comparison to the inlet CO_2 concentration. As the CO_2 concentration increased from 0.04% (air) to 10%, μ_{max} decreased by 62%, which was caused by the increasing acidity of the medium. However, the highest X_{max} was observed at 5% CO_2 cultivation. Further increasing the CO_2 concentration above 5% appeared to inhibit cell growth because the cells experienced a lower pH (6.42-6.65) in the lag phase caused by formation of carbonic acid. That was because *S.elongatus* PCC 7942, an alkaliphilic cyanobacterium, exhibits the optimum growth at pH values between 7.0 and 9.0 (Billini, 2008).

Table 29: Results of full factorial design in airlift photobioreactor

Light intensity ($\mu E/m^2/s$)	CO_2 %	X_{max} (g/L)	μ_{max} (1/h)
X_7	X_8		
60	0.04	0.316	0.0504
120	0.04	0.405	0.0373
60	5	1.066	0.0255
120	5	1.006	0.0234
60	10	0.765	0.0189
120	10	0.879	0.0194

Table 30 shows the significance of each factor on μ_{max}. Only CO_2 % had a significant effect on μ_{max}. The negative coefficient indicates that μ_{max} decreases as CO_2 % increases.

Table 30: Optimization of light intensity and CO_2 % for response μ_{max} in photobioreactor (R^2=0.85)

Variable	Effect	Standard error	*t*-value	*p*-value	Confidence level (%)
Base	0.02915	0.00257	11.37	0.0015	99.85*
CO_2 %	-0.0124	0.00314	-3.93	0.0293	97.07*
Light intensity ($\mu E/m^2/s$)	-0.00245	0.00257	-0.96	0.410	59.00

*significant at 95% level (p<0.05)

The statistical model for μ_{max} was represented by the following equation in terms of CO_2 %, where X_8 is the effects coding for CO_2 % (ie. -1, 0, 1):

$$\mu_{\max} = 0.02915 - 0.0124X_8 \qquad 42$$

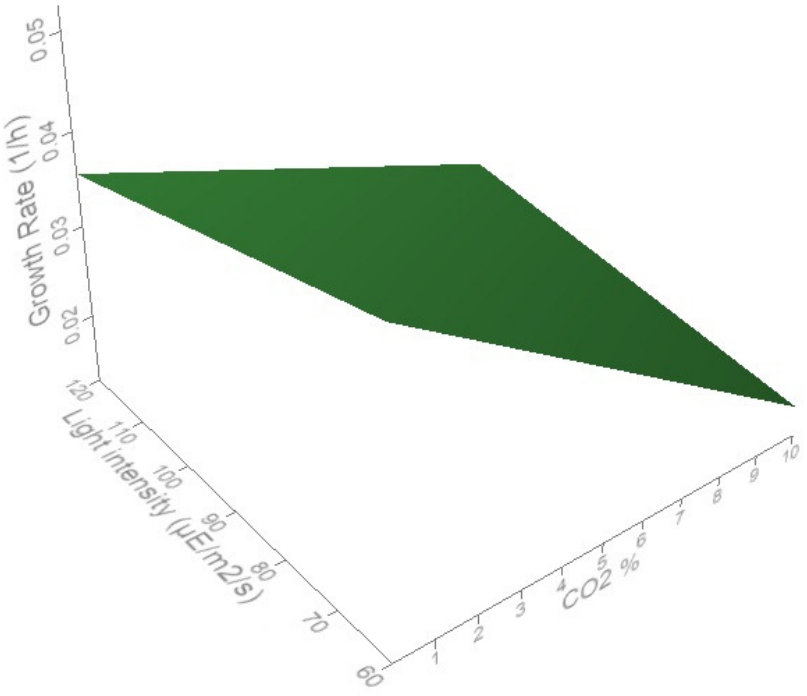

Figure 33: Response curve for μ_{max} as a function of light intensity and CO_2 % (R^2=0.85)

Figure 33 displays the response curve for μ_{max}. The light intensity had no significant effect on the response. On the other hand, increasing the CO_2 concentration to 5% and 10% reduced μ_{max} because excess carbonic acid in the medium dropped the pH below 7 for the first 60-70 hours, as shown in Figure 34. *S. elongatus* has been known to grow best at pH values between 7 and 9, and pH values below this range caused deterioration of cells and formation of toxic by-product (Billini, 2008). The low initial pH values at CO_2-enriched conditions explained why low μ_{max} values were observed. Secondly, any abrupt changes in the conditions that the cells were exposed to as they were transferred from inoculum conditions to shake flask and PBR conditions slowed growth. The more extreme the change, the longer it took for the cells to adapt to the new environment.

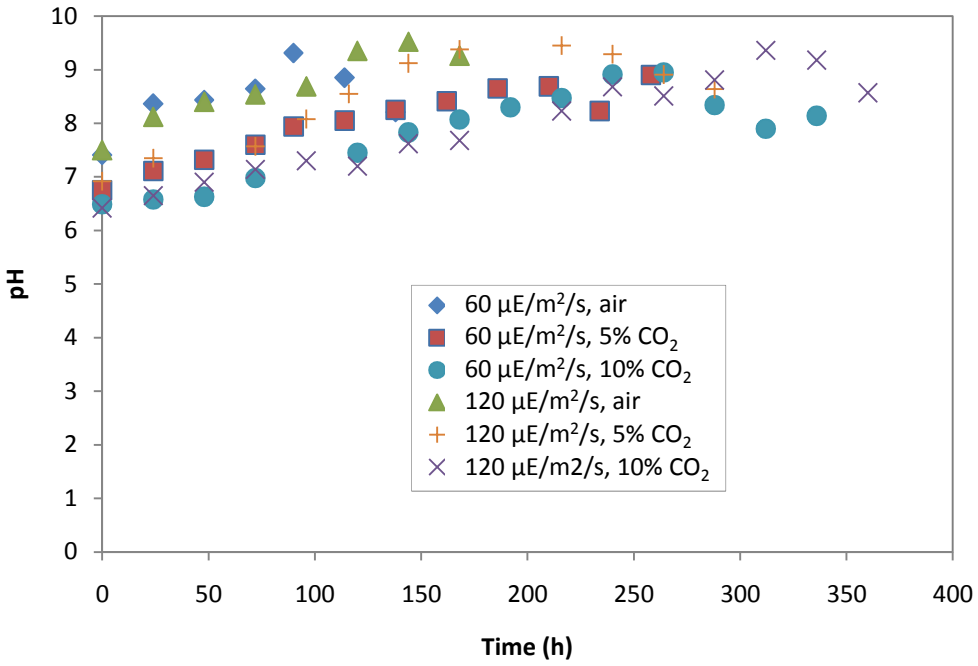

Figure 34: Culture pH at various conditions in the photobioreactor at 33°C and 1 L/min gas flow rate

The same data were also used to develop another statistical model for X_{max}. Table 31 tabulates the parameter estimates along with the corresponding confidence levels.

Table 31: Optimization of light intensity and CO_2 % for response X_{max} in photobioreactor (R^2=0.44)

Variable	Effect	Standard error	*t*-value	*p*-value	Confidence level (%)
	0.7395	0.123	6.01	0.0092	99.1*
CO_2 %	0.2308	0.151	1.53	0.223	77.7
Light intensity (µE/m^2/s)	0.0238	0.123	0.19	0.859	14.1

None of the response variables were significant at 95% confidence. Both factors had no significant effects on X_{max}, and the relationship between the factors and X_{max} was not linear. As a result, it was not possible to develop a statistical model for a first order response surface.

Figure 35 plots the data of X_{max} for CO_2 % of 0.04, 5, and 10% and light intensities of 60 and 120 µE/m^2/s.

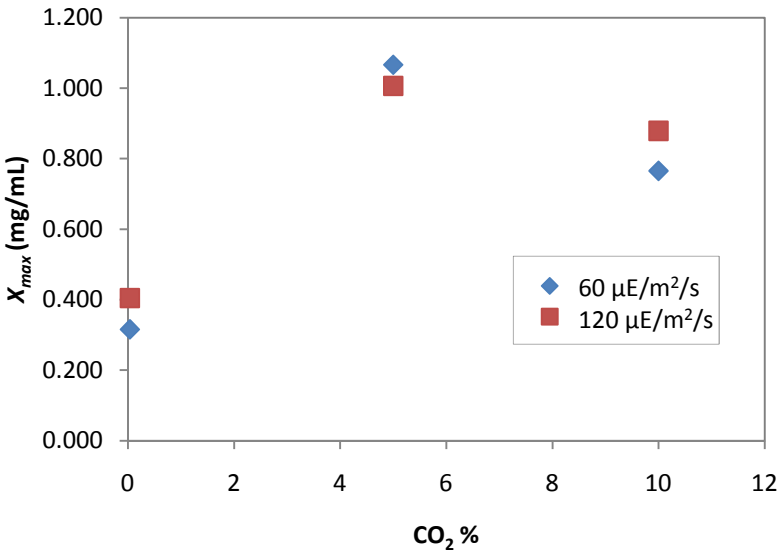

Figure 35: X_{max} for 0.04, 5 and 10% CO_2, and 60 and 120 µE/m^2/s light intensity

Figure 36 plots the data of μ_{max} for the same CO_2 % and light intensities. The fitted model provided a good representation of μ_{max} when inlet CO_2 % varied.

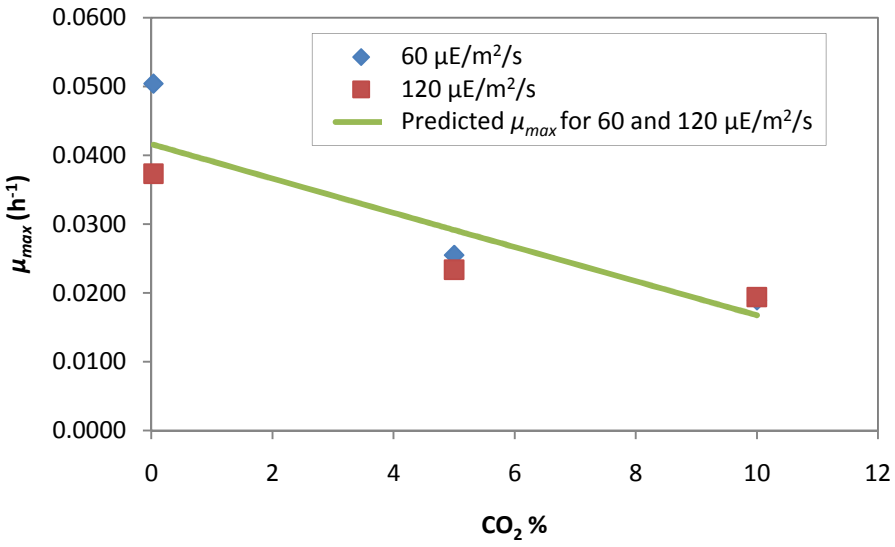

Figure 36: Specific growth rate μ_{max} for 0.04, 5 and 10% CO_2, and 60 and 120 µE/m^2/s light intensity

6.1 Effects of light intensity on growth

The first observation made was that light intensity had a small effect on X_{max} and μ_{max}. An increase from 60 to 120 µE/m^2/s resulted in an increase of X_{max} of 28% in air, a drop of 5.5% in

5% CO_2, and an increase of 14.8% in 10% CO_2. This result confirmed the findings of the light intensity experiments in shake flasks, in which the light-limiting regime was observed at light intensities below 120 µE/m^2/s.

The same increase in light intensity decreased μ_{max} by 25.9% in air, 8.3% in 5% CO_2, and increased μ_{max} by 2.4% in 10% CO_2. μ_{max} seemed to drop as CO_2 % decreased. Furthermore, it appeared that under 120 µE/m^2/s, cell growth was severely limited if dissolved CO_2 was at a limiting concentration of 0.24 ppm CO_2. No research has been conducted on the effects of CO_2 % on μ_{max} under various light intensities for *S. elongatus* PCC 7942 so a comparison with published results could not be made.

To ensure reproducibility of results, a duplicate run for 5% CO_2 at 60 µE/m^2/s was conducted. As shown in Table 32, the percent change in the measured μ_{max} was 5%. The replicate results generally agreed with the original results.

Table 32: Reproducibility of growth rate data from the photobioreactor

Conditions	Run	X_{max} (g/L)	μ_{max} (h^{-1})
33°C, 5% CO_2, 1 L/min, 60 µE/m^2/s	1	1.066	0.0255
	Replicate	0.978	0.0239

6.2 Effects of inlet CO_2 concentration on growth

A change in CO_2 concentration at the investigated parameters was shown to have a greater effect on X_{max} and μ_{max} when comparing with a change in light intensity. A higher CO_2 concentration resulted in a lower initial pH in the medium. This caused cells to grow at a slower rate. As cells adjusted to the more acidic environment, the growth rate began to accelerate by the 3rd day. It was at this point where growth curves diverged from each other. The highest X_{max} observed was 1.066 g/L at conditions of 120 µE/m^2/s and 5% CO_2. The lowest X_{max} observed was 0.316 g/L at 60 µE/m^2/s and in air. A high μ_{max} was observed when *S. elongatus* was cultivated in air. The relatively lower μ_{max} was likely caused by the formation of carbonic acid, which lowered the pH, and this was only present in the growth runs with CO_2-enriched air.

To investigate which conditions made CO_2 concentration a limiting factor on cell growth, the logistic equation (Eq. 20), CO_2 mass balance equation (Eq. 21), and Rand and Marshall equation

(Eq. 3) were solved and graphed using Polymath 6.0. Appendix D details the defining equations, parameters, and initial values for each experiment.

Figure 37 plots the total carbon content in medium and the total carbon content in biomass at 1 L/min air flow rate, 33°C and 60 μE/m^2/s. All of the CO_2 absorbed into the medium was taken up by the algae cells, indicating that the growth was limited by the low availability of CO_2. The total mass of carbon takes into account the CO_2 absorbed from gas bubbles, CO_2 originally saturated in the medium at the beginning of the experiment, sodium carbonate in the medium, and the carbon from biomass. A closer inspection showed that the total carbon content in the medium slightly exceeded the total amount of carbon in the biomass, indicating that an extremely small amount of dissolved CO_2 in the medium was present throughout the cultivation.

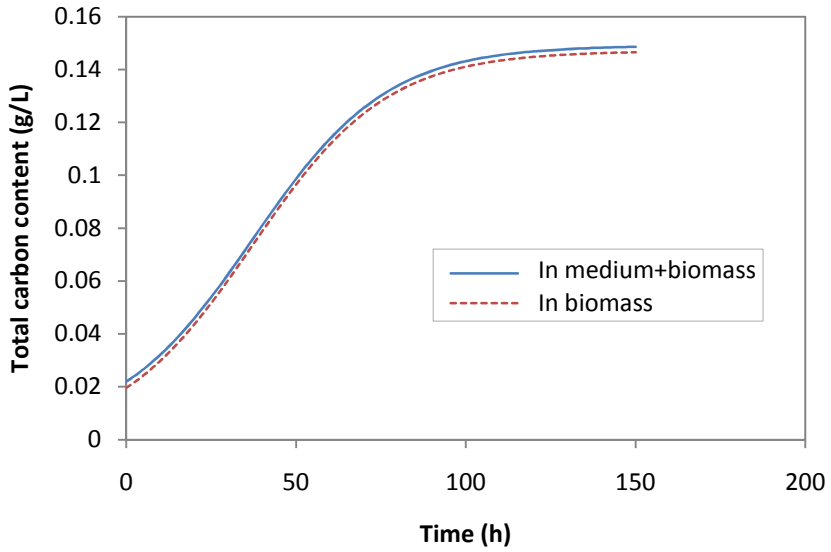

Figure 37: Carbon balance from *S. elongatus* growth in air at 1 L/min, 33°C, 60 μE/m^2/s

A similar trend was observed for 5% CO_2 in Figure 38. There was a greater difference in mass of carbon between the two curves because of the higher dissolved CO_2 concentration in the medium. This reinforced the hypothesis that CO_2 % was a limiting factor of growth for cultivations with air.

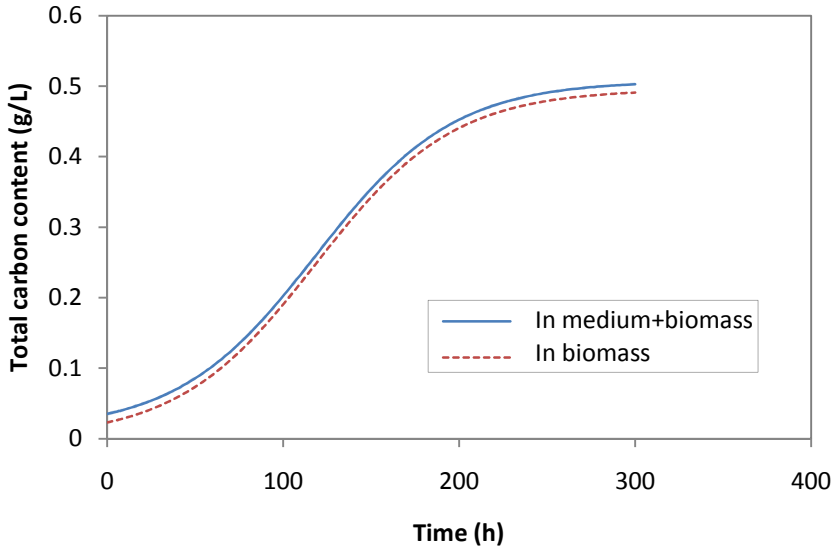

Figure 38: Carbon balance from *S. elongatus* growth in 5% CO_2 at 1 L/min, 33°C, 60 µE/m^2/s

By comparing the carbon content of 5% in Figure 38 and 10% CO_2 in Figure 39, a few observations were made. Increasing the inlet CO_2 concentration from 5% to 10% increased the amount of dissolved CO_2 but lowered X_{max}. As concluded from observations made in Figure 33, dissolved CO_2 was available in excess but the higher acidity limited cell growth. The effect of excess carbonic acid was more pronounced beyond 5% CO_2, leading to the hypothesis that an optimal CO_2 % must exist somewhere close to 5%. At this optimal concentration, the highest X_{max} may be achieved, assuming all other parameters are held constant.

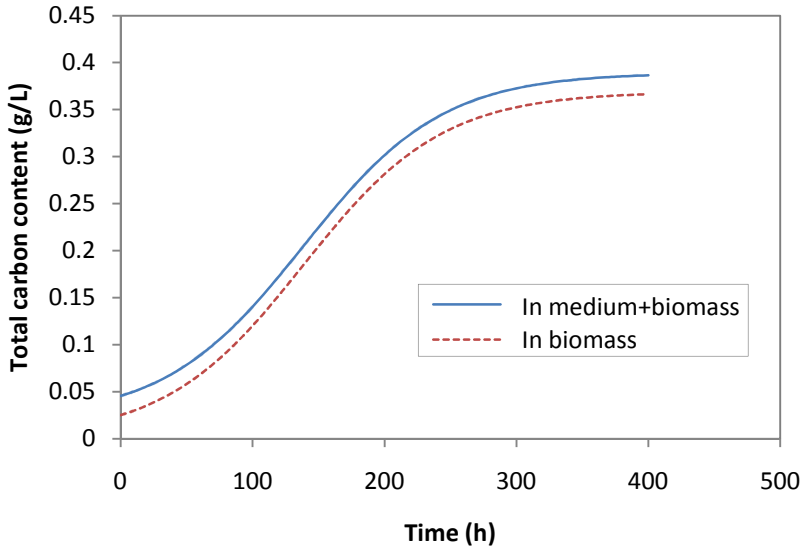

Figure 39: Carbon balance from *S. elongatus* growth in 10% CO_2 at 1 L/min, 33°C, 60 µE/m^2/s

A review of literature has shown similar trends based on research using the same freshwater strain and *Chlorella vulgaris*. Kajiwara (1997) showed that 5% CO_2 yielded the highest X_{max} (0.98 g/L) amongst growth runs of 0.04%, 5%, 10%, and 15% CO_2. However, because Kajiwara utilized HEPES buffer in the BG-11 medium, μ_{max} was about 0.044 h^{-1}, which was 73% higher than μ_{max} obtained in this experiment. This can be attributed to the alkalinic pH and shorter lag phase in Kajiwara's research. In Sasi's research with *Chlorella vulgaris*, the highest X_{max} was also recorded at 5% CO_2 (Sasi, 2009). Any further increase in CO_2 % led to a drop in biomass yield. This was evidenced that inhibition of cell growth was a common response of microalgae at high dissolved CO_2 concentrations and it was important to determine the optimal inlet CO_2 % for economical cultivations. However, growth of *S.elongatus* at other CO_2 concentrations (between 0.04 and 10%) and other gas flow rates (between 1 and 2 L/min) merits further investigation as the concentration of dissolved CO_2 can be adjusted by changing both parameters. This may lead to improved X_{max} and μ_{max} values.

6.3 Effect of 12:12 h light/dark cycle on *S. elongatus* growth

To investigate whether the introduction of light/dark cycles can potentially improve cell growth of *S. elongatus* compared to conditions in continuous lighting, an experiment was implemented for the purpose of culturing cells under 12:12 h light/dark cycle. The experimental conditions

were chosen based on the conditions that yielded the best biomass growth from the previous photobioreactor runs; ie. 33°C, 60 µE/m^2/s, 5% CO_2 @ 1 L/min.

Figure 40 showed that X_{max} for growth under continuous lighting was 64.6% higher than X_{max} for growth under the light/dark cycle. Similarly, μ_{max} for growth under continuous lighting was 27.0% higher than μ_{max} for growth under the light/dark cycle.

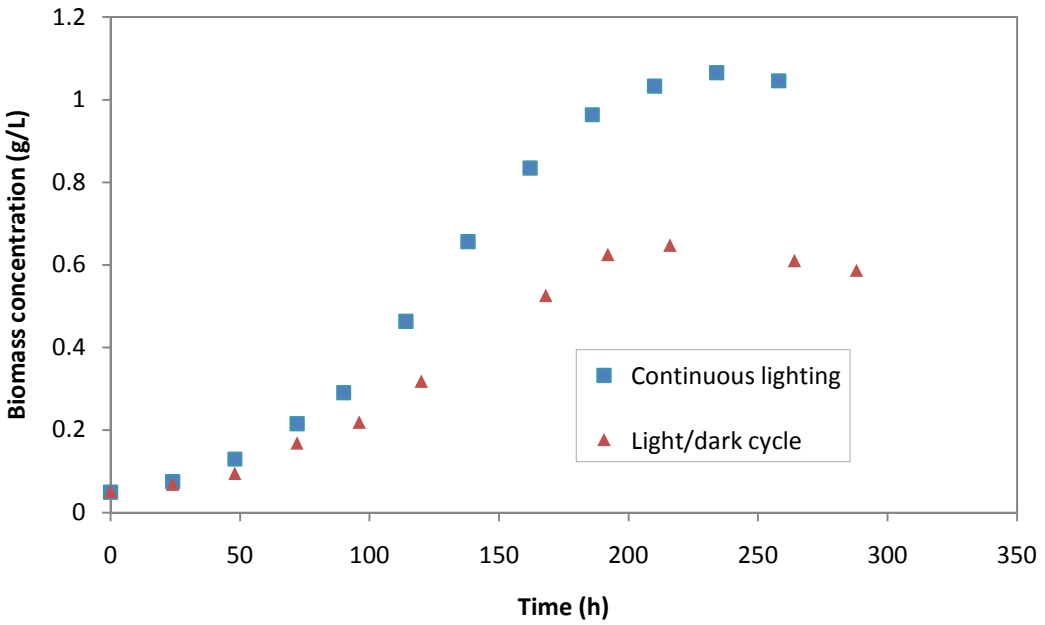

Figure 40: Comparison of growth in continuous light and 12:12 light/dark cycle at 33°C, 60 µE/m^2/s, 5% @1 L/min

Table 33 lists X_{max} and μ_{max} values for each condition. It appeared that the light/dark cycle had a significant negative effect on cell growth using the response variables as a basis for comparison.

Table 33: Results for growth under continuous light and 12:12 light/dark cycle

Light intensity (µE/m^2/s)	CO_2 %	X_{max} (g/L)	μ_{max} (h^{-1})
X_7	X_8		
60 - Continuous	5	1.066	0.0255
60 - 12:12 light/dark	5	0.648	0.0201

Nonetheless, it was also important to analyze the energy consumption in cultivating the cells under the two difference lighting conditions to see whether energy savings can be incurred without compromising cell growth. Normalizing input power per gram biomass gives:

Table 34: Energy input required for growth at continuous light and 12:12 light/dark cycle

Light intensity (µE/m^2/s)	Input power/g biomass (W/g)
60 - Continuous	30.0
60 - 12:12 light/dark	24.7

It appeared that growth under light/dark cycle was 17.7% more energy efficient in producing biomass. To put this in perspective, using a 12:12 light/dark cycle saved 17.7% in energy usage but resulted in a drop of 39.2% for X_{max} and 21.3% for μ_{max}. This probably would not be an economical trade-off. For the purpose of cultivating *S. elongatus* to achieve a high biomass yield under economical conditions, continuous light would be recommended.

7 Conclusion

A response surface method was adequate for determining the effects of each BG-11 medium component in order to maximize growth of *S. elongatus* PCC 7942. At the investigated range of component concentrations, results from an optimization experiment to determine the specific concentrations of these components generated the following response surface model for X_{max} (g/L) in terms of effects coding X_i:

$$X_{\max} = 0.386 - 0.032X_1 + 0.018X_2 + 0.022X_4 + 0.022X_5 \quad (36)$$

as well as for μ_{max}:

$$\mu_{\max} = 0.326 - 0.0052X_2 - 0.0033X_3 - 0.0021X_4 \quad (37)$$

Where:

X_1 = $NaNO_3$

X_2 = K_2HPO_4

X_3 = $CaCl_2$

X_4 = $C_6H_{11}FeNO_7$

X_5 = Na_2CO_3

Comparison of cell growth in unmodified BG-11 medium and optimized media showed that there was no significant increase in X_{max} and μ_{max}, indicating that the unmodified medium was suitable enough for high algal productivity.

Studies conducted in a shake flask scale demonstrated that an optimal temperature of 33°C and an optimal light intensity of 120 μE/m^2/s gave the highest X_{max}, 0.496 g/L, and the highest μ_{max}, 0.0519 h^{-1}, for the tested range of growth parameters. Below 30°C, the cells experienced a remarkable drop in both X_{max} and μ_{max}. Light intensity had little effect on both responses. Cells experienced a slight decrease in both responses as the light intensity increased, which may possibly indicate the presence of photoinhibition at light intensities greater than 150 μE/m^2/s. Equations represents the statistical model for X_{max} and μ_{max}, respectively.

$$X_{\max} = 0.490 + 0.0307X_6 - 0.0641X_6^2 \quad (38)$$

$$\mu_{\max} = 0.0504 + 0.00463X_6 - 0.00669X_6^2 \quad (39)$$

Where X_6 is the effects coding of temperature. These optimized parameters were subsequently used for the optimization experiments in the flat-plate photobioreactor.

To identify the best operating range of inlet gas flow rates in the photobioreactor, it was important to analyze changes in axial mixing in terms of the Bodenstein number *Bo*. As the gas flow rate increased from 0.25 L/min to 1 L/min, *Bo* dropped from 48.7 to 11.9. Beyond 1 L/min, *Bo* was observed to stabilize at approximately 11, meaning that any further increase in gas flow rate had no significant improvement in axial mixing.

To determine the photobioreactor conditions in which cell growth was CO_2-limited, experiments which studied the effects of inlet CO_2 %, gas flow rate, and temperature on the volumetric mass transfer coefficient k_La were conducted. In general, increases of each factor enhanced k_La values. k_La values increased 10-24% when the inlet CO_2 % doubled from 5% to 10%. Ramping up the gas flow rate improved gas-liquid mixing and consequently k_La values. A rise in temperature from 23°C to 33°C resulted in 19-31% increase in k_La due to the decrease in surface tension of the gas-liquid interface, creating smaller bubbles. Additionally, increasing the inlet CO_2 concentration from 5% to 10% doubled the saturation concentration of dissolved CO_2. Similar changes in k_La values of dissolved O_2 were also observed. These results led to the decision to cultivate algae at the optimal temperature of 33°C and gas flow rate of 1 L/min.

Results from the algae cultivation experiments in the photobioreactor presented several significant discoveries. As the CO_2 concentration increased from 0.04% (air) to 10%, μ_{max} dropped by 62%, and this was caused by the increasing acidity of the medium which hindered cell growth. However, the highest X_{max} was observed at 5% CO_2 for each investigated light intensity. In comparison, X_{max} at 0.04% and 10% CO_2 were noticeably less. Cell growth using air was CO_2-limited, which was confirmed by performing a mass balance on carbon; cultivations were not CO_2-limited at higher CO_2 %. Formation of excess carbonic acid at 10% CO_2 lowered pH and hindered reproduction. A change in light intensity did not significantly affect the responses. To attain the highest biomass concentration at a relatively fast rate, it is recommended to operate the photobioreactor at 33°C, 120 μE/m^2/s, and 1 L/min at 5% CO_2.

Including a 12 hour dark phase to the photobioreactor did not improve X_{max} or μ_{max}. However, when normalizing the input power per gram of biomass produced, growth under light/dark cycle

was 17.7% more energy efficient in producing biomass when compared to growth in continuous illumination. Yet this resulted in a drop of 39.2% for X_{max} and 21.3% for μ_{max}, which was not desirable from a productivity standpoint.

Ultimately, this work has demonstrated that there is a future for commercial production of high-value microalgal products. By utilizing enhanced photobioreactor design and proper selection of operating parameters, the growth rate of *S. elongatus* can be significantly enhanced. Additional research is still required to realize the full potential of microalgae for production of recombinant product in a commercial scale. Nevertheless, continued studies on the effects of various parameters on *S. elongatus* growth will lead to more breakthroughs that can eventually establish economical production of microalgae-derived high-value products. Ecological engineering such as this serves as a prime example of the current paradigm shift towards the "green" movement and places algae at the forefront of clean biotechnology.

8 Future Work

The use of flashing lights to increase the frequency of light and dark cycles in photosynthesis and possibly biomass productivity can be investigated by using LEDs. The flashing light effect has the potential to increase growth rate by better matching the time scales of photosynthetic reactions or save energy by minimizing wasted irradiation (Lunka, 2013).

Several areas have been identified which have the potential to improve the cultivation economics. Additional research on cultivation under sunlight or LEDs needs to be explored. Although limited by weather and geographic location, availability of sunlight is an attractive alternative to using CFL bulbs for cost savings. LEDs are also known to save in energy costs as they require relatively low power. Another approach is to use the microalgae to fixate CO_2 from pre-treated flue gases. Power-plant flue gas can serve as a source of CO_2; however the costs in removing toxic SO_x and NO_x gases harmful to microalgae are a subject of investigation.

To assess the viability of using microalgae as a vehicle for production of value-added compounds, a trial run with a recombinant strain that produces an enzyme with commercial potential should be conducted. Examples of test enzymes may include cellulases and research enzymes with high profit margins.

Finally, the possibility of using Aspen Plus to conduct the economic optimization of the photobioreactor conditions should be explored. Aspen Plus can be used to generate mass, energy, and utility balances over a range of cultivation conditions. In terms of scale-up production, design of a photobioreactor is crucial because a high cultivation volume is desired without compromising biomass productivity. These data can then be exported to Microsoft Excel where an economic analysis can be conducted. Economic optimization could be performed within Aspen Plus utilizing the optimization tool, and as a result a complete set of optimum process conditions could be determined. Improved optimization of reactor conditions would reduce cultivation costs.

Bibliography

Alabi, A., Tampier, M., & Bibeau, E. (2009). *Microalgae technologies and processes for Biofuels/Bioenergy production in British Columbia*. British Columbia: Seed Science Ltd.

Andersen, R. A. (2005). *Algal culturing techniques* Academic Press.

Beltran, F., Fernandez, L., Alvarez, P., & Rodriguez, E. (1998). Comparison of ozonation kinetic data from film and Danckwerts theories. *Ozone: Science & Engineering, 20*(5), 403-420.

Ben-Amotz, A. (2008). *Bio-fuel and CO2 capture by algae.* Seambiotic.

Benemann, J. R. (1997). CO2 mitigation with microalgae systems. *Energy Conversion and Management, 38, Supplement*(0), S475-S479.

Benemann, J. R., & Oswald, W. J. (1996). *Systems and economic analysis of microalgae ponds for conversion of CO2 to biomass*. Pittsburgh, PA: Pittsburgh Energy Technology Center.

Billini, M., Stamatakis, K., & Sophianopoulou, V. (2008). Two members of a network of putative Na+/H+ antiporters are involved in salt and pH tolerance of the freshwater cyanobacterium Synechococcus elongatus. *Journal of Bacteriology, 190*(19), 6318-6329.

Bird, R. B., Stewart, W. E., & Lightfoot, E. N. (2007). *Transport phenomena.* Wiley.

Blenke, H. (1979). Loop reactors. In T. K. Ghose, N. Blakebrough & A. Fiechter (Eds.), (pp. 121-214). Springer Berlin Heidelberg.

Boogerd, F. C., & Kuenen, J. G. (1990). Oxygen and Carbon Dioxide Mass Transfer and the Aerobic, Autotrophic Cultivation of Moderate and Extreme Thermophiles: A Case Study Related to the Microbial Desulfurization of Coal. *Biotechnology and Bioengineering*. *35*, 1111-1119.

Borowitzka, M. (1995). Microalgae as sources of pharmaceuticals and other biologically active compounds. Springer Netherlands.

Bulgakov, G., & Levich, P. (1999). *The nitrogen : Phosphorus ratio as a factor regulating phytoplankton community structure : Nutrient ratios*. Stuttgart, ALLEMAGNE: Schweizerbart.

Carlsson, A. S., van Beilen, J., Möller, R., & Clayton, D. (2007). *Micro- and macro-algae: Utility for industrial applications*. UK: University of York.

Chisti, Y., & Moo-Young, M. (1988). Gas holdup behaviour in fermentation broths and other non-Newtonian fluids in pneumatically agitated reactors. *The Chemical Engineering Journal, 39*(3), B31-B36.

Chisti, Y., & Moo-Young, M. (1993). Improve the performance of airlift reactors. *Chemical Engineering Progress,* , 38-45.

Dauvillée, D., & Delhaye, S. (2010). Engineering the chloroplast targeted malarial vaccine antigens in *chlamydomonas* starch granules. *PLoS ONE, 5*(12)

De Philippis, R., Colica, G., & Micheletti, E. (2011). Exopolysaccharide-producing cyanobacteria in heavy metal removal from water: Molecular basis and practical applicability of the biosorption process. *Applied Microbiology and Biotechnology, 92*(4), 697-708.

Deshmukh, D., Mane, A., Vhare, P., & Harke, S. (2013). Optimization of media component affecting phycocyanin production from *microcystsis* sp. Isolated from salim ali lake, aurangabad. [null] *Journal of Algal Biomass Utilization, 4*(2), 42-46.

Dhir, S., Morrow, K. J., Rhinehart, R. R., & Wiesner, T. (2000). Dynamic optimization of hybridoma growth in a fed-batch bioreactor. *Biotechnology and Bioengineering, 67*(2), 197-205.

Doran, P. M. (2012). *Bioprocess engineering principles* Elsevier Science.

Dos Santos, A. P., & Levin, Y. (2010). Surface tensions and surface potentials of acid solutions. *The Journal of Chemical Physics, 133*, 154107.

Doucha, J., Straka, F., & Lívanský, K. (2005). Utilization of flue gas for cultivation of microalgae chlorella sp.) in an outdoor open thin-layer photobioreactor. *Journal of Applied Phycology, 17*(5), 403-412.

Dunwell, J. M., & Ford, C. S. (2005). *Technologies for biological containment of GM and non-GM crops* . UK: University of Reading.

Environment Canada. (2012a). *Canada's emission trends*. Canada: Government of Canada.

Environment Canada. (2012b). *Reducing Greenhouse Gases.* Canada: Government of Canada.

Environment Canada. (2012c). *National inventory report 1990-2010*. Canada: Government of Canada.

Enzing, C., & Nooijen, A. (2012). *Algae and genetic modification*. Netherlands: COGEM.

Espinosa, J., Forchhammer, K., & Contreras, A. (2007). Role of the synechococcus PCC 7942 nitrogen regulator protein PipX in NtcA-controlled processes. *Microbiology, 153*(3), 711-718.

Flaherty, J. M. (2009). *Canada's economic action plan*. Canada: Department of Finance.

Gavrilescu, M., & Tudose, R. Z. (1999). Modelling mixing parameters in concentric-tube airlift bioreactors. *Bioprocess Engineering, 20*(6), 491-497.

Geider, R. J., & Osborne, B. A. (1992). *Algal photosynthesis* Chapman and Hall.

Goudar, C. T., Joeris, K., Konstantinov, K. B., & Piret, J. M. (2005). Logistic equations effectively model mammalian cell batch and fed-batch kinetics by logically constraining the fit. *Biotechnology Progress, 21*(4), 1109-1118.

Guerin, M., Huntley, M. E., & Olaizola, M. (2003). Haematococcus astaxanthin: Applications for human health and nutrition. *Trends in Biotechnology, 21*(5), 210-216.

Haynes, W. M., Lide, D. R., & Bruno, T. J. (2012). *CRC handbook of chemistry and physics* CRC Press.

Higuchi, D. (2012). *U.S. EPA recognizes kuehnle AgroSystems for innovative algae biofuel work.* Retrieved Mar 18, 2013, from http://yosemite.epa.gov/opa/admpress.nsf/0/AD6501A1BEE2D38485257A5A007785BA

Hodge, N. (2009). *Carbon intensity of algae biofuels.* Retrieved 03/04, 2013, from http://www.greenchipstocks.com/articles/carbon-intensity-of-algae-biofuels/462

Hong, D., et al. (2013). Combined effects of nitrate concentration and illumination conditions on the growth of microalga Haematococcus pluvialis. *Journal of Biology, 34*(4), 493-499.

Hu, Q., Westerhoff, P., & Vermaas, W. (2000). Removal of nitrate from groundwater by cyanobacteria: Quantitative assessment of factors influencing nitrate uptake.

Hu, Q., Kurano, N., et al. (1998). *Ultrahigh-cell-density culture of a marine green alga chlorococcum littorale in a flat-plate photobioreactor* Springer Berlin / Heidelberg.

Hu, Q., Guterman, H., & Richmond, A. (1996). A flat inclined modular photobioreactor for outdoor mass cultivation of photoautotrophs. *Biotechnology and Bioengineering, 51*(1), 51-60.

Jacob-Lopes, E., Scoparo, C. H. G., Lacerda, Lucy Mara Cacia Ferreira, & Franco, T. T. (2009). Effect of light cycles (night/day) on CO2 fixation and biomass production by microalgae in photobioreactors. *Chemical Engineering and Processing: Process Intensification, 48*(1), 306-310.

Jain, A., Verma, D., & Bagchi, D. (2006). Catalytic and regulatory properties of sulphur metabolizing enzymes in cyanobacterium synechococcus elongatus PCC 7942. *Indian Journal of Experimental Biology, 44*(9), 767-772.

Kajiwara, S., Yamada, H., Ohkuni, N., & Ohtaguchi, K. (1997). Design of the bioreactor for carbon dioxide fixation by synechococcus PCC 7942. *Energy Conversion and Management, 38, Supplement*(0), S529-S532.

Kilonzo, P. M., & Margaritis, A. (2004). The effects of non-newtonian fermentation broth viscosity and small bubble segregation on oxygen mass transfer in gas-lift bioreactors: A critical review. *Biochemical Engineering Journal, 17*(1), 27-40.

Kim, N., Suh, I. S., et al. (2002). *Simple monodimensional model for linear growth rate of photosynthetic microorganisms in flat-plate photobioreactors*

Kim, J., & Lee, C. (2005). *Systemic optimization of microalgae for bioactive compound production* The Korean Society for Biotechnology and Bioengineering.

Kobayashi, K., & Fujita, K. (1997). Tube diameter on tubular photobioreactor for microalgal culture and its biomass productivity. *Journal of Chemical Engineering of Japan, 30*(2), 339-341.

Konopka, A., & Brock, T. D. (1978). Effect of temperature on blue-green algae (cyanobacteria) in lake mendota. *Applied and Environmental Microbiology, 36*(4), 572-576.

Krüger, G. H. J., & Eloff, J. N. (1978). The effect of temperature on specific growth rate and activation energy of microcystis and synechococcus isolates relevant to the onset of natural blooms. *Journal of the Limnological Society of Southern Africa, 4*(1), 9-20.

Krupa, Z., Öquist, G., & Gustafsson, P. (1991). Photoinhibition of photosynthesis and growth responses at different light levels in psbA gene mutants of the cyanobacterium *synechococcus*. *Physiologia Plantarum, 82*(1), 1-8.

Kusnadi, A.,R., Nikolov, Z.,L., & Howard, J.,A. (1997). Production of recombinant proteins in transgenic plants: Practical considerations. *Biotechnology and Bioengineering, 56*(5), 473-484.

Lai, C., Dietrich, D., & Bowman, M. (2005). Global warming and the mining of oceanic methane hydrate. *Topics in Catalysis, 32*(3-4), 95-99.

Lee, C. (1999). Calculation of light penetration depth in photobioreactors. *Biotechnology and Bioprocess Engineering, 4*(1), 78-81.

Lee, J. N., Lee, J. S., Shin, C. S., Park, S. C., & Kim, S. W. (2000). Methods to enhance tolerances of chlorella KR-1 to toxic compounds in flue gas. *Applied Biochemistry and Biotechnology, 84-86*, 329-342.

Lee, J., & Lee, J. (2003). Review of advances in biological CO2 mitigation technology. *Biotechnology and Bioprocess Engineering, 8*(6), 354-359.

Lin, J., Lee, S., Lee, H., & Koo, Y. (2000). Modeling of typical microbial cell growth in batch culture. *Biotechnology and Bioprocess Engineering, 5*(5), 382-385.

Lönneborg, A., Kalla, S. R., Samuelsson, G., Gustafsson, P., & Öquist, G. (1988). Light-regulated expression of the psbA transcript in the cyanobacterium anacystis nidulans. *FEBS Letters, 240*(1–2), 110-114.

Loo, C. L., & Sudesh, K. (2007). Polyhydroxyalkanoates: Bio-based microbial plastics and their properties. *Malaysian Polymer Journal, 2*(2), 31-57.

Lundquist, T., Woertz, I., Quinn, N., & Benemann, J. R. (2010). A realistic technology and engineering assessment of algae biofuel production. *Energy Biosciences Institute,* , 1.

Lunka, A., & Bayless, D. (2013). Effects of flashing light-emitting diodes on algal biomass productivity. *Journal of Applied Phycology*, 1-7.

Mayer, D. (2008). Simple photosynthesis overview.

Mazel, D., Houmard, J., & Marsac, N. (1988). A multigene family in calothrix sp. PCC 7601 encodes phycocyanin, the major component of the cyanobacterial light-harvesting antenna. *Molecular and General Genetics MGG, 211*(2), 296-304.

Merchuk, J. C., & Gluz, M. (2002). Bioreactors, air-lift reactors. *Encyclopedia of Bioprocess Technology,*

Mirón, A. S., Camacho, F. G., Gómez, A. C., Grima, E. M., & Chisti, Y. (2000). Bubble-column and airlift photobioreactors for algal culture. *AICHE Journal, 46*(9), 1872-1887.

Mirón, A. S., Gómez, A. C., Camacho, F. G., Grima, E. M., & Chisti, Y. (1999). Comparative evaluation of compact photobioreactors for large-scale monoculture of microalgae. In R. Osinga, J. Tramper, J.G.Burgess and R.H.Wijffels (Ed.), *Progress in industrial microbiology* (pp. 249-270) Elsevier.

Molina , E., Belarbi, E., Acién Fernández, F. G., Robles Medina, A., & Chisti, Y. (2003). Recovery of microalgal biomass and metabolites: Process options and economics. *Biotechnology Advances, 20*(7–8), 491-515.

Monod, J. (1949). The growth of bacterial cultures. *Annual Review of Microbiology, 3*(1), 371-394.

National Research Council. (2012). *Sustainable development of algal biofuels in the united states* The National Academies Press.

Oilgae. (2009). *Oilgae report academic edition*. India:

Onken, U., & Träger, M. (1990). A simplified model of hydrodynamics in airlift loop reactors. *Bioprocess Engineering, 5*(3), 129-139.

Petrović, D. L., Posarac, D., & Duduković, A. (1995). Prediction of mixing time in airlift reactors. *Chemical Engineering Communications, 133*(1), 1-9.

Phillips, J. N. Jr., & Myers, J. (1954). Growth rate of chlorella in flashing light. *Plant Physiology, 29*(2), 152-161.

Pond Biofuels. (2011). *Algae biofuels.* Retrieved Dec 3, 2012, from http://www.pondbiofuels.com/Technology/AlgaeBiofuels/AlgaeBiofuels.html

Pope, D. (1975). Effects of light intensity, oxygen concentration, and carbon dioxide concentration on photosynthesis in algae. *Microbial Ecology, 2*(1), 1-16.

PowerplantCCS. (2010). *Algae CO_2 Capture costs and cost components.* Retrieved January 29, 2013, from http://www.powerplantccs.com/ccs/cap/fut/alg/algae_co2_capture_costs.html

Prezelin, B. B. (1981). Light reactions in photosynthesis. *Can.Bull.Fish.Aquat.Sci, 210*, 1-43.

Pulz, O., & Gross, W. (2004). Valuable products from biotechnology of microalgae. *Applied Microbiology and Biotechnology,* (65), Jan. 7, 2013-635-648.

Rasala, B. A., Muto, M., Lee, P. A., Jager, M., Cardoso, R. M., Behnke, C. A., et al. (2010). Production of therapeutic proteins in algae, analysis of expression of seven human proteins in the chloroplast of chlamydomonas reinhardtii. *Plant Biotechnology Journal, 8*(6), 719-733.

Sasi, D. (2009). Biokinetic behaviour of chlorella vulgaris in a continuously stirred bioreactor and a circulating loop photobioreactor. (M.Sc., University of Saskatchewan).

Schillberg, S., Fischer, R., & Emans, N. (2003). Molecular farming of recombinant antibodies in plants. *Cellular and Molecular Life Sciences CMLS, 60*(3), 433-445.

Schwarz, D., Nodop, A., Hüge, J., Purfürst, S., Forchhammer, K., Michel, K., et al. (2011). Metabolic and transcriptomic phenotyping of inorganic carbon acclimation in the cyanobacterium synechococcus elongatus PCC 7942. *Plant Physiology, 155*(4), 1640-1655.

Seambiotic Ltd. (2010). *Algae pilot plant*. Ashkelon, Israel: Seambiotic Ltd.

Shcolnick, S., Summerfield, T. C., Reytman, L., Sherman, L. A., & Keren, N. (August 2009). The mechanism of iron homeostasis in the unicellular cyanobacterium synechocystis sp. PCC 6803 and its relationship to oxidative stress. *Plant Physiology, 150*(4), 2045-2056.

Shelp, B. J., & Canvin, D. T. (1980). Photorespiration and oxygen inhibition of photosynthesis in chlorella pyrenoidosa. *Plant Physiology, 65*(5), pp. 780-784.

Siegesmund, S. (2011). *Stone in architecture: Properties, durability* Springer.

Sierra, E., Acién, F. G., Fernández, J. M., García, J. L., González, C., & Molina, E. (2008). Characterization of a flat plate photobioreactor for the production of microalgae. *Chemical Engineering Journal, 138*(1–3), 136-147.

Specht, E., Miyake-Stoner, S., et al. (2010). *Micro-algae come of age as a platform for recombinant protein production* Springer Netherlands.

Srivastava, A. K., Rai, A. N., & Neilan, B. A. (2013). *Stress biology of cyanobacteria: Molecular mechanisms to cellular responses* Taylor & Francis Group.

Suh, I. S., & Lee, S. B. (2001). Cultivation of a cyanobacterium in an internally radiating air-lift photobioreactor. *Journal of Applied Phycology, 13*(4), 381-388.

Suh, I. S., Park, C. B., Han, J., & Lee, S. B. (1998). Cultivation of cyanobacterium in various types of photobioreactors for biological CO2 fixation. *Studies in surface science and catalysis* (pp. 471-474) Elsevier.

Summerfield, T. C., & Sherman, L. A. (2008). Global transcriptional response of the alkali-tolerant cyanobacterium synechocystis sp. strain PCC 6803 to a pH 10 environment. *Appl Environ Microbiol., 17*(74), 5276-5284.

Suzuki, L., & Johnson, C. H. (2001). Algae know the time of day: Circadian and photoperiodic programs. *Journal of Phycology, 37*(6), 933-942.

Todar, K. (2012). *Nutrition and growth of bacteria.* Retrieved Feb 25, 2013, from http://textbookofbacteriology.net/nutgro.html

UTEX. (2009). *BG-11 medium.* Retrieved 07/08, 2010, from http://www.sbs.utexas.edu/utex/mediaDetail.aspx?mediaID=26

Wageningen UR. (2011). *Research on microalgae within wageningen UR.* Retrieved Feb 27, 2012, from http://www.algae.wur.nl/UK/factsonalgae/growing_algae/temperature/

Walker, T., Purton, S., Becker, D., & Collet, C. (2005). Microalgae as bioreactors. *Plant Cell Reports, 24*(11), 629-641.

Watkins, K. (2002). *Fighting the clock.* Retrieved January 28, 2013, from http://www.pubs.acs.org/cen/coverstory/8004/8004pharmaceuticals.html

Wyszecki, G., Stiles, W. (1982). *Color Science: Concept and Methods, Quantitative Data and Formulæ*. Wiley.

Yamada, H., Ohkuni, N., Kajiwara, S., & Ohtaguchi, K. (1997). CO_2-removal characteristics of anacystis nidulans R2 in airlift bioreactors. *Energy, 22*(2–3), 349-352.

Yang, J., Rasa, E., Tantayotai, P., Scow, K. M., Yuan, H., & Hristova, K. R. (2011). Mathematical model of chlorella minutissima UTEX2341 growth and lipid production under photoheterotrophic fermentation conditions. *Bioresource Technology, 102*(3), 3077-3082.

Yun, Y., Lee, S. B., Park, J.M., Lee, C., & Yang, J. (1997). Carbon Dioxide Fixation by Algal Cultivation Using Wastewater Nutrients. *J. Chem. Tech. Biotechnol*, *69*, 451-455.

Zhang, K., Kurano, N., & Miyachi, S. (2002). Optimized aeration by carbon dioxide gas for microalgal production and mass transfer characterization in a vertical flat-plate photobioreactor. *Bioprocess Biosyst Eng, 25*(2), 97-101.

Appendices

Appendix A: Sample calculations

1) Calculation for biomass concentration *X* from optical density reading

X (g/L) = 0.3543*OD_{600} – 0.004

For OD=1,

X=0.3543*1-0.004

X=0.3503 g/L

2) CO_2 electrode calibration

Dissolved CO_2 concentration (g/L) = exp[(mV+1.2)/8.2082]

For mV=30,

Dissolved CO_2 conc. = exp[(30+1.2)/8.2082]

= 44.7 mg/L

3) Calculation of theoretical mixing time (95% homogeneity)

$$t_m = 53.5 U_G^{-0.31} \left(\frac{H}{D}\right)^{0.12} V_R^{0.19} V_D^{0.5} V_S^{-0.26}$$

Calculate characteristic diameter *D*:

Assuming *D* is equal to the diameter of a circle with an area equivalent to that of the cross-sectional area of the reactor.

$$\pi\left(\frac{D}{2}\right)^2 = L \cdot W$$

$$D = 2\sqrt{\frac{L \cdot W}{\pi}}$$

For a photobioreactor of 2.54 cm width and 16.61 cm:

$$D = \frac{2}{100}\sqrt{\frac{2.54 \cdot 16.61}{\pi}}$$

D = 0.0731 m

For U_G = 0.25 cm/s, H = 0.17145 m, D = 0.0731 m

$$t_m = 53.5 * 0.1987^{-0.31} * \left(\frac{0.17145}{0.0731}\right)^{0.12} * 0.000346^{0.19} * 0.000359^{0.5} * 0.00016^{-0.26}$$

t_m = 4 s

4) Calculation of Bodenstein number

$$c_r = \sum (c_r)_{x_U} = \sum_{x_U=\tau_U-2}^{x_U=\tau_U+2} \left(\frac{Bo}{4\pi\tau_U} \right)^{1/2} \exp\left[-\frac{(x_U - \tau_U)^2}{4\tau_U} Bo \right]$$

An initial guess of 10 was first applied to *Bo*. For τ_U of 4,

$$c_r = \sum_{x_U=2}^{x_U=6} \left(\frac{10}{4\pi \cdot 4} \right)^{1/2} \exp\left[-\frac{(x_U - 4)^2}{4 \cdot 4} 10 \right] = 0.997$$

The residual sum of squares taken from the theoretical c_r and experimental c_r was minimized. Using the solver function in Excel, *Bo* was determined to be 11.5. c_r was calculated to be 0.999.

Appendix B: Bubble size in photobioreactor (33°C)

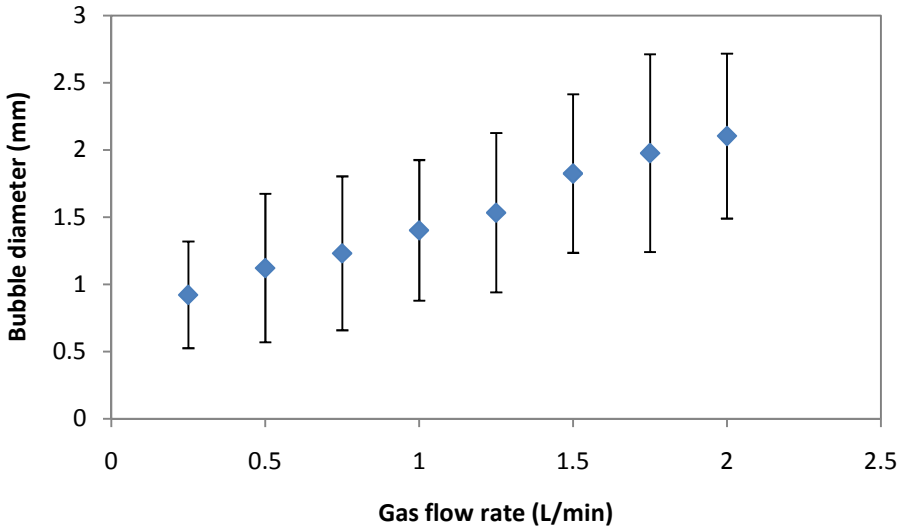

Appendix C: *S. elongatus* growth at various conditions in 2D photobioreactor

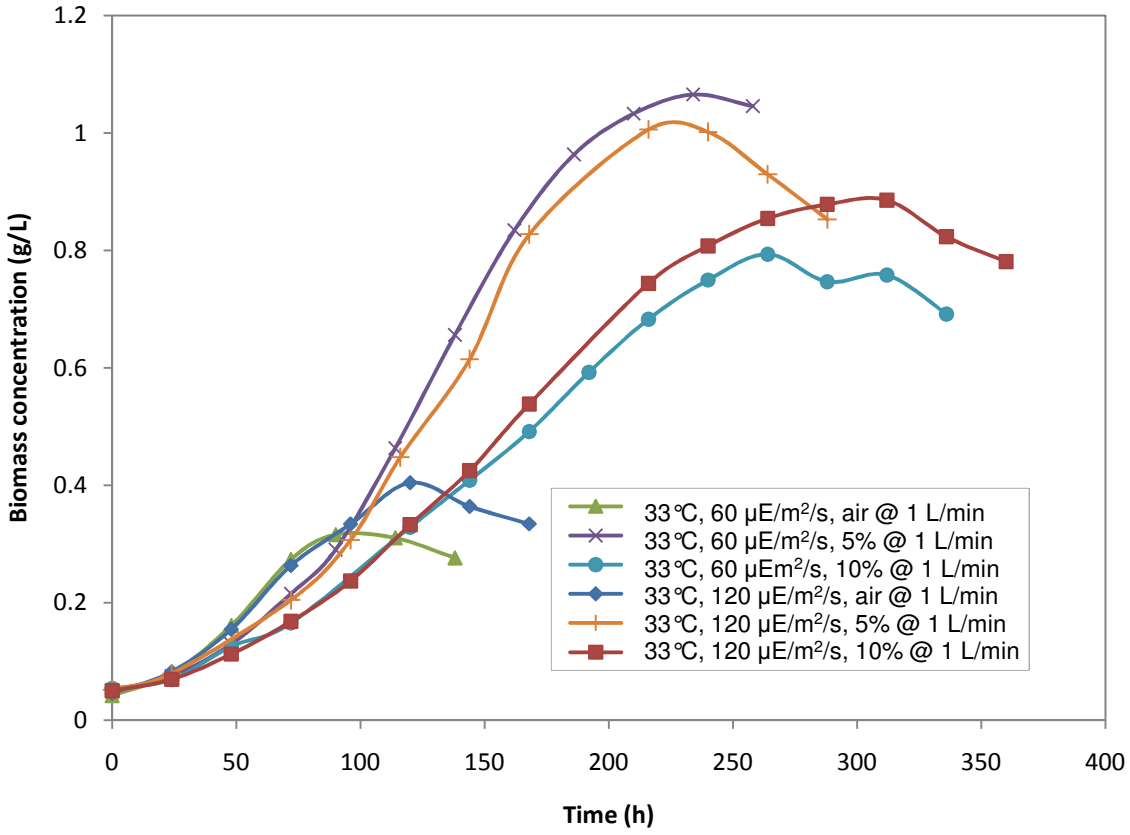

Appendix D: Polymath program for calculating carbon content

```
# air @ 1 L/min
d(C)/d(t) = kLa * (Cs - C) - r # carbon dioxide mass balance in medium (g/L/h)
X = Xo * Xm * exp(u * t) / (Xm - Xo + Xo * exp(u * t)) # logistic growth model (g/L)
Xo = 0.0421617 # initial biomass concentration (g/L)
C(0) = 0.000654 # initial dissolved CO2 concentration in medium (g/L)
u = 0.05038517 # maximum specific growth rate (1/h)
kLa = 45.50 # volumetric mass transfer coefficient  (1/h)
Xm = 0.3160356 # maximum biomass concentration (g/L)
t(0) = 0 # initial time (h)
t(f) = 150 # final time (h)
Cs = 0.000474 # estimated saturation concentration of CO2 in medium (g/L)
r = u * (1 - X / (1 + Xm)) * X * 0.465 * 44 / 12 # carbon uptake rate (g/L/h)
Ca = C * 12 / 44 + X * 0.465 + 0.00216 # Total carbon (from CO2 and Na2CO3) in medium (g/L)
Cx = X * 0.465 # Total carbon content in biomass (g/L)

# 5% @ 1 L/min
d(C)/d(t) = kLa * (Cs - C) - r
X = Xo * Xm * exp(u * t) / (Xm - Xo + Xo * exp(u * t))
Xo = 0.049602
C(0) = 0.0367
u = 0.025514
kLa = 5.76
Xm = 1.065734
t(0) = 0
t(f) = 300
Cs = 0.0367
r = u * (1 - X / (1 + Xm)) * X * 0.465 * 44 / 12
Ca = C * 12 / 44 + X * 0.465 + 0.00216
Cx = X * 0.465

# 10% @ 1 L/min
d(C)/d(t) = kLa * (Cs - C) - r
X = Xo * Xm * exp(u * t) / (Xm - Xo + Xo * exp(u * t))
Xo = 0.053854
C(0) = 0.067
u = 0.018948
kLa = 5.37
Xm = 0.793632
t(0) = 0
t(f) = 300
Cs = 0.067
r = u * (1 - X / (1 + Xm)) * X * 0.465 * 44 / 12
Ca = C * 12 / 44 + X * 0.465 + 0.00216
Cx = X * 0.465
```